December 2020

Evaluating Hydration and Artificial Aging Effects on the Paleointensity in Natural Glass

Sebastian Fearn
University of Wisconsin-Milwaukee

EVALUATING HYDRATION AND ARTIFICIAL AGING EFFECTS ON THE PALEOINTENSITY IN NATURAL GLASS

by

Sebastian Fearn

A Thesis Submitted in

Partial Fulfillment of the

Requirements for the Degree of

Master of Science

in Geosciences

at

The University of Wisconsin-Milwaukee

December 2020

ABSTRACT

EVALUATING HYDRATION AND ARTIFICIAL AGING EFFECTS ON THE PALEOINTENSITY IN NATURAL GLASS

by

Sebastian Fearn

The University of Wisconsin-Milwaukee, 2020
Under the Supervision of Dr. Julie Bowles

Young natural volcanic glasses have been successfully used to recover Earth's geomagnetic field intensity (paleointensity). However, the magnetic stability and reliability of volcanic glass as a paleomagnetic recorder over geologic time is unclear. Paleointensity estimates may be influenced by natural processes that alter magnetic mineralogy. Previous results from paleointensity and rock magnetic experiments suggest that post-emplacement hydrothermal alteration can alter the magnetic remanence and can possibly cause paleointensity experiments to fail. Low-temperature hydration and natural relaxation of the glass structure over time may also adversely impact paleointensity results. In this study, rhyolitic and basaltic glass specimens underwent artificial aging and artificial hydration treatments to observe how the magnetic mineralogy and resulting magnetic properties are affected. The fresh rhyolitic glass contained pseudo-single-domain to multidomain low-Ti titanomagnetite, and basaltic glass contained single-domain and superparamagnetic grains of medium to low-Ti titanomagnetite. Artificial aging took place by heating in air at 200-400°C under anhydrous conditions for up to 240 days. Hydration was induced at 200 MPa pressure with elevated temperatures of 300°C and

450℃ at different time intervals. Before and after aging or hydration, samples underwent experimental procedures to assess the impact of the aging or hydration treatments on magnetic mineralogy and behavior during paleointensity experiments. Aged samples were subject to a modified Thellier-Thellier paleointensity experiment, isothermal remanent magnetization (IRM) acquisition experiments, hysteresis and first order reversal curve (FORC) experiments, and thermal demagnetization of a three-component IRM. Hydrated samples were subject to hysteresis and FORC experiments, and IRM acquisition experiments. IRM acquisition experiments on artificially aged samples showed increases in saturation IRM and a decrease in coercivity in both rhyolitic and basaltic glass specimens. These trends in magnetic properties are believed to have arisen from a growth of existing grains within the basaltic and rhyolitic glasses. Paleointensity experiments showed that with increased aging temperature, basaltic glasses experience more alteration during paleointensity laboratory reheating experiments. This is not seen in rhyolitic glasses. Hydration experiments resulted in inconsistent changes in coercivity and magnetization over treatment. Changes in coercivity and magnetization in basaltic glasses were much greater than rhyolitic glasses. These changes may be explained by magnetic grain growth, loss of material, select dissolution of the finest magnetic grains, and possible oxidation in basaltic glass samples based on IRM experiments. Hydration rims appeared prominently in nearly all hydrated samples, with some rhyolitic glasses experiencing a hydrated interior while only one basaltic sample showed hydration within the interior. While young volcanic glass could be used as a good paleomagnetic recorder, results of this study suggest that older material might pose several problems. Older material could be hydrated, rehydrated, or have a change in the glass structure that results in a change in the magnetic mineral assemblage and therefore incorrect paleointensity and paleomagnetic data. It is recommended that the glass properties and

hydration states of older glasses should be further studied before carrying out paleomagnetic studies.

To

Mum and Bill,

Thank you for supporting my Journey

TABLE OF CONTENTS

LIST OF FIGURES

LIST OF TABLES

LIST OF ABBREVIATIONS

NRM – Natural Remanent Magnetization

ARM – Anhysteretic Remanent Magnetization

TRM – Thermal Remanent Magnetization

IRM – Isothermal Remanent Magnetization

FTIR – Fourier Transform Infrared Spectroscopy

FORC – First Order Reversal Curve

TM60 – Titanomagnetite 60.

DRATS – Sum of Difference Ratios

MORB – Mid-Ocean Ridge Basalt

B – Magnetic Field

B_{cr} – Coercivity of Remanence

B_c – Coercivity

sIRM – Saturation Isothermal Remanent Magnetization

M_s – Saturation Magnetization

M_r – Saturation Remanent Magnetizaiton

T_c – Curie Temperature

T_g – Glass Transition Temperature

SD – Single-Domain

SP – Superparamagnetic

PSD – “Pseudo-single” domain

MD – Multi-Domain

ACKNOWLEDGEMENTS

There are several people and institutions that I would like to express my deepest gratitude making this thesis possible. First, to my advisor Dr. Julie Bowles, I would not have been able to carry out this thesis without your invaluable commentary and assistance throughout my graduate education. Thank you so much for your time and patience through this current, soon to be historic COVID-19 pandemic. Second, I would like to thank Fatimah Abdulghafur for collecting samples, and starting early measurements of artificially aged samples. I would like to thank my Master's committee, Dr. Barry Cameron and Dr. Lindsay Henry for their comments and ideas.

There are several institutions I would like to thank for their support in this project, first, I would like to thank the National Science Foundation for funding this project (grant 1547483). Secondly, I would like to thank Dr. Bryan Dreyer of the Monterey Bay Aquarium Research Institute for providing the submarine basaltic glass samples for this study. And finally, I would like to thank everyone at the Institute for Rock Magnetism at the University of Minnesota for all their equipment and their help with the hysteresis data sets.

I would like to thank everyone at UWM for being so welcoming, and all of the graduate students in the Geosciences department. Personally, I would like to thank Ji-in Jung, Gayantha Loku Kodikara, Leslie Bychinski, Falyn Strey, Chase Glenister, and his partner Sarah Whitaker for helping me and having fun in Milwaukee, along with their inspiration and support through my graduate career. Finally, I would like to thank my parents, Kathleen Mayer-Solosy and William Solosy Jr. for all their help and support in my endeavors to understand the world around us, and its natural history.

Chapter 1: BACKGROUND

1.1 General Paleomagnetism Background

1.1.1 Earth's Magnetic Field: A Brief History

The history of Earth's geomagnetic field is crucial to understanding the evolution and habitability of Earth. Earth's geomagnetic field varies in both space and time, and these variations can be used to determine tectonic reconstructions, geodynamo formation, geodynamo behavior, and planetary evolution (e.g., Glatzmaier and Roberts, 1996; McElhinny and McFadden, 2000). Long-term variations are linked to planetary evolution, geodynamo formation, and core formation while shorter-period variations can provide insight into paleosecular variation. A possible source of energy for the movement of material throughout the mantle is thermal buoyancy derived from the latent heat of freezing the inner core material (Jacobs, 1953). Additionally, a compositional buoyancy originates from the exclusion of light elements from the inner core (Glatzmaier and Roberts, 1996). The resulting magnetohydrodynamical system can create a self-maintaining dynamo (Glatzmaier and Roberts, 1996). Planetary magnetic fields are thought to be one of the key factors for life to exist on planetary bodies, leading to further questions about how these magnetic fields originally formed.

There are several different theories on both the age of inner core formation and the age of the Earth's magnetic field. It is believed that the Earth's magnetic field existed as early as ~3.4 Ga, with some findings showing the formation of Earth's magnetic field at ~4.3 Ga (Tarduno et al., 2010, Tarduno et al., 2015). Estimates of inner core formation span from ~1.5 Ga to ~500 Ma (e.g., Biggin et al., 2015, Bono et al., 2019). These timings are based in part on paleomagnetic estimates of magnetic field intensity (paleointensity). However, one of the difficulties in determining paleointensity in deep time is the lack of suitable material that has retained its

magnetization for millions or billions of years. Young basaltic volcanic glass has been shown to be a reliable paleointensity recorder (e.g., Pick and Tauxe, 1993b; Carlut and Kent, 2000; Gee et al., 2000; Carlut et al., 2004; Bowles et al., 2005; 2006; 2011). This study attempts to show the benefits and drawbacks of using volcanic glasses of variable compositions and ages as a possible paleomagnetic recorder from which we may gain insight into the evolution of the ancient magnetic field.

1.1.2 Suitable Paleointensity Materials

There are numerous materials that can record the geomagnetic field with varying degrees of success. Most absolute paleointensity experimental protocols involve replacing a natural thermal remanent magnetization (TRM) with a laboratory-imparted TRM in a known field. This protocol assumes that the remanence recording minerals in the sample are the same for both the natural TRM and the laboratory TRM. Therefore, to accurately recover paleointensity, the magnetic mineralogy of the sample must remain unchanged since formation. It also must not change during laboratory reheating. Finally, only the finest-grained magnetic particles will faithfully retain a magnetization for billions of years and also satisfy further assumptions in the paleointensity methodology (see Sec. 1.1.5). An ideal paleointensity recorder is therefore one that contains fine-grained (titano)magnetite (for example) and resists alteration. Basaltic lava flows are often used in paleointensity studies, but they do not always contain exclusively fine-grained magnetic particles and the matrix material will sometimes alter during laboratory heating. For the recent past, anthropogenic sources such as pottery fragments or tools that can be accurately dated can be used for paleomagnetic studies. Single silicate crystals with magnetic inclusions have shown some success, as the silicate material typically shields the magnetic particles from alteration (e.g. Tarduno et al., 2015, Tarduno et al., 2020). For a look at deeper

time, single-silicate zircons have been used to analyze paleointensity in the Hadean (Tarduno et al., 2015; Tarduno et al., 2020). Similar to the silicate crystals, volcanic glass typically contains fine-grained magnetic particles and the glass seems to protect these particles from alteration, at least over short timescales (hundreds of thousands of years) (e.g, Pick and Tauxe, 1993b; Carlut and Kent, 2000; Gee et al., 2000).

Figure 1.1: Examples of materials used in paleointensity studies. (A) An image of a single silicate grain used to find paleointensity estimates, zircon is in the "o" on the face of a dime (Tarduno et al., 2020). (B) An image of rhyolitic glass used in this paleomagnetic study. The sample is approximately 30 cm × 25 cm × 15 cm.

A) **B)**

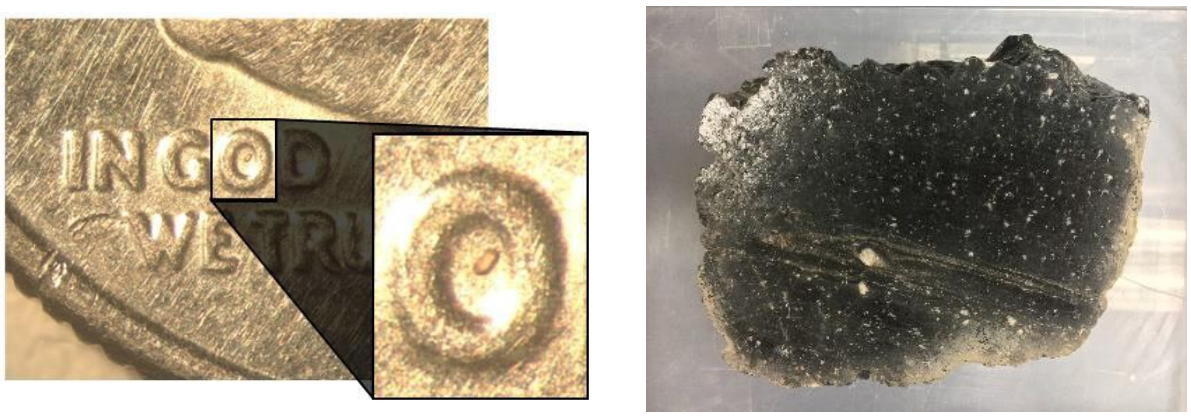

The focus of this thesis is these volcanic glasses. Glasses have some properties that make them desirable as paleomagnetic recorders, but their magnetic stability over geologic time is uncertain. Despite this, basaltic glasses have been used to derive paleointensity estimates in the Cretaceous and Jurassic (Pick and Tauxe, 1993a; Tauxe and Staudigel, 2004; Tauxe, 2006; Tauxe et al., 2013). The oldest abundant volcanic glass on Earth is in New South Wales, Australia. The glass, an ignimbrite, is 332 +/- 4 Ma, and was proven to be glass through X-ray diffraction and electron diffraction (Hamilton, 1992). However, over the course of geologic

history these volcanic glasses can be altered, possibly altering the magnetic mineralogy and the magnetization they hold. This thesis examines the potential effects of alteration by hydration and by simple age-induced glass relaxation.

1.1.3 Magnetic Remanence

There are two types of magnetization: induced magnetization and remanent magnetization. Induced magnetization occurs when a sample is exposed to a magnetic field (Butler, 1992), but the magnetization is not permanent. Induced magnetization can be calculated using the equation, $M_i = \chi H$, with M_i being the induced magnetization, H the magnetic field strength, and χ is the magnetic susceptibility of the material (Butler, 1992). Remanent magnetization is a type of magnetization that persists once the field is removed. This form of magnetization can therefore provide information about the history of Earth's magnetic field. It arises from ferromagnetism, which results from strong interactions between neighboring electron spins that occur in certain magnetic materials (Tauxe et al., 2018).

The natural remnant magnetization (NRM) is the magnetization that remains in the rock before any laboratory experiments. There are several different ways for a sample to acquire an NRM, including thermal, viscous, and chemical remanences. Thermal remanence (TRM) is when a sample cools from above the Curie temperature (T_c) and the magnetization aligns with the geomagnetic field. Viscous remanent magnetization (VRM) is when the magnetization realigns at temperatures lower than T_c due to changes in the ambient field (Tauxe et al., 2018). A VRM can replace some or all the preexisting NRM (Tauxe et al., 2018). Chemical remanence (CRM) is when a chemical alteration occurs below T_c, creating, destroying, or modifying ferromagnetic minerals (Tauxe et al., 2018). When magnetic mineral assemblages in paleomagnetic samples are altered, this can have a negative effect on the paleointensity estimates

because the TRM acquired in the lab will not be carried by the same minerals that acquired a TRM in nature.

1.1.4 Grain Size, Domain State, and Coercivity

Coercivity is the magnetic field required to reverse the magnetization direction of a magnetized particle over the anisotropy energy barrier (Tauxe et al., 2018). The ease with which a sample may become remagnetized in the absence of any chemical transformations is partly a function of its coercivity. Analyzing the coercivity is critical to seeing if a material has physically changed compared to its unaltered state. Coercivity is a function of mineral composition and grain size, and grain size is linked to the magnetic domain state. Magnetic domain states describe the way electron spins organize within a single crystal in order to minimize the total energy (Tauxe et al., 2018). The minimum energy configuration varies based on the size, shape, and composition of the individual mineral. Schematic end-member domain states of grains are shown in **Figure 1.2**. At small grain size, a single-domain (SD) state exists where the grain is uniformly magnetized, and all electron spins act together to align parallel (or anti-parallel). SD materials typically have high coercivity and carry a stable magnetization. For magnetite, the SD size range is approximately 50-90 nm (Dunlop and Özdemir, 1997). As particle sizes get larger the total energy is minimized by a divergence of spin directions, leading to a 'pseudo-single domain' state of non-uniform magnetization (Tauxe et al., 2018). In the multi-domain (MD) states found in larger crystals, spins organize themselves into separate distinct regions with quasi-uniform magnetization. MD materials typically have low coercivity and less stable magnetization. Superparamagnetic particles, which are the smallest grain sizes, have uniform magnetization throughout, but the total magnetic energy is exceeded by thermal energy, leading to an unstable magnetization and no remanence (Tauxe et al., 2018).

Figure 1.2: Domain sizes. A single-domain grain (L) and a multi-domain grain (R) showing sub-grain magnetization directions. The best paleomagnetic recorders are single-domain samples and have good paleomagnetic retention (Modified from Butler, 1992).

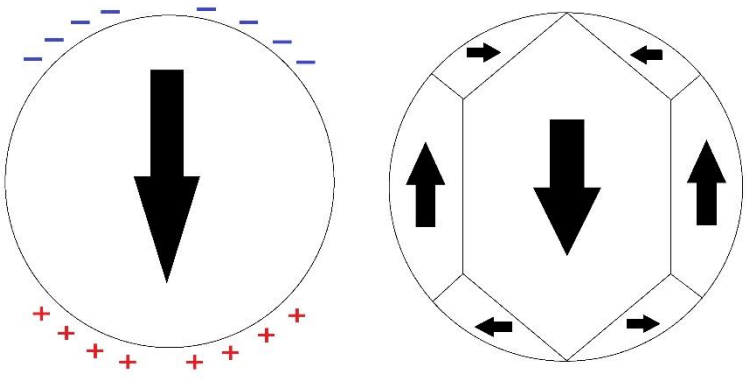

Paleomagnetic samples such as rocks or pottery can contain an assemblage of magnetic grains with a distribution of grain sizes. A distribution of grain sizes in a sample will have a distribution of coercivities.

1.1.5 Curie and Blocking Temperatures

Curie temperatures in paleomagnetic materials are explored to determine grain composition. Above the Curie temperature (T_C) cooperative spin behavior ceases due to crystal expansion (Tauxe et al., 2018). Different materials have different Curie temperatures based on the characteristics of each crystal type and exchange energy between atoms. For example, the Curie temperature of magnetite (Fe_3O_4) is 580°C, meaning that an NRM is removed after being exposed to that temperature. Compositional variations can influence Curie temperature, and an example of a mineral with a wide range of Curie temperatures is titanomagnetite. Titanomagnetite ($Fe_{3-x}Ti_xO_4$, $0 \leq x \leq 1$) is the solid solution between magnetite and ulvöspinel (Fe_2TiO_4), and Curie temperatures varies with Ti-content, ranging from -150°C (x = 1) to ~580°C (x = 0) (**Fig. 1.3**).

Spins behave cooperatively below T_c, but remanence will not be locked in until the sample cools below its blocking temperature(s). At the blocking temperature, magnetic relaxation time is a few hundred seconds, and grains with these relaxation times will be in equilibrium with the field (Tauxe et al., 2018). Cooling below the blocking temperature increases relaxation time, so magnetization is essentially blocked, and the sample acquires a TRM (Tauxe et al., 2018). Blocking temperature is always less than T_c and is typically a function of grain size.

Figure 1.3: Titanomagnetite Curie temperature as a function of titanium substitution. (Modified from Tauxe et al., 2018). TM60 represents a titanomagnetite with x = 0.6, and the Curie temperature is ~200°C.

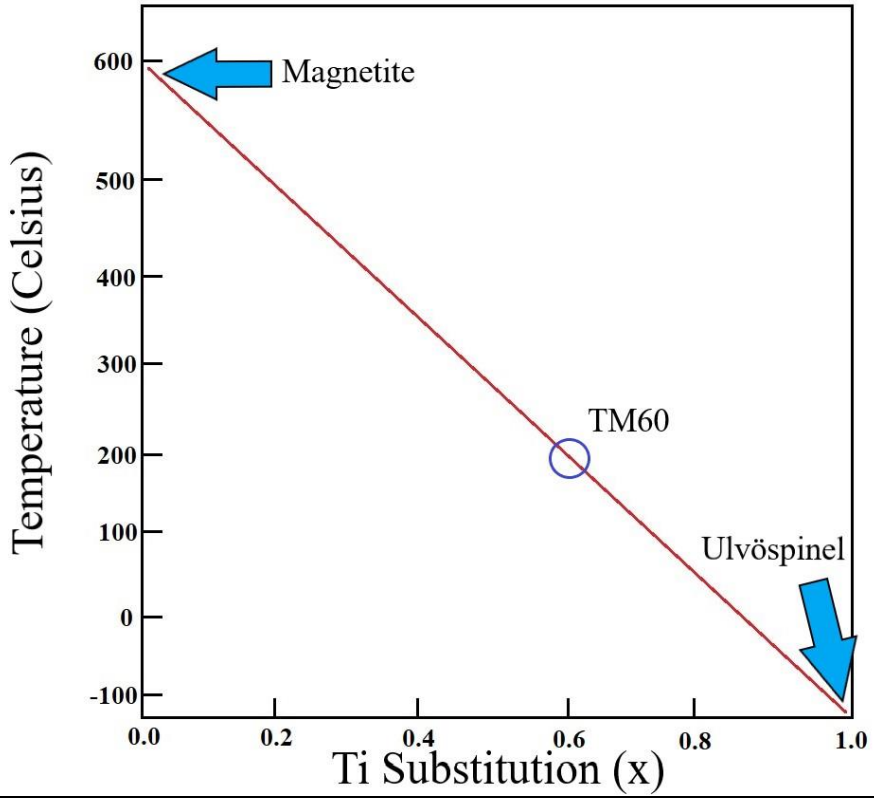

1.1.6 Paleointensity

Paleointensity experiments provide estimates of the strength of Earth's magnetic field at the time an NRM is acquired. Experimental protocols for paleointensity commonly involve comparing the NRM to a TRM imparted in the lab in a known field (Tauxe et al., 2018). A sample is heated up in a stepwise temperature experiment. The NRM is progressively removed or "unblocked" due to the heating of the material. The NRM is replaced by an artificially created TRM in a known field as seen in **Figure 1.4**. The ratio of NRM/TRM is related to the strength of the paleofield and can be used to estimate the strength of the ancient geomagnetic field.

Methods for determining absolute paleointensity assume the NRM is a TRM acquired on cooling through the sample's blocking temperatures. The protocol also rests on the assumptions of additivity and reciprocity of partial TRM which are only valid for SD particles. SD samples are therefore the best for recovering a paleointensity estimate of Earth's magnetic field due to their grain size but are unfortunately rare in nature. Submarine, subglacial, and subaerial volcanic glasses are some of the few natural materials that contain SD particles.

Figure 1.4: Schematic representation of paleointensity estimation. At low fields (such as Earth's field), there is a linear relationship between applied field and remanent magnetization. Once the NRM is measured, the sample can be given a magnetization in a known laboratory field. This provides the ratio of M/B which can be used to infer the ancient field required to produce the NRM. (After Tauxe et al., 2018)

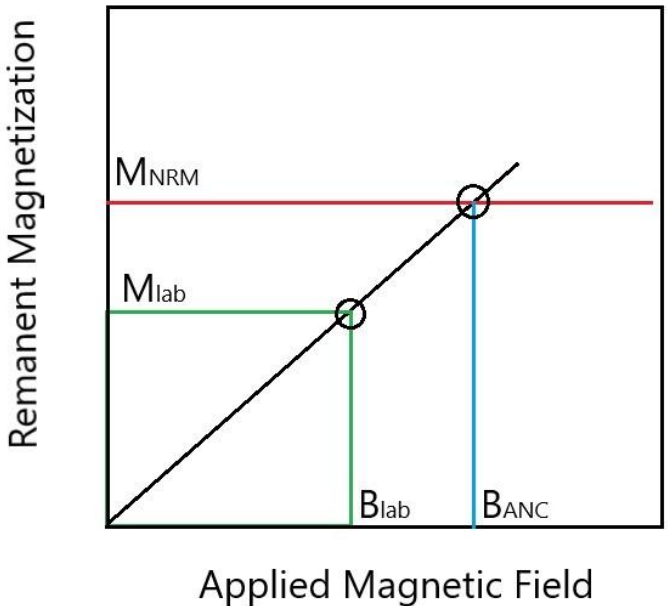

There are several different paleointensity methodologies that have been used to find absolute paleointensity. Heating methods include the Thellier-Thellier stepwise heating method (Thellier and Thellier, 1959), a variation of which is described in Section 2.2.7. In the modified Shaw method (Shaw, 1974), the NRM is alternating field demagnetized before a TRM is acquired. There are methodologies for paleointensity that do not involve heating, but rather involve normalizing by an isothermal remanent magnetization (IRM) or an anhysteretic remanent magnetization (ARM) instead of a TRM. However, the these "quasi-absolute" estimates (Tauxe et al., 2018) need to be carefully calibrated and typically have high uncertainty.

1.1.7 Possible changes in Magnetic Mineralogy

Determining how well a magnetic mineral assemblage retains a magnetic remanence over deep time is an important caveat for possible paleointensity experiments. Changes in magnetic mineral assemblage after the primary TRM is acquired will likely lead to failure or bias in paleointensity experiments. In this thesis, I will focus on two parameters when interpreting

changes in magnetic mineralogy over the course of the aging and hydration experiments. Saturation IRM (sIRM), which is explored in Ch. 3, is a function of mineral composition, domain state, and the volume abundance of grains within the sample. Coercivity is a function of grain size or domain state, and a decrease in coercivity is typically linked to an increase in grain sizes of magnetic mineral assemblages. By contrast, an increase in coercivity typically indicates a decrease in overall grain size. Coupling changes in coercivity and magnetization into a "quadrant" like graph allows us to place constraints on changes in the magnetic mineral assemblage over the course of treatments seen in this thesis. **Figure 1.5** shows an example of simple changes within the magnetic mineralogy based on coercivity and magnetization treatments over treatment.

Figure 1.5: Possible changes in magnetic mineralogy linked to changes in sIRM and coercivity. These are some of the simplistic reasons magnetization and coercivity changed over treatment time. With the exception of the upper left quadrant, the other quadrants assume no change in mineral composition.

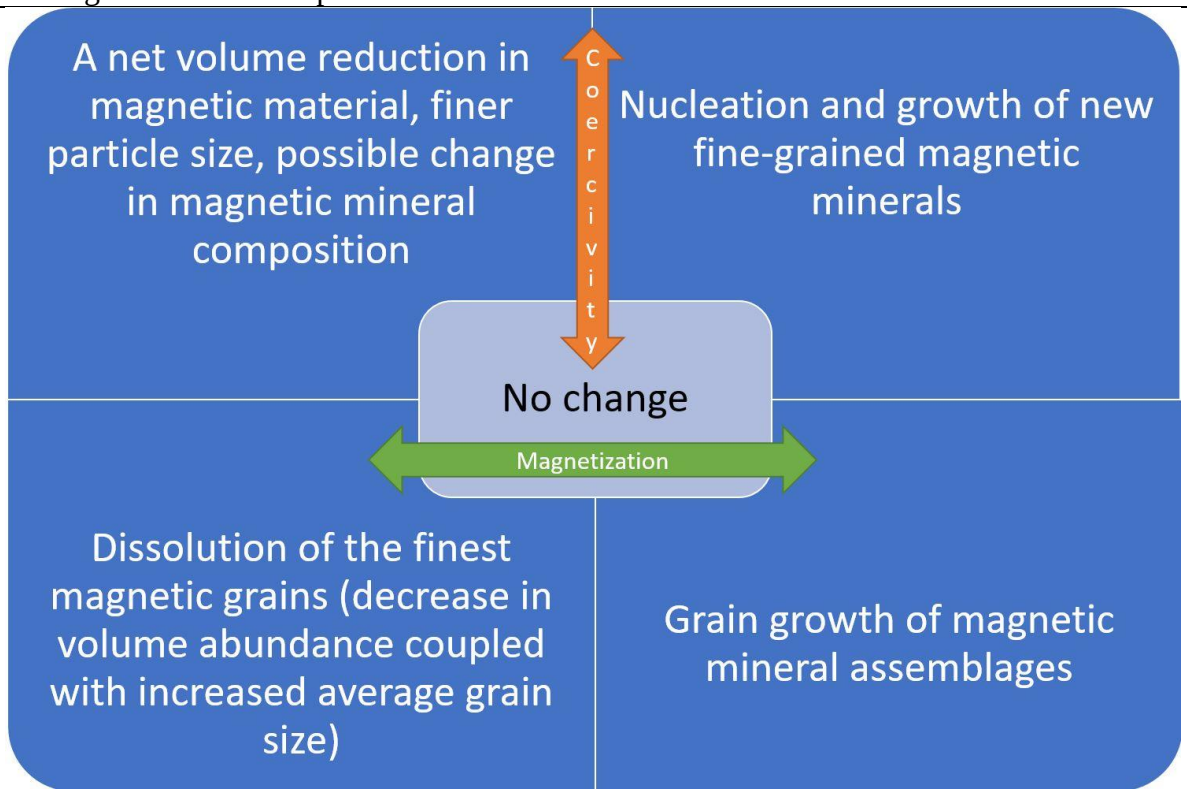

For example, increased coercivity and an increased magnetization are consistent with nucleation and growth of fine-grained materials. The formation of new material would increase the saturation IRM, and if the particles are smaller than the preexisting grains, the sample average coercivity will increase. A decrease in coercivity and increase in magnetization would be consistent with growth of existing grains. A decrease in magnetization would suggest a net volume loss of magnetic particles and/or a change in the magnetic mineral composition.

1.2 Volcanic Glass

1.2.1 Volcanic Glass: Why use as a paleomagnetism target?

Volcanic glasses may be considered ideal paleointensity recorders for two reasons: 1) they often contain SD titanomagnetite or magnetite particles as a result of rapid quenching from a melt; and 2) the glass surrounding these particles may protect them from thermochemical alteration during the paleointensity experiment itself (e.g., Bowles et al., 2011). Young (<100 ka) submarine basaltic volcanic glasses have been shown to provide insight into the short-term behavior of Earth's magnetic field strength (e.g., Pick and Tauxe, 1993b; Carlut and Kent, 2000; Gee et al., 2000; Carlut et al., 2004; Bowles et al., 2005; 2006; 2011). The abundance of volcanic glasses on the surface of Earth would help provide better, more evenly distributed data compared to archaeomagnetic sources (Ferk et al., 2011).

However, the viability of paleomagnetic measurements using older volcanic glass has been questioned because volcanic glasses often alter over time. Paleointensity experiments assume that the laboratory induced TRM is completely analogous to the original process by which the sample acquired its magnetization upon cooling from a melt. This assumption can be

violated in at least two ways. 1) The NRM no longer corresponds to the original primary TRM, either due to overprinting by (thermo)viscous processes or by acquisition of a CRM during chemical alteration in nature. 2) The sample may still hold its primary NRM and original magnetic mineralogy, but that mineralogy may alter during the paleointensity experiment itself. This means that the laboratory TRM will be held by a different mineral assemblage than the NRM.

Because volcanic glass is meta-stable, it may undergo alteration as the sample ages, meaning that the magnetic mineralogy may change after acquisition of the original NRM. Changes to the magnetic remanence carriers may occur during devitrification as the glass relaxes over geologic time, influencing the reliability of recorded paleointensities and paleodirections. Even without (magnetic) mineralogical changes in nature, older glass may be more likely to alter upon reheating during laboratory paleointensity experiments (Smirnov and Tarduno, 2003; Bowles et al., 2011). Devitrification at these lower temperatures may lead to the undetected crystallization of new magnetic material that would render the paleointensity result unreliable.

1.2.2 Structural Properties and Evolution of Volcanic Glasses

The structural state of the glass is often described by the glass transition temperature (T_g). If a material is above the T_g, then the material behaves like a liquid, and if it is below the T_g it behaves like a solid. T_g also tells you something about the relative structural equilibrium of the sample. As the melt cools, the liquid has a temperature-dependent equilibrium structure arising from Si-O configuration and bonding. This structural order remains in equilibrium until it passes through the glass transition, at which point the structure is "frozen". So T_g tells you the temperature at which the glass was last at equilibrium. Measured glass transition temperatures

vary due to several factors including melt composition, water content, cooling rate, and the timescale of observation (Dingwell and Webb, 1990; Deubener et al., 2003).

Glasses are inherently thermodynamically unstable and can devitrify if given adequate time (Lofgren, 1971). This results from structural relaxation, is accompanied by a reduction in T_g, and may be linked to the formation of new magnetic minerals at ambient temperatures during incipient devitrification. If T_g is low enough, paleointensity experiments may result in samples being heated to temperatures close to or above T_g, resulting in crystallization during the experiment. It has been observed that at temperatures just below or above T_g new magnetic minerals can precipitate out of the glass (Leonhardt et al., 2006; Bowles et al., 2011; Smirnov and Tarduno, 2003), and this would have a deleterious effect on the paleointensity result.

1.2.3 Previous Natural Glass Paleointensity Studies

Most preserved basaltic glass is submarine, where a glass rind (usually < 1 cm thick) forms when the hot lava quenches against the cold seawater (Anovitz et al., 2008). Basaltic glasses have been studied extensively and have been previously used as a paleomagnetic recorder. Pick and Tauxe (1993) first showed that Holocene basaltic glass samples were ideal in terms of magnetic domain state and experimental behavior. Selkin and Tauxe (2000) expanded on this work and concluded that that submarine basaltic glasses were well suited for future paleointensity studies. Zero-age basaltic glass from the East Pacific Rise and the Juan de Fuca Ridge accurately recover the known field intensity (Carlut and Kent, 2000; Bowles et al., 2006) or show a slight offset interpreted to arise from preexisting magnetic topography which generates local magnetic anomalies that distort the ambient field (Carlut and Kent, 2000).

Technically successful paleointensity experiments have also been carried out on much older submarine basaltic glasses (Selkin and Tauxe, 2000; Tauxe and Love, 2003; Tauxe and

Staudigel, 2004; Tauxe, 2006; Tauxe et al., 2013). These samples range from ~420 kyr to Jurassic in age. However, because we do not know what the field should be, it is hard to assess accuracy.

Paleointensity values recovered from the glass can be compared to those determined from the more slowly cooled crystalline interior. Many of these particular studies were done on pillow basalts, which have a varying glass rim based on the quenching rate. Carlut and Kent (2002) performed Thellier-Thellier experiments in zones between the glassy surface and coarser interiors and found a significant dependence between the location of the sample compared to the glassy margin. Tauxe and Love (2003) studied samples from the Hawaiian Drilling Project and found that the coarse interior materials typically overestimated the ancient geomagnetic field (Tauxe and Love, 2003) compared to the glass.

Nearly all of the submarine basaltic glass samples from these studies contain superparamagnetic to SD-sized titanomagnetite with a wide range of blocking temperatures which appear to correspond to a wide range in Ti content and/or grain size (Zhou et al., 2000; Bowles et al., 2006; 2011).

Rhyolitic glass, or obsidian, is a glass with a high silica (SiO_2) content and forms when felsic lava cools rapidly with nominal crystal growth during the cooling process (Stevenson et al., 1995). Fewer paleointensity studies have been carried out on rhyolitic glass, but magnetic remanence carriers have been shown to be predominantly low-Ti titanomagnetites in the SD to PSD size range (e.g., Leonhardt et al., 2006, Ferk et al., 2010, Ferk et al., 2011, Frahm and Feinberg, 2013). In at least one study, the NRM unblocking temperature is at around 550°C, corresponding to a Ti concentration of $x \leq 0.05$ (Leonhardt et al., 2006).

Paleointensity studies of rhyolitic glasses have shown that the effects of magnetic anisotropy and a difference in laboratory cooling rate compared to the natural cooling rate can result in biased paleointensity estimates (e.g., Elmwood et al., 1982, Leonhardt, 2006). Slight variations in the domain state of the magnetic mineral assemblage can change the TRM dependency on cooling rate (Leonhardt et al., 2006; Ferk et al., 2010). However, these effects are well understood and can be corrected for experimentally and during data analysis. An investigation of a rhyolitic obsidian flow dated to ~543 AD from Lipari, Italy revealed paleointensity values similar previous volcanic rock and archaeomagnetic studies in the same area (Leonhardt et al., 2006).

Some rhyolitic glasses have been previously analyzed and showed that devitrification processes altered rock magnetic parameters and lead to a decrease in paleointensity estimates (Ferk et al., 2011; 2012). In these cases, the devitrification was related to hydration. A common form of devitrification in glasses is "perlisation", or the process of weathering the surface of a material. Ferk et al. (2012) found that with increasing perlisation of naturally occurring obsidian, the glass transition temperature remained static and coercivity of remanence decreased with increased volatile content from perlisation. **Figure 1.6** show a decrease in coercivity of remanence, saturation magnetization, and saturation remanent magnetization as total volatile content increased.

In both basaltic and rhyolitic glass, some studies have shown or suggested glass transition temperatures lower than the highest unblocking temperatures, which leads to problems in paleointensity estimates. If a sample has unblocking below T_g, then magnetic mineralogy should not alter during laboratory reheating. However, if unblocking occurs above T_g, alteration can occur and affect the paleointensity estimate (Smirnov and Tarduno, 2003). This means that

measurements of T_g may be necessary to determine the relationship between T_g and unblocking temperatures in paleointensity studies (Leonhardt et al., 2006).

Figure 1.6: Magnetic properties of hydrated rhyolitic glass (from Ferk et al., 2012). **P**erlitised obsidian and hyaloclastite samples paleomagnetic properties compared to total volatile content of water (wt%). Ferk et al. (2012) collected samples in transects from obsidian to hyaloclastite with perlitization increasing toward hyaloclastite in Blahnukur in Iceland. Error bars are 10%. Magnetic properties shown are coercivity of remanence (B_{cr}), coercivity (B_c), saturation magnetization (M_{rs}), and remanent magnetization (M_r). Two different sites were analyzed as seen below, with similar trends being seen at both sites (Ferk et al., 2012).

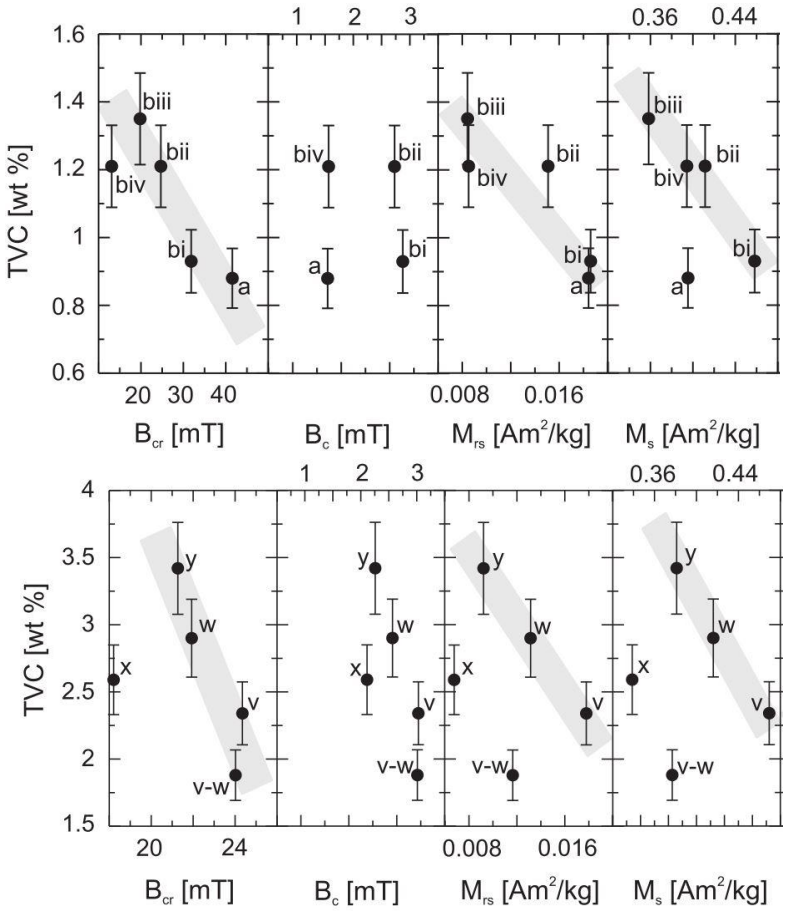

1.3 Aging of natural glasses via structural relaxation

As noted above (Sec. 1.2.2), glasses are thermodynamically unstable and the glass structure will relax over time, but this process can take millions of years. To speed up the processes, the aging experiments in this study are conducted at elevated temperatures (200-400°C). However, there is no numerical model that will accurately describe the relaxation process at these temperatures which remain far below the equilibrium T_g temperatures of ~600-750°C. The numerical models developed for relaxation typically appear in material science papers and are not geared toward geological interests (e.g., Angell et al., 2000; Jantzen et al., 2010). These models describe structural relaxation at higher temperatures close to equilibrium and fail to simulate relaxation at far lower temperatures (Moynihan et al., 1991). There is therefore no easy way to extrapolate the laboratory timescales in our study to geological timescales. Ultimately, results from this study will be linked to naturally aged samples by using T_g as a proxy for the structural "age" of the sample. That is, however, beyond the current scope of this thesis.

1.4 Hydration of Volcanic Glasses

Normally, fully-degassed, unrehydrated natural glasses have a water content << 1 wt% once surface water is removed from the sample (Newman et al., 1988). The magmatic water content of several obsidian domes in California ranges between 0.060 and 0.126 wt% (DeGroat-Nelson et al., 2001). In submarine eruptions hydrostatic pressure results in less degassing and a slight increase water content. Submarine basaltic glasses have a relatively narrow range of water contents (~0.12 – 0.49 wt%) (Danyushevsky et al., 2000; Heide et al., 2008; Kelley and Cottrell, 2009).

There are many ways that natural glasses could become hydrated, at higher temperature and lower temperature. The earliest hydration events take place at high temperature during cooling from a melt. In many cases, magmatic degassing processes deposit primary magmatic

water in unknown quantities while material is molten (Newman et al., 1988, Seligman et al., 2016). During primary hydration on the seafloor during an eruption, bubbles of steam interact chemically and physically with water (Perfit et al., 2003). In higher-temperature hydration, if the natural glass is immersed in deionized water, glass modifier cations diffuse outward as the positively charged water species diffuse inwards toward the glass (Verney-Carron et al., 2011).

Major fractures in volcanic glasses form due to cooling contraction (Denton et al., 2012). This contraction leads to fractures where water may enter and diffuse into the glass structure, leading to arcuate perlitic fractures (Ferk et al., 2012), commonly found in obsidian. The most significant perlitic fractures are believed to form right below the glass transition temperature (Ferk et al., 2012). The total volatile content increases with increasing perlitization of obsidian (Denton et al., 2012), and this increase appears to come from secondary meteoric water (Seligman et al., 2016).

At ambient surface temperatures, it is unknown how long it takes for mafic and felsic glass to become secondarily hydrated (Seligman et al., 2016). Several proposed models for rehydration include a simple linear increase (Friedman et al., 1966) to a square root of time dependence (Nolan and Bindeman, 2013), but in general, diffusion would take place on much longer timescales (Ferk et al., 2012) than at high temperatures. In both felsic and mafic volcanic glasses, a thin layer of hydrated glass, or a 'gel layer' is formed during rehydration processes (Seligman et al., 2016). This 'gel layer' is believed to protect the glassy interior due to the closure of pores (Seligman et al., 2016).

Rhyolitic glass rehydration is believed to have started in an exchange of hydrogen and deuterium ions with water soluble ions (K^+, Na^+, Ca^{2+}), and then absorption of H_2O_{mol} (Cerling et al., 1985; Valle et al., 2010). The rehydration of basaltic glass is slightly different in this case, as

it forms palagonite-rich areas (~10wt.% water) on the outer rind of the glass (Stroncik and Schmincke, 2002; Parruzot et al., 2015).

Previous studies further our understanding of alteration and rehydration of volcanic glasses on the seafloor. Kruber et al. (2008) found that incipient low-temperature alteration occurred in basaltic glasses on the seafloor. Zoned yellow-brown amorphous gel zones of palagonite were found on basaltic glass samples (Kruber et al., 2008). Microorganisms were located on some of the surficial areas and surrounded the fractures of the palagonite rims. The microbial growth of these organisms could influence the porosity and texture of the palagonite gel (Kruber et al., 2008). The changes in porosity and texture could lead to changes in the total chemical exchange of the glass and seawater. The palagonite also creates enriched areas of titanium oxide, iron (II) oxide, and water compared to the original unaltered glass. A second stage of alteration could occur in the basaltic glass and lead to slightly anisotropic, fibrous smectite (Kruber et al., 2008). Secondary hydration typically becomes a more prominent factor for older samples, this is due to the time exposed to hydration conditions.

Chapter 2: METHODOLOGY

2.1 Sample Selection

Young, unaltered volcanic glass samples representing basaltic and rhyolitic endmembers were selected for experiments. Two different types of volcanic glasses were used in this study. Rhyolitic glass (obsidian) samples were gathered in 2014 by Dr. Julie Bowles and Fatimah Abdulghafur from the base of the ~650 yr old South Deadman Creek Dome (**Figure 2.1**) in California. Submarine basaltic glass samples from the 2011 eruption on Axial Seamount (**Figure 2.2**), Juan de Fuca Ridge, were provided by Dr. Brian Dreyer (Monterey Bay Aquarium Research Institute). The Axial samples were gathered using remotely operated vehicle (ROV) *Doc Ricketts* during 2011 and 2014 expeditions on the R/V *Western Flyer*.

Figure 2.1: Rhyolitic sampling site. Rhyolitic glass samples were collected from the Deadman Creek Dome in California. Image below is from Google Earth.

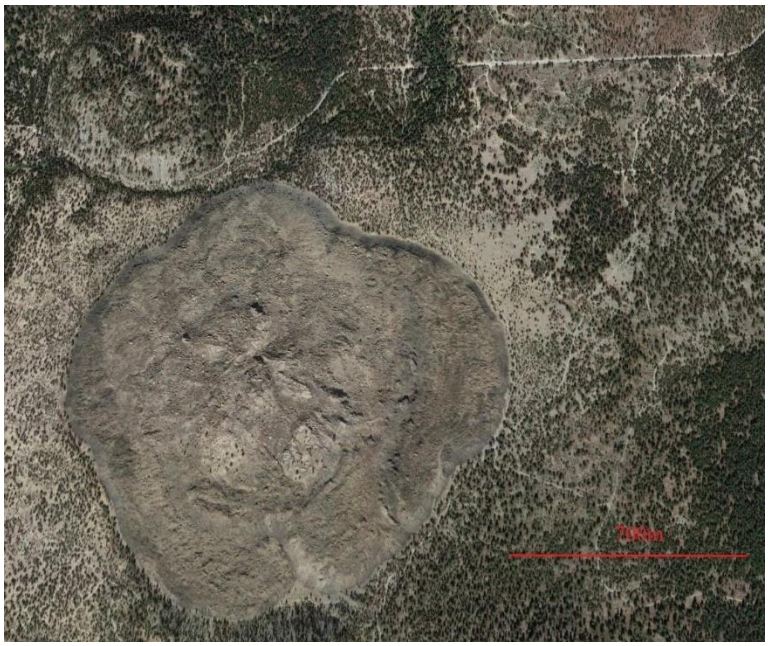

Figure 2.2: Axial Seamount bathymetry and location of 2011 eruption (from Stewart et al., 2019). Basaltic glass samples were collected by submersible from the 2011 eruption (outlined in thin black lines from Caress et al., 2012).

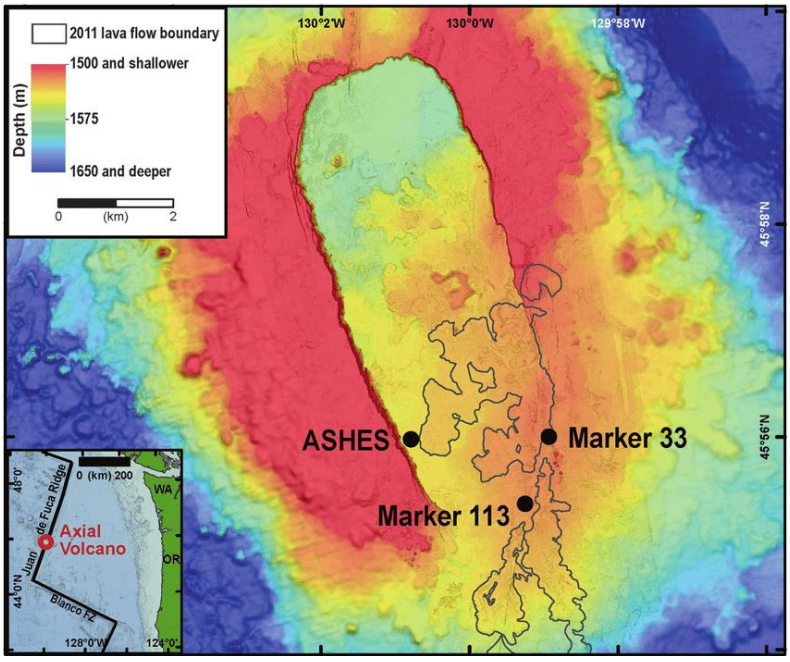

The ~650-year-old (Millar et al., 2006) rhyolitic glass used in this study is from Deadman Creek obsidian dome in California (**Figure 2.1**). The vents at this location all trend north to south, and most likely result from a magmatic dike (Miller, 1985). The three vents began with an initial phreatic explosion, caused by the heating of groundwater due to the intruding magma dike (Millar et al., 2006). The Deadman Creek Dome erupted in the topographic margins of the Long Valley Caldera and contains some residual plagioclase phenocrysts material. The sample selected for this study has an approximate water content of 0.2 wt% percent based on loss on ignition experiments (F. Abdulghafur, pers. comm.).

Homogeneity in mass normalized measurements of these samples was taken as a crude estimate of homogeneity in starting magnetic mineral assemblage. Individual specimens (sub-samples) for both artificial aging and hydration experiments were therefore selected based on the

normalized NRM data (Am^2/kg). Basaltic glass had a range of 3.85×10^{-6} Am^2/kg to 6.0×10^{-4} Am^2/kg, with a geometric mean of 4.93×10^{-5} Am^2/kg. Rhyolitic glass samples had a range of 2.08×10^{-4} Am^2/kg to 8.83×10^{-4} Am^2/kg, with a geometric mean of 2.78×10^{-4} Am^2/kg.

Specimens were named based on treatment type undergone. Specimens designated with a "B" were part of the original artificial aging experiment (e.g., B-01, B-02). Specimens with the "E" designation indicate a second, abbreviated artificial aging experiment for rhyolitic samples to address questions with repeatability in the first set of experiments. Any sample designated with a "C" underwent hydration treatment. Specimen IDs and treatment conditions are given in **Tables 2.1 and 2.2**.

2.2 Experimental Methodology

2.2.1 Artificial Aging Process

To accelerate the natural aging process, samples were "aged" in air at 200˚C, 300˚C, and 400˚C for times ranging from 15 days to 240 days. One specimen for each composition and each temperature treatment was subjected to a detailed IRM acquisition experiment before the heat treatments and then this IRM was repeated after 15, 30, 60, and 240 days of heating. This was designed to monitor changes in the coercivity spectrum over the course of the experiment. Additional specimens were selected to be removed from the experiment and set aside after set heating durations. These were reserved for later rock magnetic and glass transition temperature experiments. Specimens undergoing glass transition temperature experiments (not reported on here) were first subjected to hysteresis, FORC, and backfield IRM measurements. **Table 2.1** shows sample experiment and treatment information.

Table 2.1: Aging experiment specimen summary. Experiments conducted key: (G = Glass Transition Temperature, H = Hysteresis Experiments, P = Paleointensity, I = IRM-Repeat). (Glass transition data are not reported in this thesis.)

Specimen ID	Temperature (°C)	Composition	Treatment Time (Days)	Mass Normalized NRM (Am^2/kg)	Experiments Conducted
B-06	300	Basaltic	15	7.42×10^{-5}	G, H
B-07	300	Basaltic	60	4.11×10^{-5}	G, H
B-11	300	Basaltic	15	4.94×10^{-5}	P
B-12	200	Basaltic	240	1.47×10^{-4}	P
B-13	200	Basaltic	60	5.92×10^{-4}	P
B-14	200	Basaltic	240	3.67×10^{-4}	P
B-15	300	Basaltic	60	3.56×10^{-5}	P
B-16	300	Basaltic	60	4.56×10^{-5}	P
B-17	300	Basaltic	240	2.93×10^{-5}	P
B-18	300	Basaltic	240	2.23×10^{-5}	P
B-26	Untreated	Rhyolitic	N/A	2.41×10^{-4}	P
B-27	300	Rhyolitic	240	2.56×10^{-6}	I, H
B-28	400	Rhyolitic	240	2.39×10^{-4}	I, H
B-29	200	Rhyolitic	240	2.81×10^{-4}	I, H
B-30	300	Rhyolitic	15	2.43×10^{-4}	G, H
B-31	300	Rhyolitic	60	2.58×10^{-4}	G, H
B-32	300	Rhyolitic	240	2.43×10^{-4}	G, H
B-33	300	Rhyolitic	15	2.26×10^{-4}	P
B-34	Untreated	Rhyolitic	N/A	2.86×10^{-4}	P
B-35	300	Rhyolitic	15	2.30×10^{-4}	P
B-36	Untreated	Rhyolitic	N/A	2.17×10^{-4}	P
B-37	300	Rhyolitic	60	2.28×10^{-4}	P
B-38	300	Rhyolitic	60	2.80×10^{-4}	P
B-39	300	Rhyolitic	240	2.42×10^{-4}	P
B-40	400	Basaltic	15	2.59×10^{-4}	G, H
B-41	300	Basaltic	240	2.78×10^{-4}	I, H
B-42	400	Basaltic	240	1.01×10^{-5}	I, H
B-44	200	Basaltic	240	5.93×10^{-5}	I, H
B-45	Untreated	Basaltic	N/A	1.09×10^{-3}	P
B-46	400	Basaltic	60	1.60×10^{-4}	G, H
B-48	400	Basaltic	240	3.23×10^{-4}	G, H
B-49	400	Basaltic	15	8.41×10^{-5}	P
B-50	400	Basaltic	15	9.70×10^{-6}	P
B-53	400	Basaltic	60	2.09×10^{-5}	P
B-56	400	Basaltic	60	1.47×10^{-5}	P
B-57	400	Basaltic	240	6.95×10^{-6}	P
B-58	400	Basaltic	240	4.51×10^{-5}	P
B-60	200	Basaltic	15	5.63×10^{-5}	P

B-64	200	Basaltic	15	2.38×10^{-5}	G, H
B-65	200	Basaltic	60	2.52×10^{-5}	G, H
B-66	200	Basaltic	240	3.85×10^{-6}	G, H
B-68	200	Basaltic	15	5.33×10^{-6}	P
B-70	300	Rhyolitic	240	2.51×10^{-4}	P
B-73	400	Rhyolitic	15	2.31×10^{-4}	G, H
B-74	400	Rhyolitic	60	2.50×10^{-4}	G, H
B-75	400	Rhyolitic	240	2.39×10^{-4}	G, H
B-76	400	Rhyolitic	15	2.28×10^{-4}	P
B-77	400	Rhyolitic	15	2.46×10^{-4}	P
B-78	400	Rhyolitic	60	2.08×10^{-4}	P
B-79	400	Rhyolitic	60	2.51×10^{-4}	P
B-80	400	Rhyolitic	240	2.31×10^{-4}	P
B-81	400	Rhyolitic	240	2.55×10^{-4}	P
B-85	200	Rhyolitic	15	2.56×10^{-4}	G, H
B-87	200	Rhyolitic	60	2.18×10^{-4}	G, H
B-88	Untreated	Basaltic	N/A	3.05×10^{-4}	P
B-89	200	Rhyolitic	240	2.40×10^{-4}	G, H
B-90	Untreated	Basaltic	N/A	2.46×10^{-4}	P
B-91	200	Rhyolitic	15	2.61×10^{-4}	P
B-92	200	Rhyolitic	15	2.41×10^{-4}	P
B-93	200	Rhyolitic	60	2.40×10^{-4}	P
B-94	200	Rhyolitic	60	2.49×10^{-4}	P
B-95	200	Rhyolitic	240	2.50×10^{-4}	P
B-96	200	Rhyolitic	240	2.56×10^{-4}	P
E-39	400	Rhyolitic	30	8.29×10^{-4}	I
E-42	300	Rhyolitic	30	8.82×10^{-4}	I
E-43	200	Rhyolitic	30	8.42×10^{-4}	I

2.2.2 Hydration Experimental Process

The artificial hydration treatment was used to replicate the effects of hydration on both the rhyolitic and basaltic glass. The experimental protocol was modeled after Lofgren (1971). For each intended treatment temperature and duration, four small (21 mg – 128 mg) chips were sealed in silver capsules with 10 wt% water. They were then pressurized to 200 MPa and heated to either 300˚C or 450˚C for 1 day to 15 days (**Table 2.2**). Before and after hydration, one chip from each experiment underwent detailed IRM acquisition to assess changes in the coercivity

spectrum. Following hydration, hysteresis and FORC measurements were also conducted. **Table 2.2** shows the sample hydration treatment conditions and experiments.

Table 2.2: Hydrated samples summary. Experiments conducted key: (G = Glass Transition Temperature, H = Hysteresis Experiments, F = Fourier Transform Infrared Spectroscopy, I = IRM-Repeat). Untreated samples used in FTIR experiments are included in this list and have different naming conventions than hydrated samples.

Specimen ID	Temperature (°C)	Composition	Treatment Time (Days)	Experiments Conducted
C-02	300	Rhyolitic	1.0	I, H, F
C-06	300	Rhyolitic	2.5	I, H, F
C-11	300	Rhyolitic	6.3	I, H, F
C-15	300	Rhyolitic	15	I, H, F
C-19	450	Rhyolitic	0.3	I, H, F
C-25	450	Rhyolitic	1.0	I, H, F
C-29	450	Rhyolitic	3.2	I, H, F
C-33	450	Rhyolitic	10	I, H
C-50	300	Basaltic	1.0	I, H, F
C-53	300	Basaltic	2.5	I, H, F
C-57	300	Basaltic	6.3	I, H, F
C-65	300	Basaltic	15	I, H
C-69	450	Basaltic	0.3	I, H, F
C-71	450	Basaltic	1.0	I, H
C-75	450	Basaltic	3.2	I, H, F
C-79	450	Basaltic	10	I, H
E-07	N/A	Rhyolitic	N/A	F
E-21	N/A	Rhyolitic	N/A	F
E-26	N/A	Rhyolitic	N/A	F
E-27	N/A	Rhyolitic	N/A	F
E-29	N/A	Rhyolitic	N/A	F
D270-R2	N/A	Basaltic	N/A	F
D270-R8	N/A	Basaltic	N/A	F
D270-R11	N/A	Basaltic	N/A	F

2.2.3 Hydration Analysis

Sections of hydrated specimens were polished, examined under the microscope, and analyzed with the aid of image processing software. Specimens were prepared as for Fourier transform infrared analysis (FTIR), which remains for future work. Vacuum grease was added to one side of a glass side, and the smoothest side of the glass fragment was placed face-down on the slide. Next, samples were coated with orthodontic powder. A resin liquid was added to the powder. The samples were typically left overnight to solidify. After the resin solidified, a razorblade or scalpel was used to remove the resin coated glass fragment from the slide. The fragment was polished using aluminum oxide polishing sheets with grit sizes of 60µm, 40µm, 30µm, 12µm, 9µm, 5µm, 1µm, and 0.1µm. Samples were polished approximately sixteen times in a circular pattern and then rotated 45° to ensure a flat surface on one face.

After polishing one side to mirror finish, specimens were mounted on a glass slide using Crystalbond™ heated by a low temperature setting on a hot plate. The glass fragment was pressed down on the glass slide to ensure all parts of the crystal bond were attached to the glass slide. Once the crystal bond solidified, the second side of the sample was polished. A micrometer was used to keep track of the thickness at the 60µm polish, as the sample lost most of its mass during this polish. Once the sample had an approximate thickness of 400µm, the next aluminum oxide paper grade was used to polish the sample. This process continued until a mirror finish was present on both sides of the sample and the estimated thickness of the sample was <250µm. The sample was detached from the glass slide, by reheating the slide and melting the Crystalbond™. A scalpel was used to separate the sample from the glass slide.

Figure 2.3: Polished sample. A wafer-thin basaltic glass sample within the resin after a double polish. The scale is included.

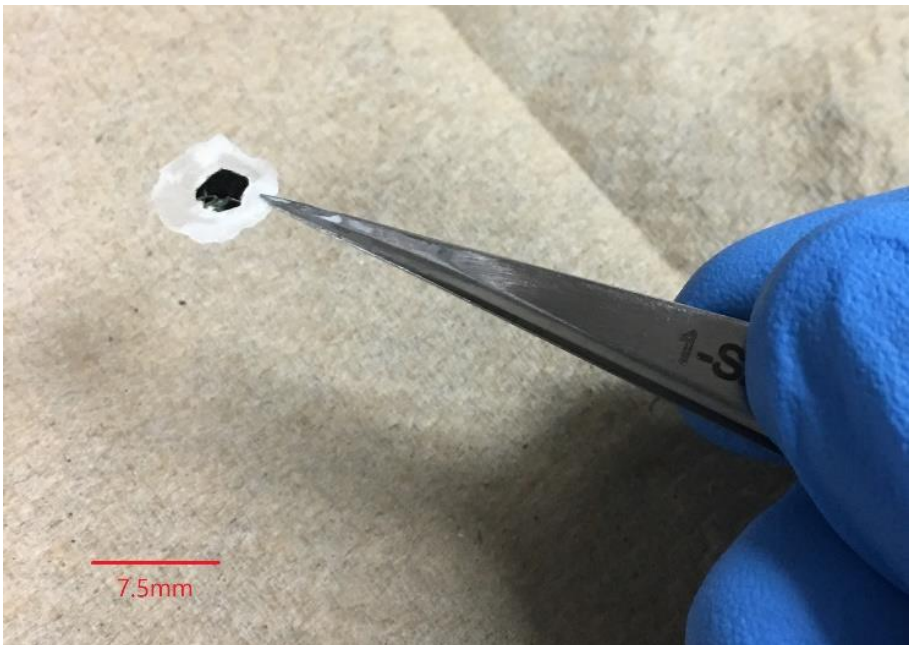

ImageJ image analysis software was used to determine the percentage of possible hydrated areas in place of FTIR experiments to study water content. Samples were converted from a “jpeg” image to a 32-bit stack, and then a color threshold was applied to approximately identify areas of hydration interiors or rims. Final area calculations were made after manually adjusting these areas where the thresholding had misidentified crystals (for example) as hydration rims.

Basaltic glass on balance showed surface hydration rims and were also more opaque which make the color threshold analysis more difficult. The image analysis was therefore only used on images of intact rhyolitic samples prepared for FTIR experimentation.

2.2.4 Isothermal Remanent Magnetization Acquisition and Unmixing

IRM acquisition and unmixing was undertaken to assess variations or changes in the coercivity distributions which may be linked to variations or changes in the magnetic mineral assemblage. First, a 1000 mT IRM is applied in one direction, saturating the magnetization.

Next, increasingly large fields are applied in the reverse direction. For the untreated and 15-day artificial aging treatment, 15 incremental steps were applied ranging from 10 mT to 1000 mT (IRM steps were 10, 15, 20, 25, 30, 40, 50, 80, 100, 150, 200, 400, 600, 800, 1000 mT). For the 30-day treatment onward, IRM was measured in 28 incremental steps ranging from 3 mT to 1000 mT (IRM steps were 3, 5, 7.5, 10, 12.5, 15, 20, 25, 30, 35, 40, 50, 60, 70, 80, 90, 100, 125, 150, 175, 200, 250, 300, 350, 400, 600, 800, 1000 mT).

The data are then analyzed using a program called MaxUnmix (Maxbauer et al., 2016). The first derivative of the IRM acquisition provides the coercivity distribution, and it can be mathematically "unmixed" to estimate different magnetic mineral populations (e.g., Robertson and France, 1994). This methodology assumes that any single mineral population has a log-normal distribution of grain size and therefore coercivity. Egli (2003) updated the fitting procedure to allow for deviations from non-normality often observed in natural samples by using a skew generalized Gaussian function. MaxUnix instead fits the IRM acquisition data with a set of skew-normal functions to represent different mineral populations. Skewness can show certain grain behaviors within samples but will be discussed in Ch. 4. The fits are first made by the user, and the program then optimizes the fits. Statistical F-tests were used to help determine the minimum number of required components. If $F > 1$ and $p < 0.05$, you can reject the null hypothesis that a less complicated (fewer-component) model is required and support a more complicated model (Maxbauer et al., 2016). It was found that all the MaxUnmix curves in this thesis supported a less complicated model than user fitted components. Both basaltic and rhyolitic glass only contained a maximum of two different coercivity components. Prior to fitting, a smoothing spine was applied with values ranging from 0.4 to 0.5. Uncertainty estimates were generated via a bootstrap resampling process with n=600.

2.2.5 Thermal Demagnetization of Three-Component IRM

To aid in magnetic mineral identification, thermal demagnetization of a multi-component IRM was carried out to assess joint variations in coercivity and blocking temperature (Lowrie, 1990). A 1 T IRM is first applied along the sample z-axis, followed by 0.3 T along the y-axis and 0.1 T along the x-axis. This IRM is then thermally demagnetized in steps of 50℃ between 100℃ and 200℃, and then in 25℃ steps until 575℃, where a majority of the IRM disappeared. The "soft" (0.1 T), "medium" (0.3 T), and "hard" (1 T) coercivity components can then be mathematically decomposed from the magnetization vector and plotted as a function of temperature to aid in determining ferromagnetic mineralogy (Lowrie, 1990).

2.2.6 Paleointensity

Modified Thellier-type paleointensity experiments (Thellier and Thellier, 1959) were carried out on forty-four artificially aged specimens and six untreated specimens (**Table 3.1**). This method works best when repeating steps at lower temperatures to show that the capacity of the sample to acquire a thermal remanence has not changed (Tauxe et al., 2018). These repeat steps are also called partial TRM (pTRM) checks (Coe, 1967) because they assess changes in pTRM acquired in discrete temperature intervals. Changes in pTRM indicate possible alteration of the magnetic mineral assemblage during the experiments. In addition to pTRM checks, the order of the in-field and zero-field steps was reversed at each temperature step according to the IZZI protocol (Tauxe and Staudigel, 2004) to assess non-ideal behavior arising from non-SD grain sizes. Specimens were prepared by immobilizing in glass tubes using potassium silicate and silicon glass pads. During the in-field steps, a 40 μT field was applied along the z-axis of the samples. The software package Pmagpy (Tauxe et al., 2016) was used to process the data.

While not known at the time, it was later determined that prior to aging, samples had been AF demagnetized and were given an anhysteretic remanent magnetization which was also AF demagnetized. The data therefore cannot be straightforwardly interpreted in terms of paleointensity, as the samples had little-to-no pre-existing remanence.

2.2.7 Hysteresis Experiments

Hysteresis (magnetization vs applied field) and first order reversal curve (FORC; see Sec. 2.2.8) experiments were carried out on a vibrating sample magnetometer (VSM) on a specimen from every hydrated experiment and artificial aging experiment. Specimens of >0.05g were placed in a cubic, plastic sample holder to hold in place during VSM experiments. Specimens of <0.05 g were put into gel caps and immobilized with crystal fiber. Vibration parameters were on the maximum setting to increase instrument sensitivity. Measurement averaging times for hysteresis loops ranged from 100 ms to 400 ms, with longer times used for more weakly-magnetic samples. Loops were measured in fields up to +/- 1000 mT. Backfield remanence curves were also measured to find the coercivity of remanence.

2.2.8 First Order Reversal Curve Experiments

First Order Reversal Curve (FORC) experiments are advanced hysteresis tools based on data points collected within the entire area of an enclosed hysteresis loop (Harrison and Feinberg, 2008). While simple hysteresis loops allow determination of a rough average domain state, FORCs allow the user to better identify a range of magnetic domain states and to "unmix" individual magnetic components (Harrison and Feinberg, 2008). FORCs begin by saturating a sample in the positive field, and then the external field is decreased to some value, B_a, or the reversal field (Harrison and Feinberg, 2008). The magnetization of the sample is measured as a

function of B_b, or increasing field, until saturation is achieved again (Harrison and Feinberg, 2008). This process is repeated to sample the entire area enclosed by a hysteresis loop (Harrison and Feinberg, 2008). The FORC distribution is defined as the mixed second derivative of M (B_a, B_b) with respect to B_a and B_b (Harrison and Feinberg, 2008):

$$\rho(B_a, B_b) = \frac{\partial^2 M(B_a, B_b)}{\partial B_a \, \partial B_b}$$

The data are plotted on a set of coordinates (B_u and B_c) which represent a 45° counterclockwise rotation of the FORC distribution: $B_c = (B_a - B_b)/2$ and $B_u = (B_a + B_b)/2$. The horizontal axis (B_c) represents coercivity, and the vertical axis (B_u) is a measure of magnetic interaction fields. An assemblage of SD grains is characterized by high coercivities, and the FORC distribution typically appears as a ridge along the $B_u = 0$ axis. An assemblage of MD grains, by contrast, typically shows significant vertical spread in the $+B_u$ direction near B_c=0. Measurement averaging time was between 200 ms to 300 ms. FORCs were processed using FORCinel (Harrison et al., 2008). Smoothing factors ranged from 5 to 7.

2.3 Laboratory Instrumentation

At UWM, paleointensity experiments and thermal demagnetizations were conducting using an ASC Thermal Demagnetizer equipped with a DC field coil, and IRM acquisition steps were carried out on an ASC Impulse Magnetizer. All remanence measurements were made on a 2G Enterprises 755 SRMS Superconducting Rock Magnetometer housed in a magnetically shielded room in the UWM Paleomagnetic Laboratory. All hysteresis and FORC experiments were conducted at the Institute for Rock Magnetism, University of Minnesota, on two Princeton Measurements micro-VSMs. Artificially aged samples were heated in two Thermo Scientific™

Lindberg/Blue M™ Moldatherm™ Box Furnaces. Hydration experiments were carried out by Dr. Julia Hammer at the University of Hawaii – Manoa Experimental Petrology Lab using several water-medium cold-seal pressure vessels made from waspaloy. A conventional quench and a computer-controlled pressure variator were used (Hammer, pers. comm.).

Chapter 3: RESULTS

3.1 Artificial Aging Results

3.1.1 Isothermal Remanent Magnetization Experiments

IRM acquisition experiments show how the remanent magnetization of an assemblage of magnetic particles changes with an applied field. Magnetic particles whose coercivity is below the applied magnetic field will typically flip their magnetization toward the direction of the applied field and obtain a magnetic remanence in that direction (Tauxe et al., 2018). IRM acquisition experiments therefore allow us to assess the coercivity distribution, as well as the saturation isothermal remanent magnetization (sIRM). Different magnetic mineral assemblages have different coercivity distributions and behaviors, based on their composition and grain-size distribution. If the natural glass magnetic mineral assemblage physically changes during aging treatments by nucleation of new minerals or by growth or destruction of existing magnetic grains, we would expect the coercivity distribution and/or sIRM to change.

Figure 3.1 shows example raw IRM acquisition data. Because the IRM was applied along the sample z-axis, the z-component of the magnetization is shown. From these data, sIRM and coercivity of remanence (B_{cr}) are calculated, and the data serve as the for MaxUnmix curves (Maxbauer et al., 2016). sIRM is approximated as the magnetization at 1T, and this reflects the volume abundance of magnetic material, but is also influenced by mineral composition and domain state. The B_{cr} is found where the magnetization direction changes from positive to negative (when M = 0).

Figure 3.1: Example raw z-component IRM acquisition data. These were included to show prominent changes in sIRM (rhyolite 400°C) and B_{CR} (basalt 300°C). Treatment time in days is given in legend.

Rhyolite 400°C

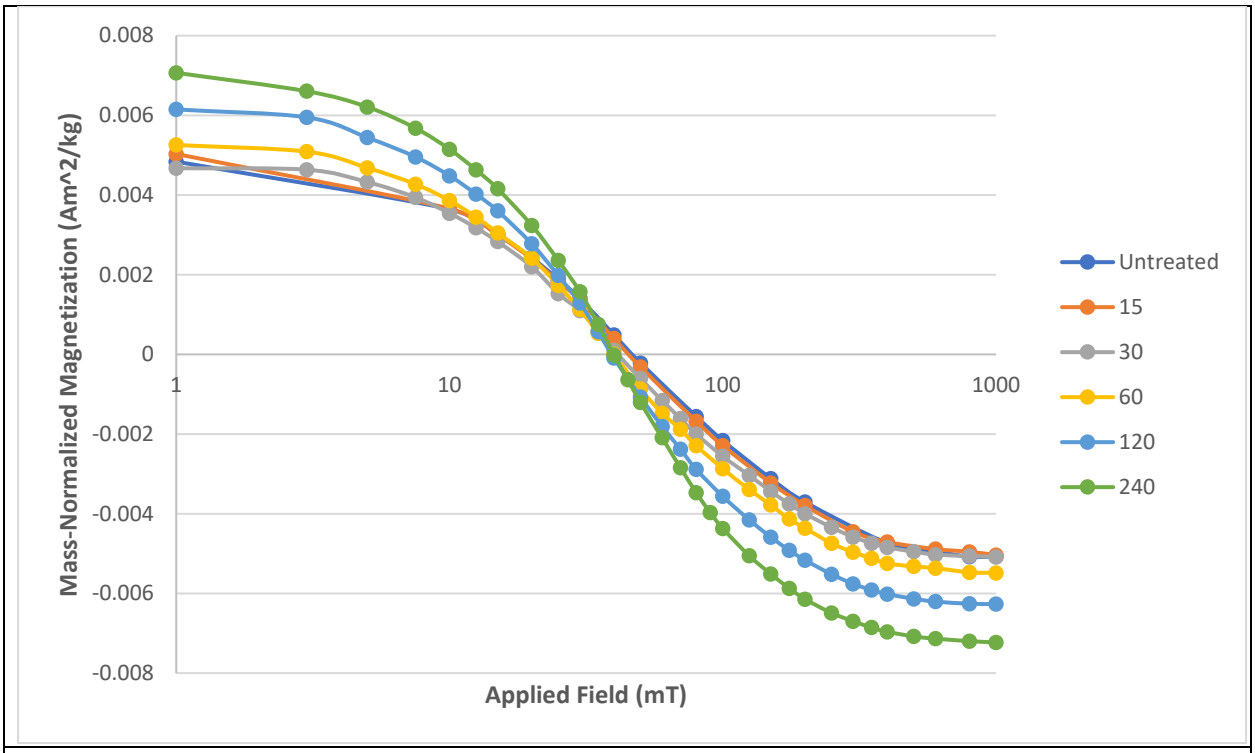

Basalt – 300°C

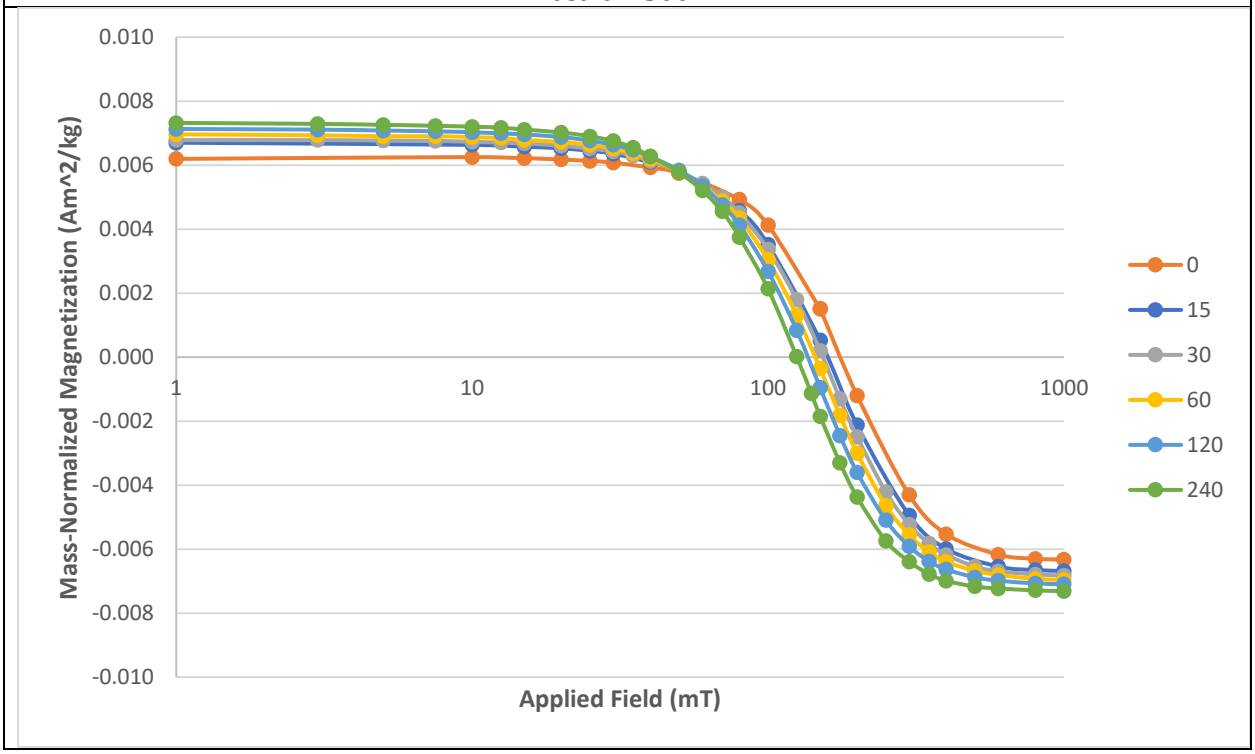

Figure 3.2 shows the sIRM (e.g., 1T IRM) normalized to the starting value at time = 0.

All the original rhyolitic specimens showed an increase, decrease, and then increase in sIRM

over the first 60 days. To determine whether these unusual and unexpected results were reproducible, the aging experiment was repeated on fresh specimens. The second rhyolitic IRM experiment showed a steady decrease for 200°C and 300°C over the same course of time, while the samples treated at 400°C showed a slight increase (**Figure 3.2**). The other rhyolitic samples in the first experiment had a slight increased magnetization over the course of the 240-day treatment. The basaltic samples all showed an increase in sIRM over treatment time, with greater increases at higher treatment temperatures. The 400°C basaltic glass sample had an approximate 40% increase in magnetization after 240 days.

Figure 3.2: Rhyolitic and basaltic glass IRM_{1T} over the course of 240 days. Data normalized to 0-day results.

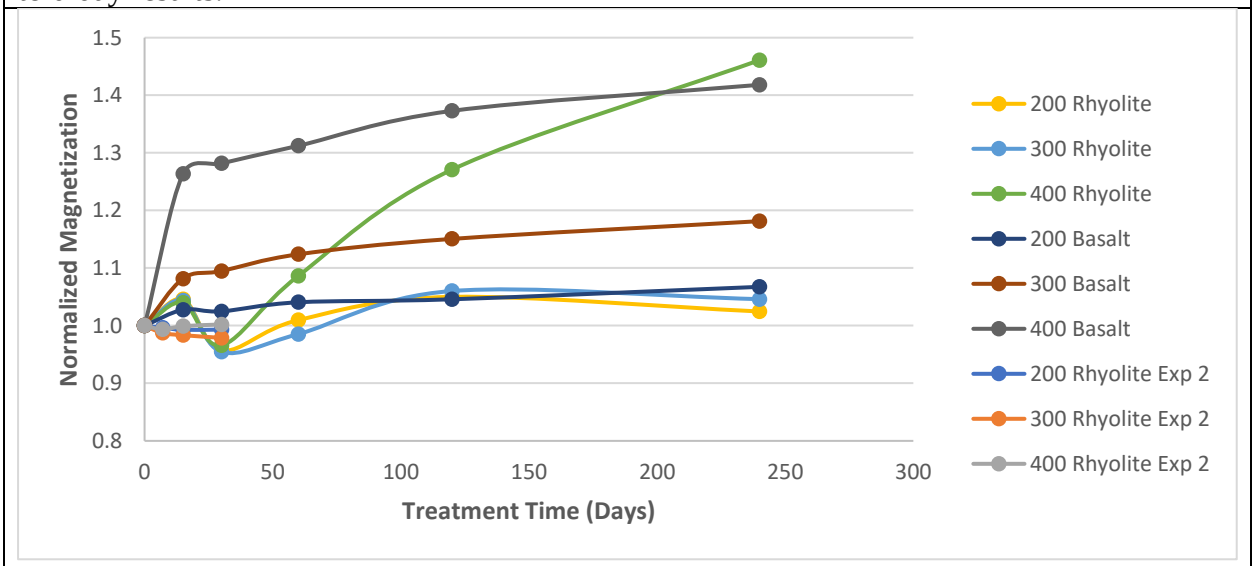

Figure 3.3 shows B_{cr} changes as a function of treatment time. B_{cr} of rhyolitic glass treated at 400°C decreased over treatment time, while the 200°C and 300°C samples fluctuated in the first aging experiment. The second rhyolitic artificial aging experiment showed a regular decrease in B_{CR} over the thirty-day treatment. Rhyolitic glasses had a B_{cr} ranging from approximately 39 mT to ~52 mT during their entire treatment. Basaltic glass had a much higher range of measured B_{cr} (Figure 3.3B). Basaltic glass B_{cr} ranged from ~96 mT to ~180 mT over the

course of treatment. The basaltic glass also showed a decrease in B_{CR} throughout the entire experiment apart from the 200°C sample between 30 and 60 days.

Figure 3.3A: Rhyolitic glass B_{cr} change over artificial aging treatment.

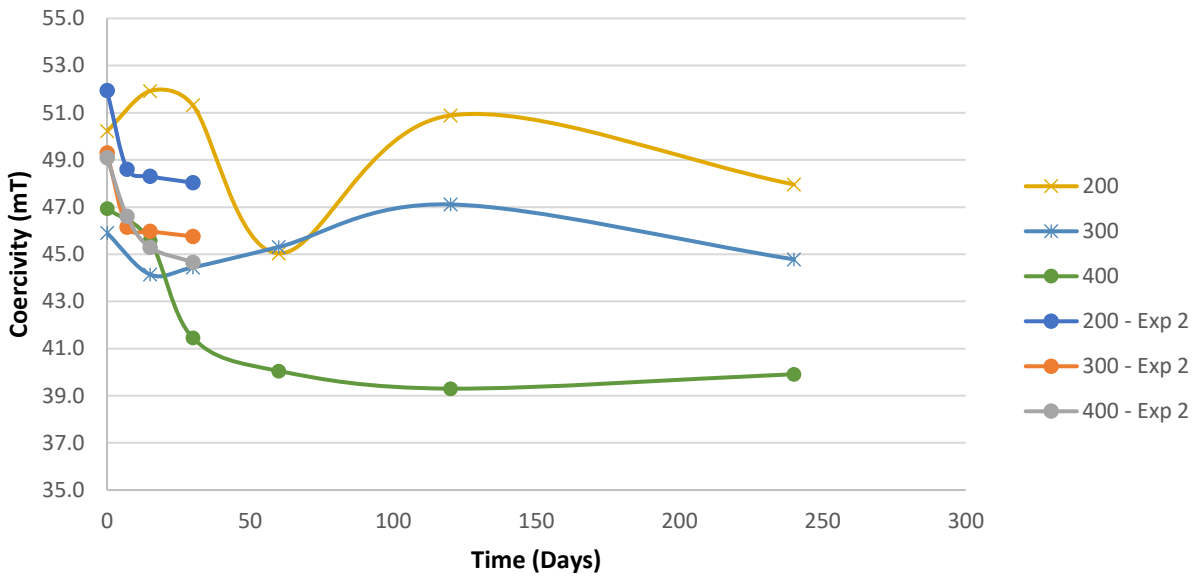

Figure 3.3B: Basaltic glass B_{cr} change over artificial aging treatment.

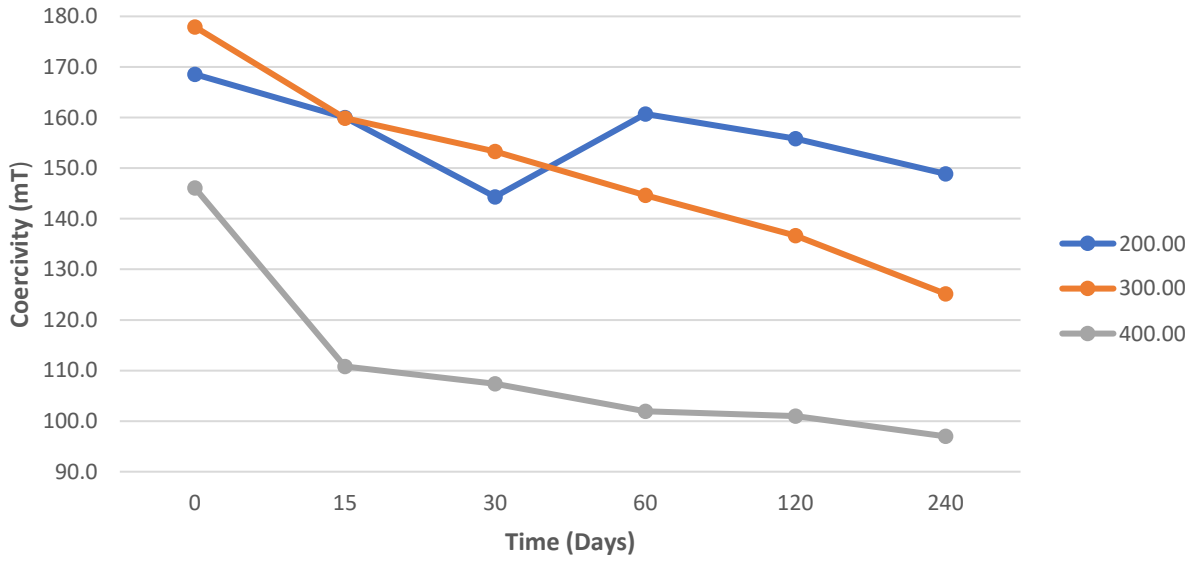

3.1.2 IRM Unmixing

The first derivative of the IRM acquisition data gives the coercivity distribution of the sample, and this distribution can be modeled as a mixture of different magnetic mineral populations whose individual coercivity distributions follow a skew-normal distribution (see Methods). By mathematically unmixing the IRM data, we can place constraints on the magnetic mineral population, chemical composition, and grain sizes within a sample (Maxbauer et al., 2016).

Figure 3.4 shows the coercivity distributions for rhyolitic glass over the artificial aging treatment. Appendix A lists all the specific calculated variables of MaxUnmix curves, which will be discussed here in terms of common trends. Most data sets were best fit by a single coercivity distribution with a mean coercivity (B_h) of about 23 to 52 mT. Some data sets additionally had a higher coercivity component with a B_h of about 172 to 281 mT. The lower coercivity component was the dominant, or primary, component in all cases. The primary coercivity component had a consistent shift to lower coercivity over the course of the 200°C experiments over 240 days. The 300°C and 400°C coercivity distributions fluctuated but had a decreased overall coercivity in both components over aging treatments. All primary components of coercivity in MaxUnmix curves skewed to the left ($S < 1$), while all secondary (purple) components skewed to the right ($S > 1$). Primary components of 200°C, 300°C, and 400°C typically skewed more to the left over 240 days with slight increased left-skewness at different times during treatment.

The relative contribution of each component to the overall coercivity distribution is estimated by extrapolating unsaturated higher-coercivity components to saturation. Based on this extrapolated contribution, the primary component of all samples in the first experiment made up

more than 85% of the entire coercivity distribution with the exception of the 400°C sample at 60 days, which made up only ~71% of the entire curve.

Figure 3.4: IRM Unmixing results for the artificially-aged rhyolitic glass. Purple and blue lines represent different skew-normal coercivity distributions, where blue is typically the dominant component. The yellow line is the sum of the individual components. Some samples only had one component to the coercivity distribution, which is then shown in yellow. The shaded areas surrounding the lines are the 95% uncertainty intervals calculated using a bootstrap resampling algorithm. Light gray dots are the raw data, and the gray line is a smoothing spline fit to these data and is obscured in most plots by the yellow fit curve.

Rhyolite 200°C		
Day 0	**Day 15**	**Day 30**
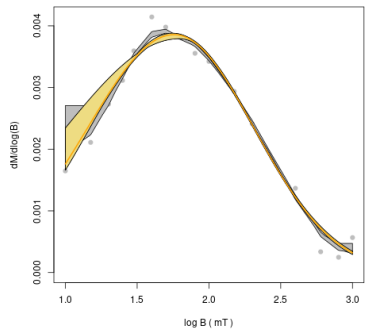	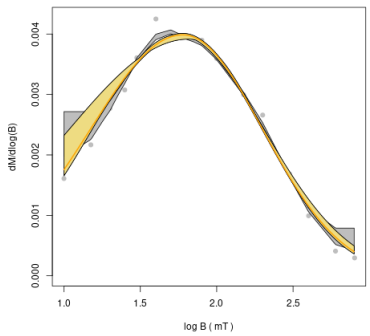	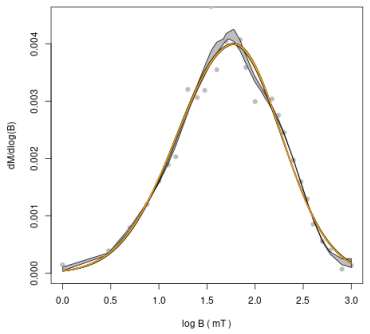
Day 60	**Day 120**	**Day 240**
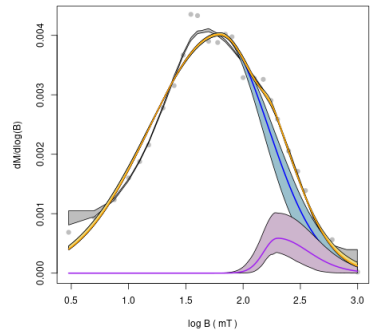	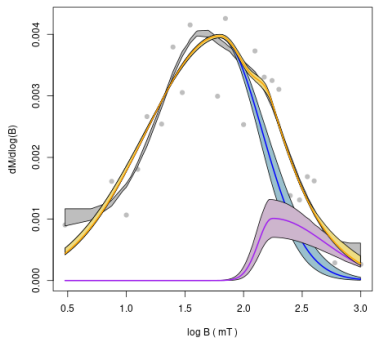	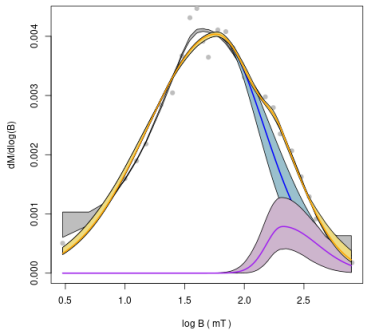
Rhyolite 300°C		
Day 0	**Day 15**	**Day 30**

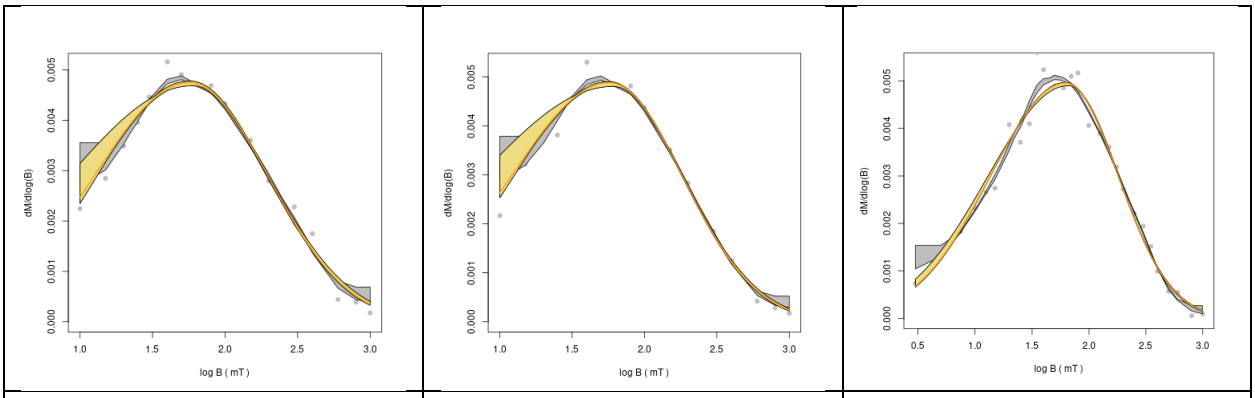

Day 60	Day 120	Day 240

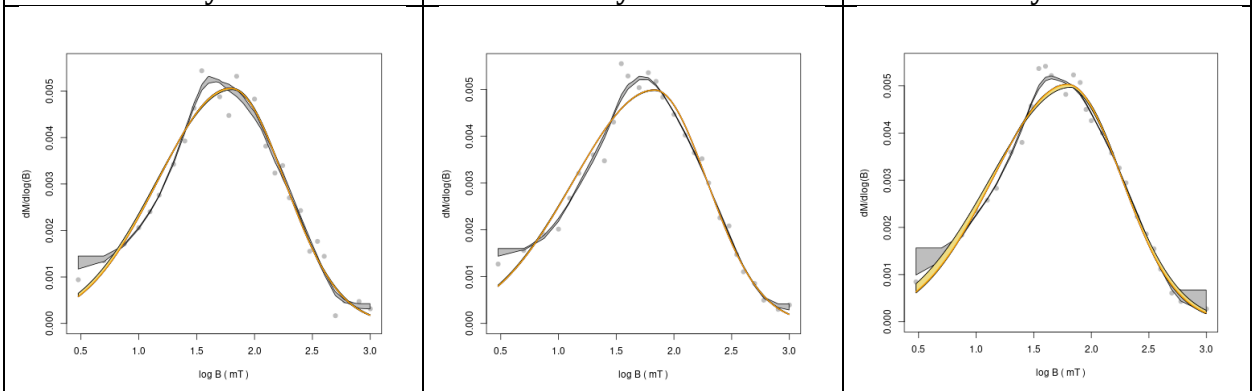

Rhyolite 400°C

Day 0	Day 15	Day 30

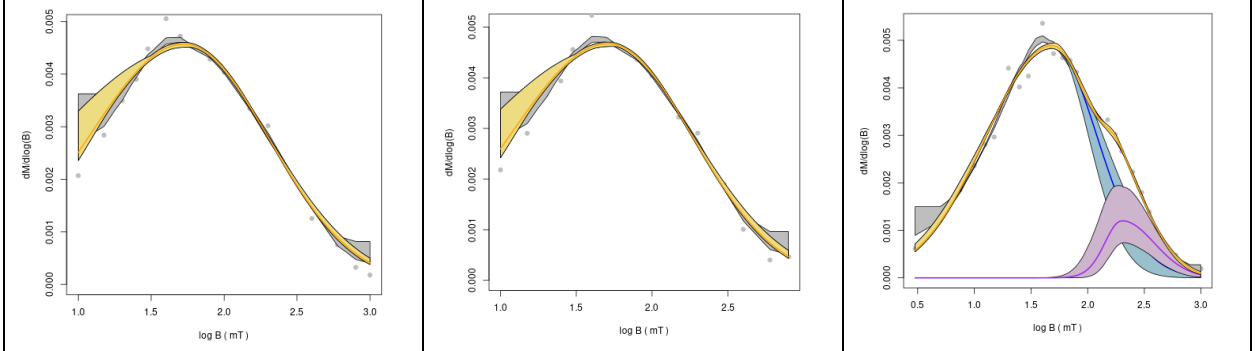

Day 60	Day 120	Day 240

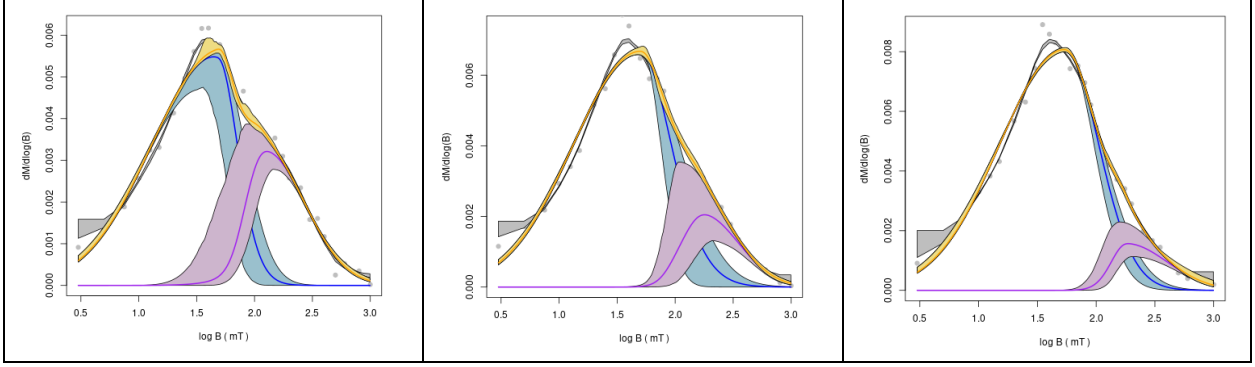

The second experiment involving rhyolitic glasses (**Figure 3.5**) used a higher density of field steps at all treatment times (see Methods) in hopes of better constraining the coercivity distribution, especially at lower coercivities. Shifts in coercivity components over treatment time can be seen in these samples over the course of the experiment. All the rhyolitic samples in the second experiment had an increase in the mean (B_h) of the primary component throughout aging treatment at all temperatures. Peaks only increased by approximately 3 mT to 6mT for 200℃ and 400℃ samples. The 300℃ samples experienced a larger peak shift of ~22 mT throughout treatment. All the rhyolitic samples primary component skewed to the right (S > 1), while the secondary components skewed to the left (S < 1) apart from untreated rhyolitic glass before the 300℃ treatment. The 200℃ samples' primary component typically skewed more to the right over treatment time. While the 200℃ and 400℃ samples had overall increased right-skewness, the skewness fluctuated over treatment time.

The primary component typically contributes >80% of the total coercivity distribution (yellow curve) (**Figure 3.5)**, apart from 300℃ at 30 days showing ~68% of the total curve. Secondary components typically made up 5% to 20% of the total curve in the second experiment, except for 300℃ at 30 days displaying ~32% of the total curve. The 200℃ and 300℃ had a decreased primary component over treatment with the contribution of the secondary component increasing over treatment time. Primary components of all temperature treatments were all > 88% the height of the total curve. One exception was the 300℃ at 30 days, which had a primary component of only ~82% of the total curve. There were no trends with the primary component height over treatment time. Secondary components proportionally had a height of 8% to 20% of the total curve, with the outlier being 300℃ at 30 days, having a ~40% height of the total curve.

The more frequent identification of two components in this second set of experiments may partially be related to the higher density of measurement steps, which were also used in the first set of experiments from 30 days onward (**Figure 3.4**).

Figure 3.5: IRM Unmixing results for the second experiment of artificially-aged rhyolitic glass. Colors and symbols as in **Fig. 3.4**. The primary component (blue) remains similar throughout each sample, with most changes in dispersion, saturation magnetic remanence, and mean coercivity of grain population taking place in the secondary component (purple).

Rhyolite 200°C	
Day 0	**Day 7**
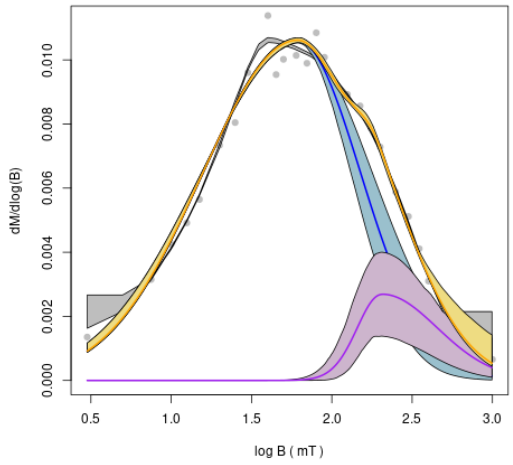	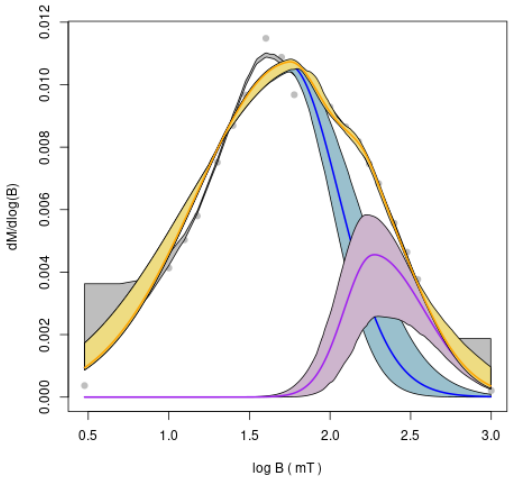
Day 15	**Day 30**
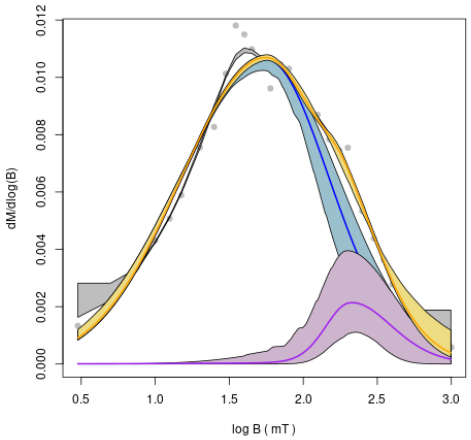	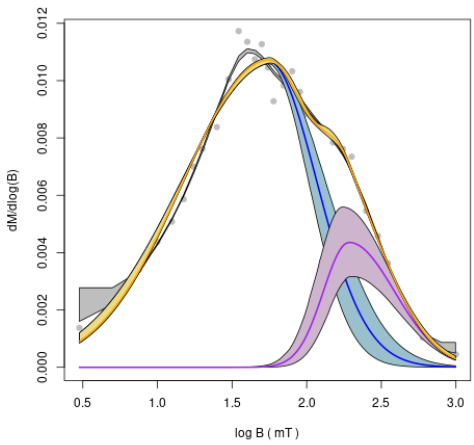
Rhyolite 300°C	
Day 0	**Day 7**

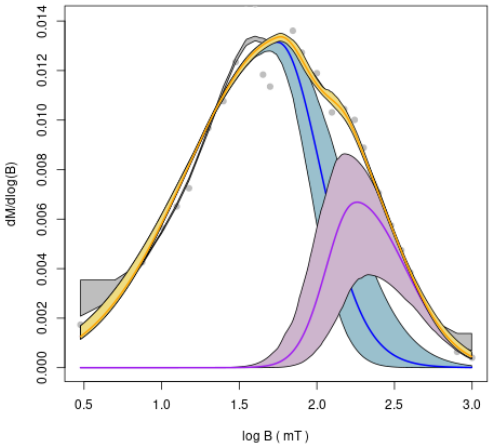

Day 15

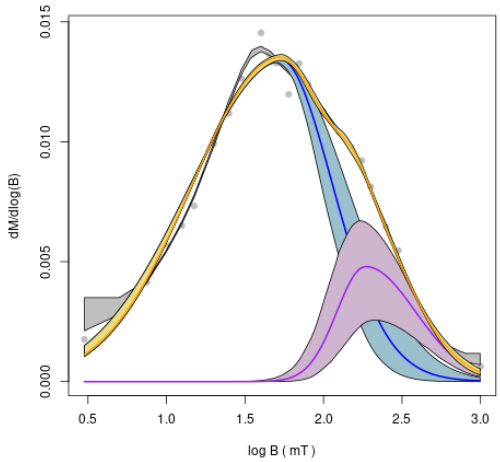

Day 30

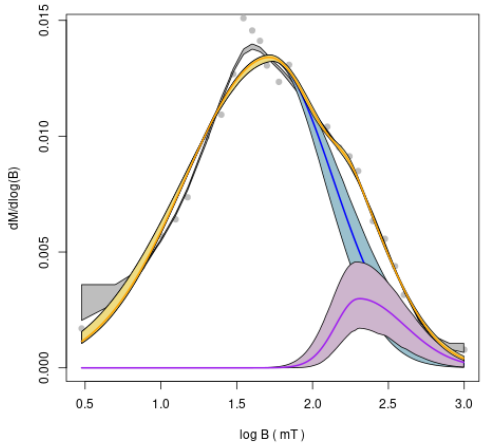

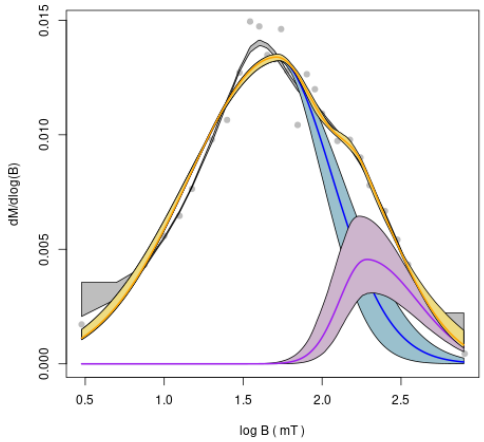

Rhyolite 400°C

Day 0

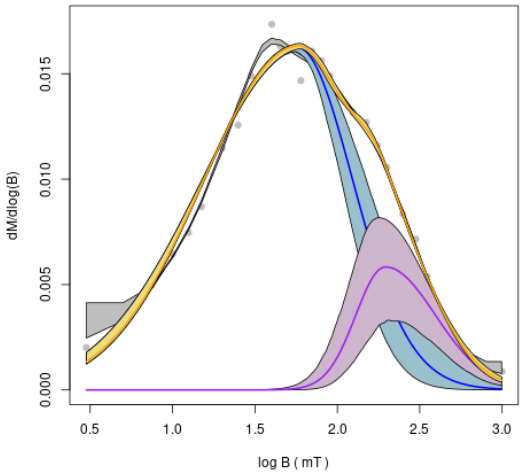

Day 7

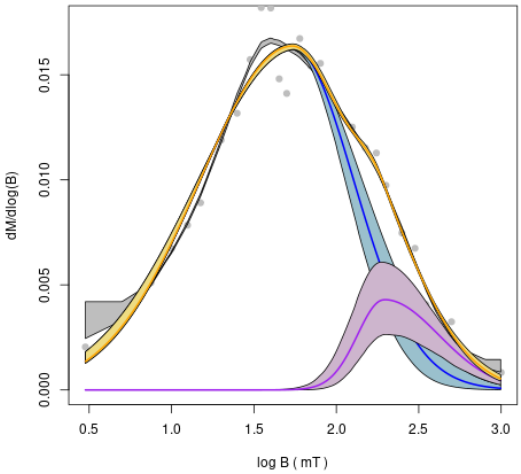

Day 15	Day 30
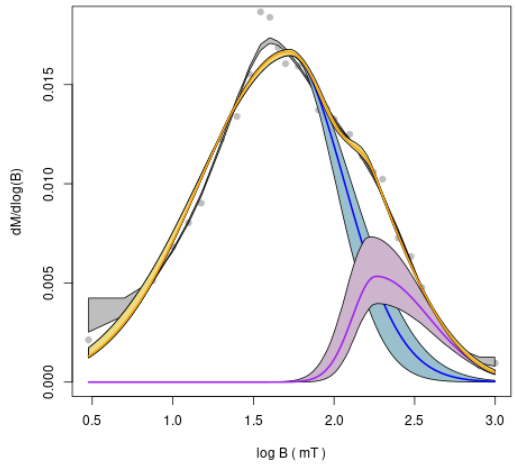	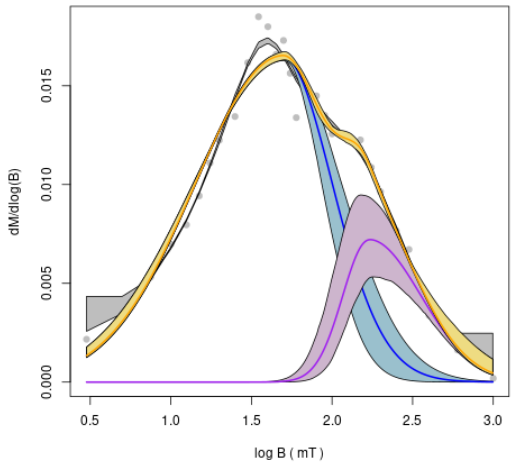

There were some changes between the first and second experiments of rhyolitic glass MaxUnmix curves. In the second suite of artificial aging treatments in the rhyolitic glass, the coercivity peak (B_h) was larger than in the first experiment in the primary component of the coercivity distribution. The first suite of experiments showed consistency of proportional height of the total curve, more than the second suite of experiments. All primary components of the first experiment skewed to the left, while all primary components in the rhyolitic samples of the second experiment skewed to the right. The proportional contribution of the secondary component was greater in the second set of experiments.

Figure 3.6 shows the data from the basaltic glass artificial aging experiment. The basaltic samples were best fit with one or two coercivity components. The dominant, or primary, component was of higher coercivity with a peak at about 165 mT, while the secondary component – when present – was of lower coercivity (~45 to 114 mT) and higher dispersion. For the samples aged at 300°C and 400°C, the peak of the primary coercivity component decreased from 176 mT to 139.5 mT over 240 days of treatment but fluctuated in between treatment times. The peak of the primary component of the 200°C sample increased over

treatment time by ~3mT, but had fluctuations of increasing and decreasing peaks in between the 240 days. All the primary components in basaltic glasses skewed to the left except for the 300℃ at 240 days, which skewed to the right. The secondary components skewed to the right apart from 300℃ at 240 days and 400℃ at 30 days. For all treatment temperatures, the relative contribution of the primary component decreased with time. The 200℃ and 400℃ samples have a decrease from 100% to ~56%. The primary component of the 300℃ sample fluctuated but overall dropped over 240 days from 100% to 84%, with the lowest point being 78% at 30 days. The secondary component extrapolated contribution typically increased over the course of treatment time at all temperatures.

Figure 3.6: IRM Unmixing results for the artificially-aged basaltic glass. All three temperatures had similar components to the overall coercivity distribution of the sample, with the dominant primary component (blue) and a slightly fluctuating secondary component (purple).

Basalt 200℃

Day 0	**Day 15**	**Day 30**
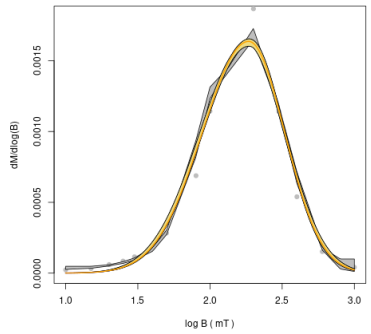	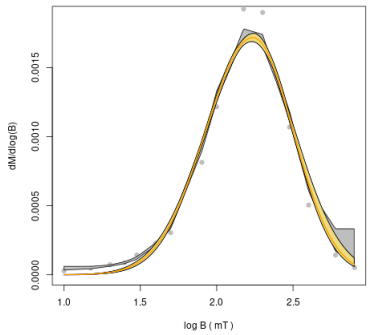	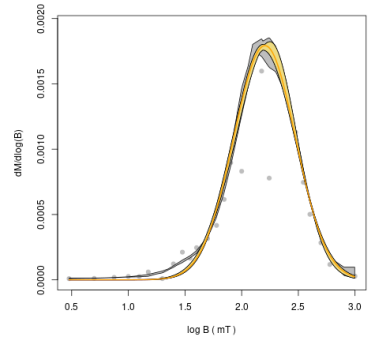
Day 60	**Day 120**	**Day 240**
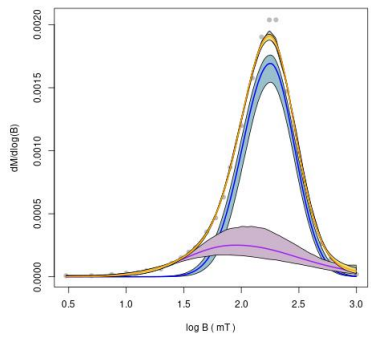	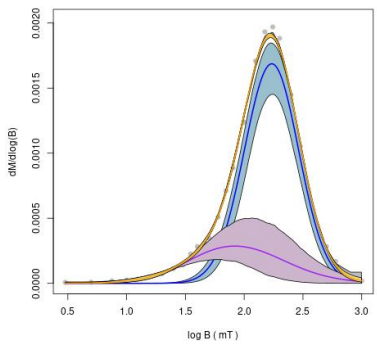	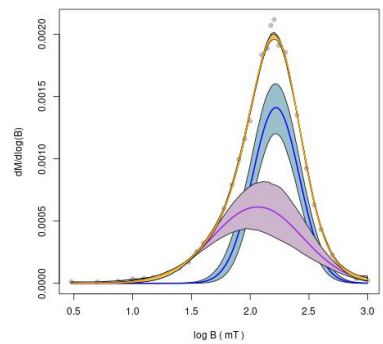

Basalt 300°C		
Day 0	**Day 15**	**Day 30**
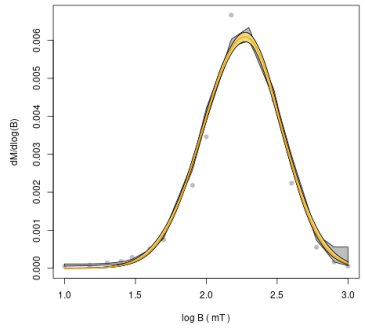	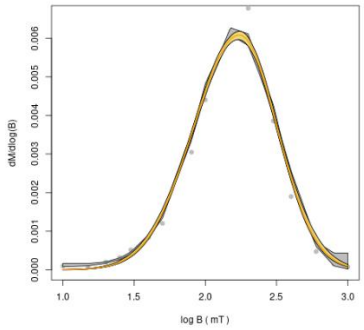	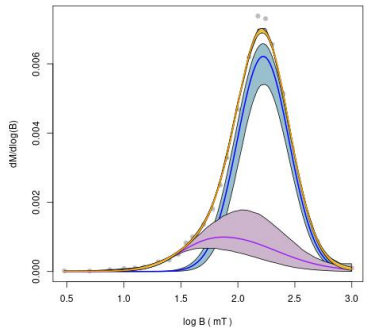
Day 60	**Day 120**	**Day 240**
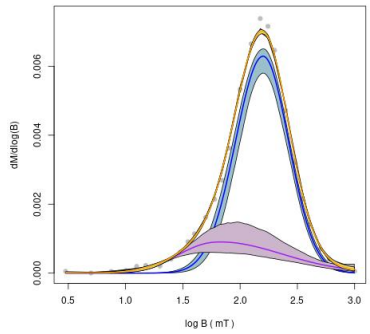	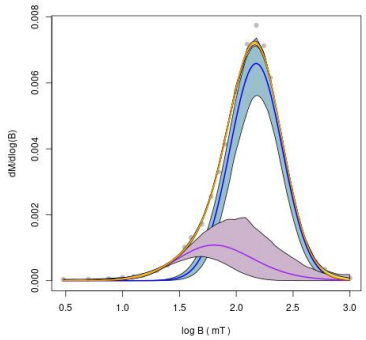	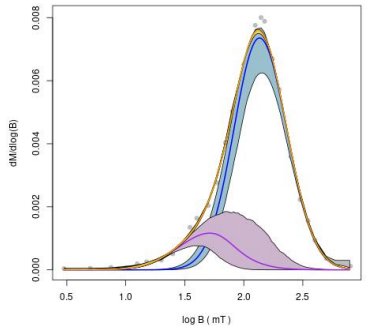
Basalt 400°C		
Day 0	**Day 15**	**Day 30**
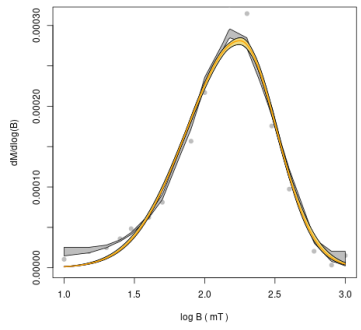	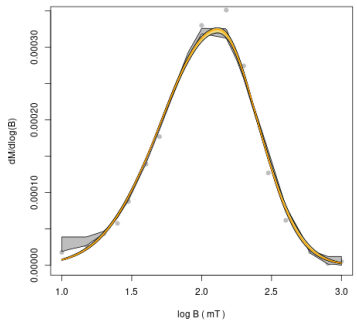	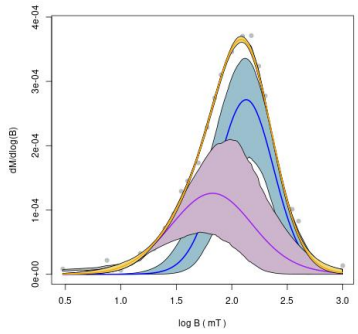
Day 60	**Day 120**	**Day 240**

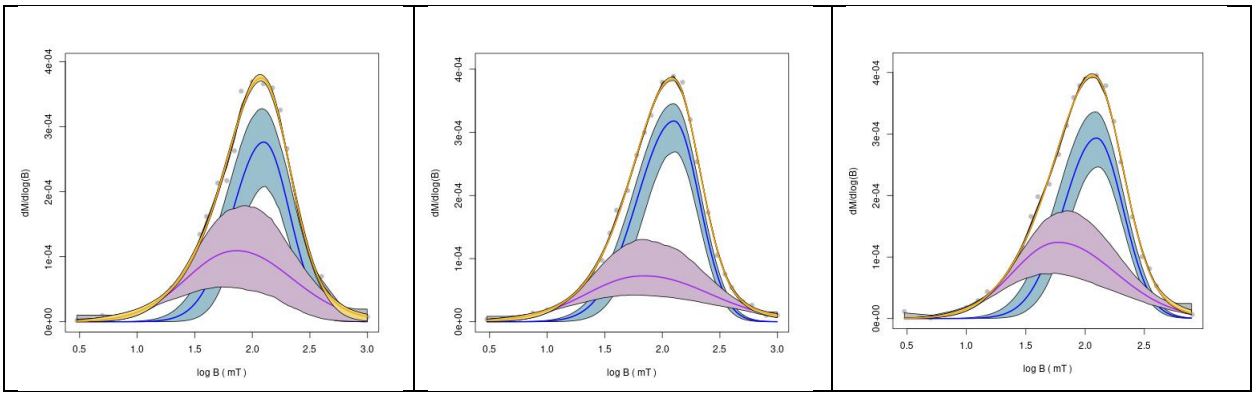

3.1.3 Three-component IRM Demagnetization

Thermal demagnetization of the three-component IRM shows unblocking temperature variations for the soft, medium, and hard coercivity fractions. Compared to basaltic glasses, rhyolitic glasses unblocked at higher temperatures. In all the rhyolitic samples there were prominent “soft’ and “medium” coercivity components, with a secondary “hard” component. All three components displayed similar behavior, with a mostly gradual loss of magnetization to about 475-500°C, and then a rapid loss of the remaining magnetization by 575°C. The maximum unblocking temperatures of 575°C are consistent with very low-Ti titanomagnetite. The distributed unblocking at lower temperatures is consistent with either relatively coarse-grained low-Ti titanomagnetite and/or a population of grains with more variable and higher Ti content. Some of the soft components display more rapid unblocking up to 150°C which is consistent with higher-Ti titanomagnetite (roughly x = 0.6). The sample aged at 400°C had a marked shift towards lower unblocking temperatures compared to the other samples.

Figure 3.7: Rhyolitic glass three-component IRM datasets. "Soft" = <100mT, "Medium" = <300 mT, "Hard" = <1T.

Untreated

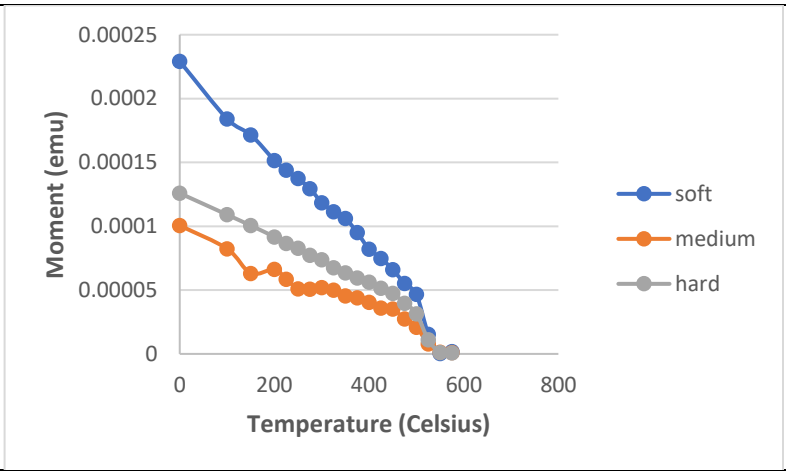

Untreated

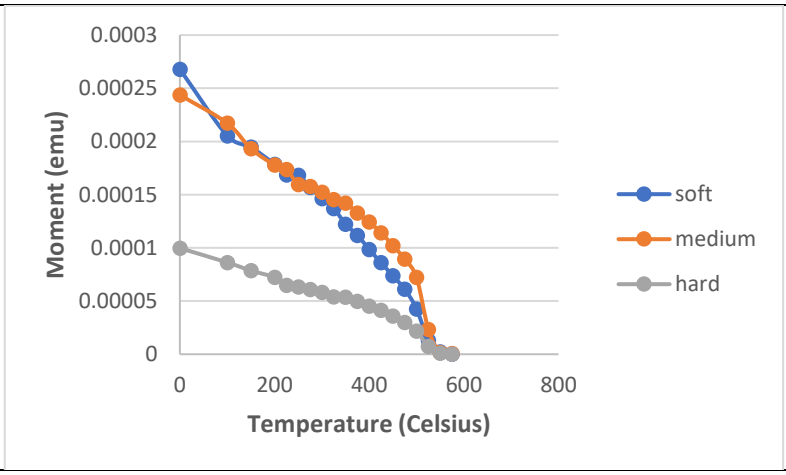

200°C

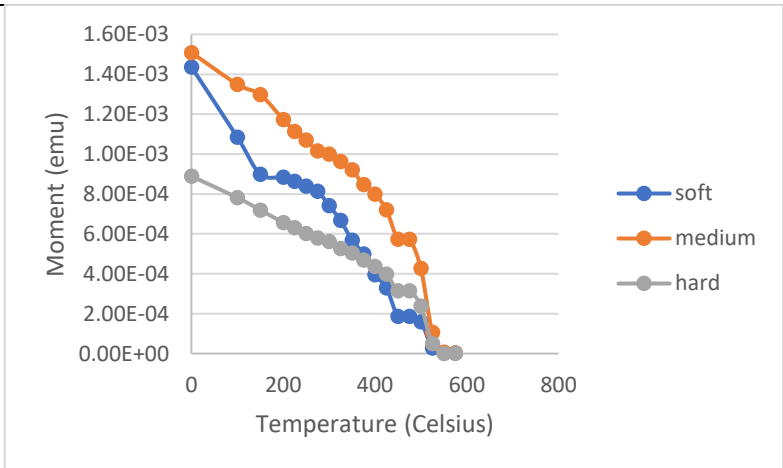

300°C

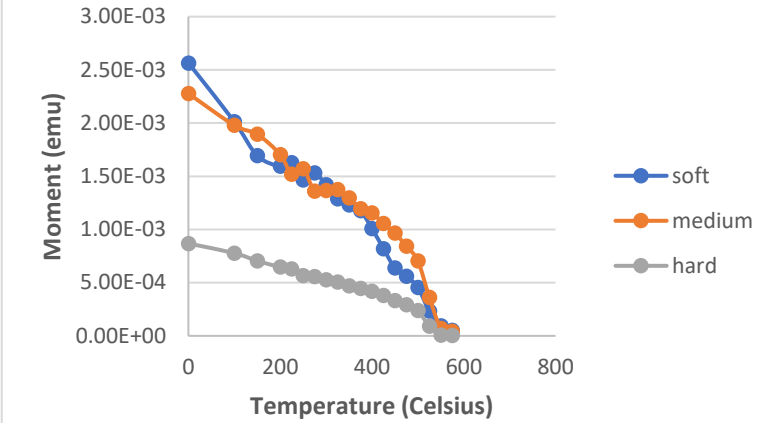

400°C

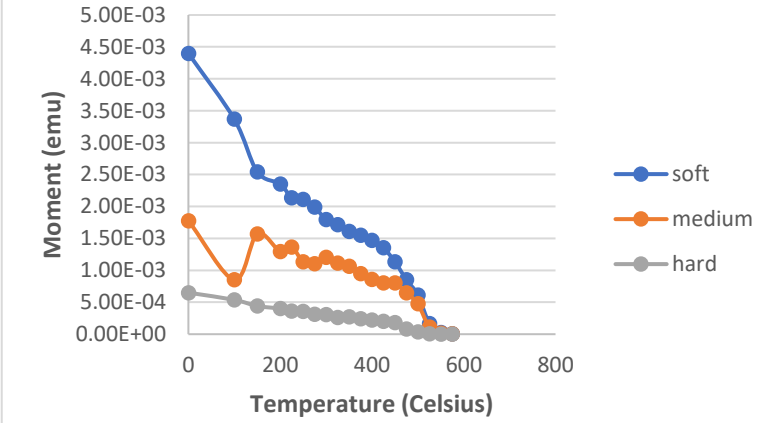

Compared to the rhyolitic glass, the basaltic glass contained a more prominent "hard" coercivity component, but the "soft" and "medium" coercivity components were still dominant. They have lower blocking temperatures on average, consistent with previous observations of a wide range of Ti concentrations in the titanomagnetite. Samples aged at 200°C, 300°, and 400°C lost 75%, 66%, and 33% respectively of their magnetic moment by 400°C. This shows progressively higher unblocking temperature at higher treatment temperatures. This could be explained by a shift to lower-Ti titanomagnetite with a higher Curie temperature. An additional possible explanation is oxidation to titanomaghemite, which is accompanied by an increase in

Curie temperature. The shift to larger average SD grain size may also be accompanied by an increase in blocking temperatures.

Figure 3.8: Basaltic glass three-component IRM datasets. "Soft" = <100mT, "Medium" = <300 mT, "Hard" = <1T.

Untreated

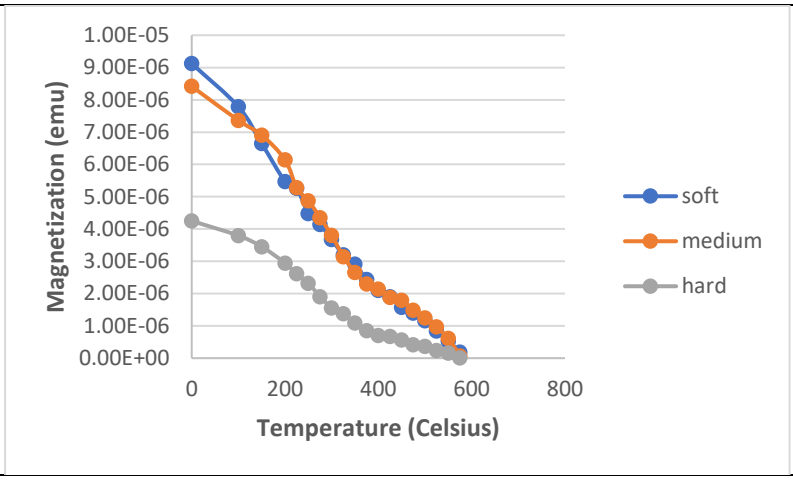

Untreated

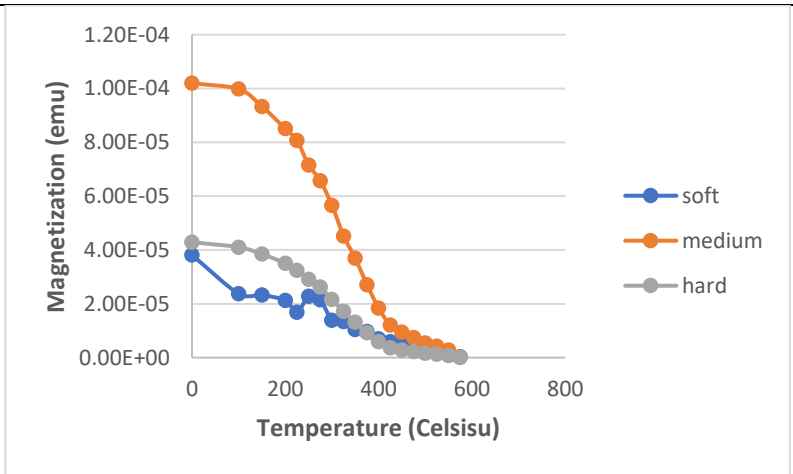

200°C

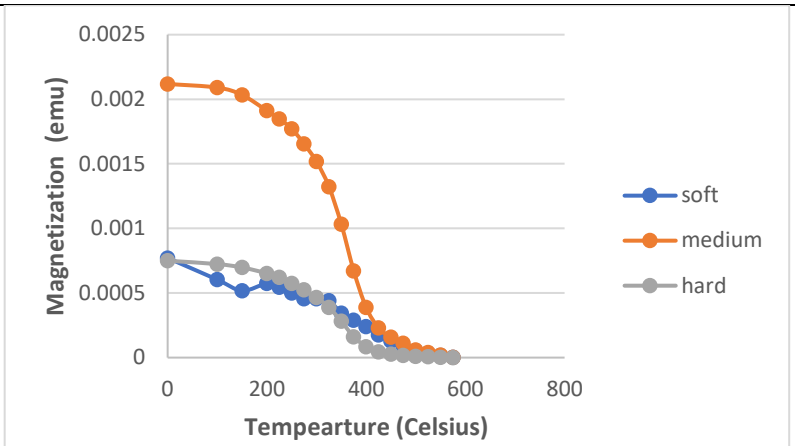
0.0025
0.002
0.0015
0.001
0.0005
0
Magnetization (emu)
0
200
400
600
800
Tempearture (Celsius)
soft
medium
hard

300°C

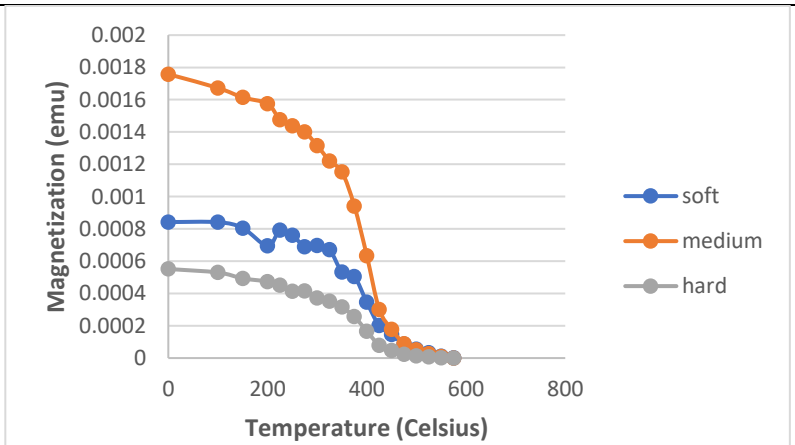
0.002
0.0018
0.0016
0.0014
0.0012
0.001
0.0008
0.0006
0.0004
0.0002
0
Magnetization (emu)
0
200
400
600
800
Temperature (Celsius)
soft
medium
hard

400°C

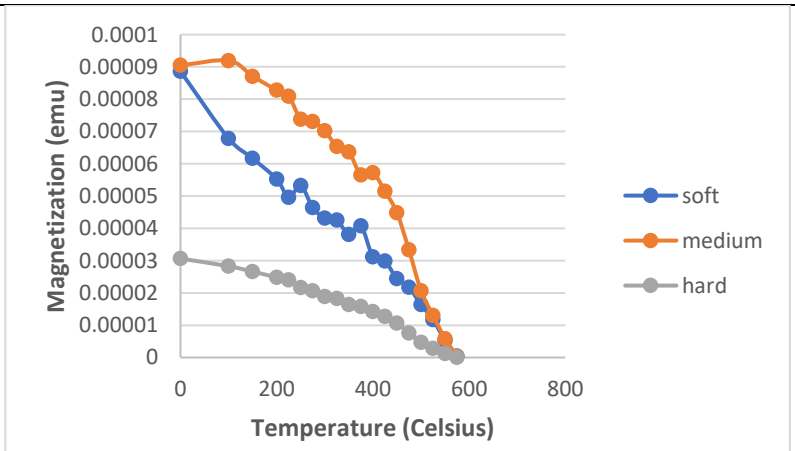
0.0001
0.00009
0.00008
0.00007
0.00006
0.00005
0.00004
0.00003
0.00002
0.00001
0
Magnetization (emu)
0
200
400
600
800
Temperature (Celsius)
soft
medium
hard

3.1.4 Hysteresis Experiments

3.1.4.1 Hysteresis Loops

Figure 3.9: An example of different domain states from hysteresis loops. The black line represents a single-domain grain, and the red line indicates a multi-domain sample. When the loop gets skinnier in the middle (low remanent magnetization and low coercivity), it indicates a shift to multi-domain behavior. Hysteresis parameters M_r, M_s, and B_c are shown in the SD hysteresis loop (see also text).

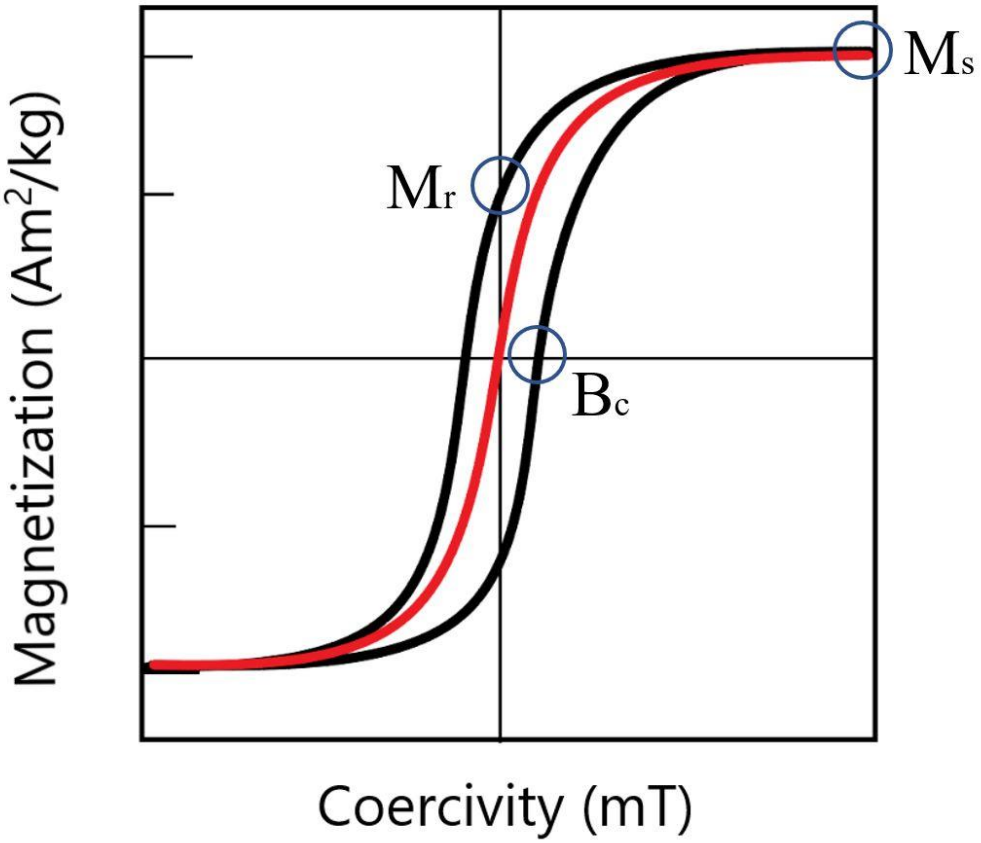

Hysteresis loops play a prominent role in our understanding of magnetic grain populations and their possible chemical composition, coercivity, and domain state. **Figure 3.9** shows an example hysteresis loop for a SD sample (black), and the red hysteresis loop is an example of a MD hysteresis loop. **Figure 3.10A** shows an example of the raw data (orange line) collected on samples for these studies. Because glass typically contains a lot of paramagnetic iron resulting in the linear slope at high field values, this paramagnetic background is subtracted

to produce the ferromagnetic loop (blue line). The rhyolitic sample in **Figure 3.10B** shows all the individual data points collected during a hysteresis experiment.

Figure 3.10A: Example hysteresis loops from a rhyolitic and basaltic glass samples. Magnetic remanence is on the y-axis while coercivity is on the x-axis. Rhyolitic glass, B-74 was artificially aged at 400℃ for 60 days. Basaltic glass, B-41 was artificially aged at 300℃ for 240 days.

Basaltic Glass)

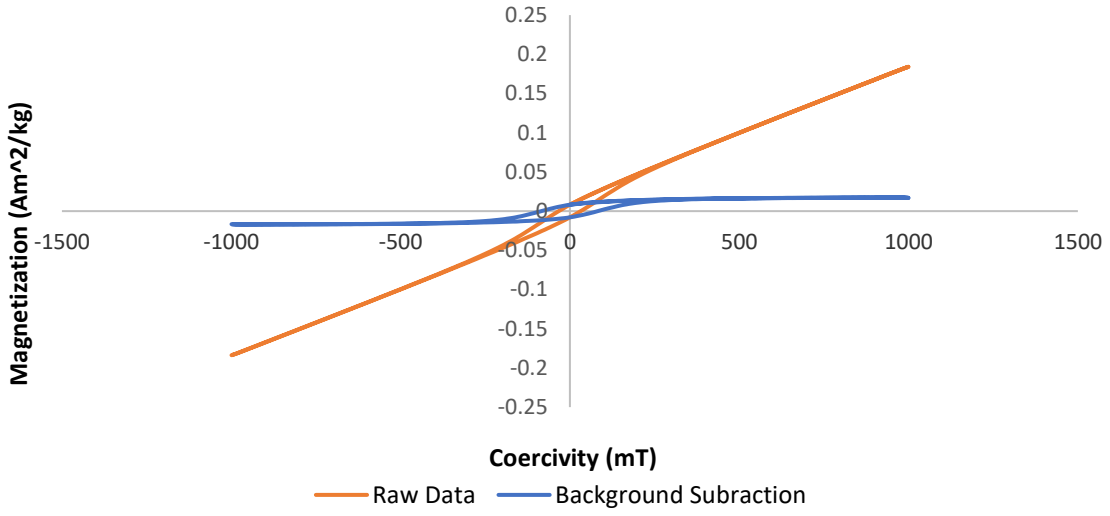

Rhyolitic Glass)

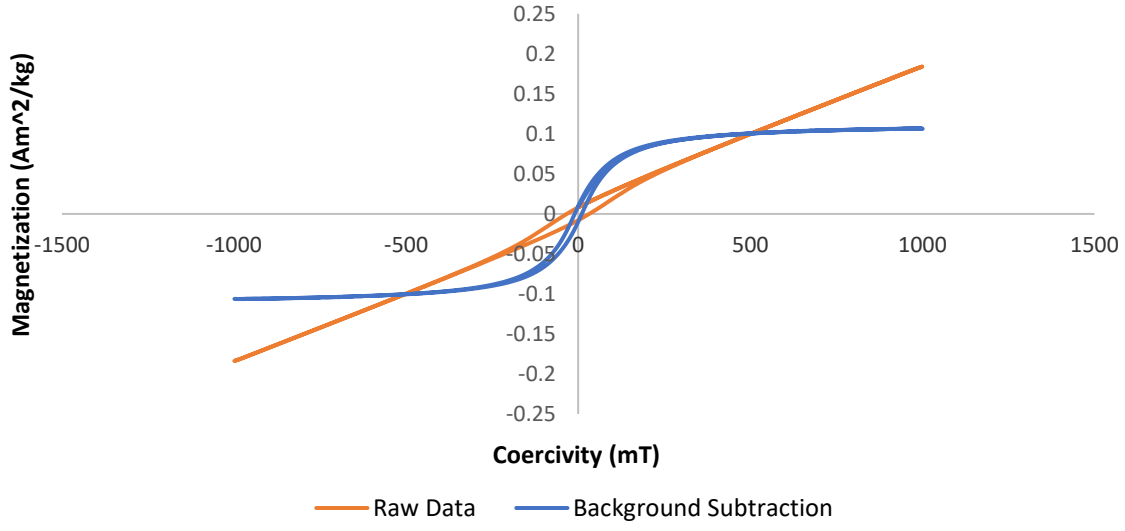

Figure 3.10B: Individual hysteresis data points. B-06, before (left) and after (right) paramagnetic subtraction from the hysteresis loop. The individual symbols show the data points collected in one hysteresis loop.

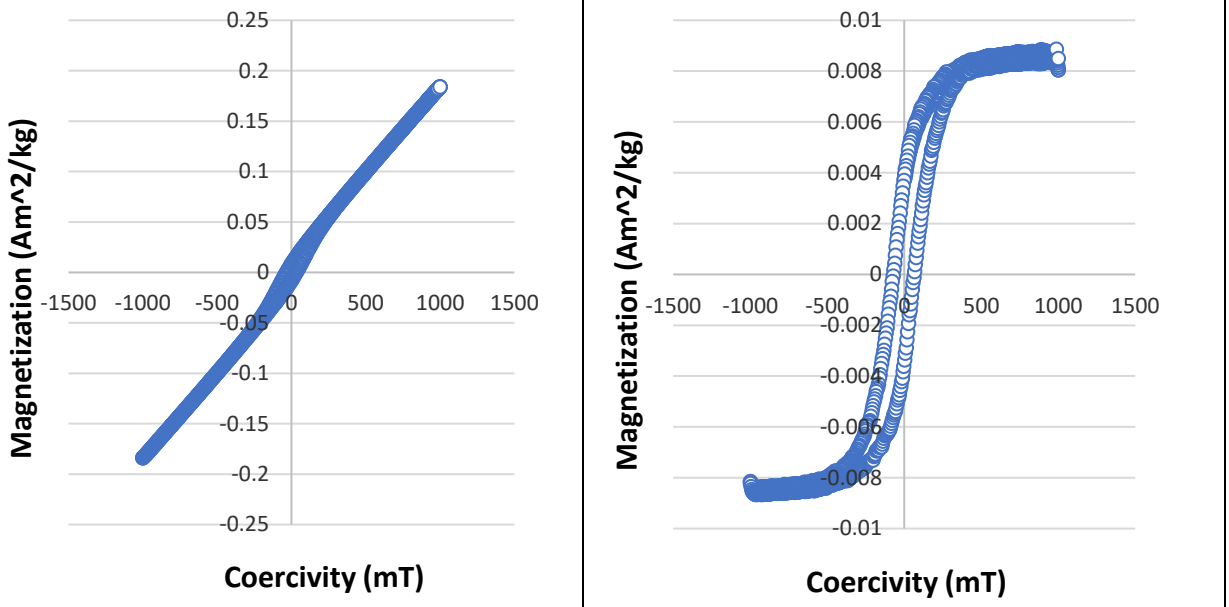

Hysteresis loops are often summarized by four parameters. M_s is the saturation magnetization, or the maximum magnetization the sample can achieve in high field. M_r is the saturation remanent magnetization, or the magnetization remaining at zero applied field ($B_c = 0$), following saturation. M_r is found at the y-axis intercept in Fig. 3.9. The field necessary to reduce the net moment to zero is the coercivity (B_c), found at the x-axis intercept in Fig. 3.9 (Tauxe et al., 2018). The coercivity of remanence (B_{cr}) can be estimated from the hysteresis loop but is more properly derived from the backfield remanence curve (see Methods). It is the field required to reduce M_r to zero when measurements are made after the applied field is turned off. It can also be defined as the field required to irreversibly flip half the magnetic moments (Tauxe et al., 2018).

To summarize results from many samples, the hysteresis parameters are frequently combined on a so-called Day plot of saturation remanent magnetization over saturation magnetization (M_r/M_s) versus coercivity of remanence over coercivity (B_{cr}/B_c) (Day et al., 1977). Plotted like this, SD samples will plot in the upper left and MD samples will plot in the lower right. While imperfect, a Day plot is commonly used to analyze magnetic domain state variations within a group of samples. Because magnetic domain state transitions can occur at unequal particle sizes for different magnetic minerals, making inferences about the overall assemblage is difficult without other information (Roberts et al., 2018). But it can still be useful to look at changes within sample populations. Dunlop (2002) calculated theoretical SD + MD mixture curves for magnetite, which are included on the Day plot shown in **Fig. 3.11**.

Table 3.1: **Hysteresis parameters for artificially aged samples.** These values were used in calculations for the Day plot of **Figure 3.11**.

Glass Type / Aging Temperature	Ms [Am/kg]	Mr [Am/kg]	Bc [mT]	Bcr [mT]
Untreated Rhyolitic Glass	0.29782	0.02179	8.60	54.86
Untreated Rhyolitic Glass	0.25679	0.01885	9.72	58.41
200°C Rhyolitic Glass, 240 days	0.11563	0.00725	8.38	48.97
200°C Rhyolitic Glass, 15 days	0.12324	0.00796	7.67	46.04
200°C Rhyolitic Glass, 60 days	0.12459	0.00665	7.29	46.43
200°C Rhyolitic Glass, 240 days	0.11738	0.00672	6.66	45.53
300°C Rhyolitic Glass, 240 days	0.11998	0.00746	7.03	47.03
300°C Rhyolitic Glass, 15 days	0.11537	0.00623	7.26	47.29
300°C Rhyolitic Glass, 60 days	0.11101	0.00639	6.82	44.15
300°C Rhyolitic Glass, 240 days	0.10612	0.00709	7.94	48.06
400°C Rhyolitic Glass, 15 days	0.12068	0.01044	11.60	41.09
400°C Rhyolitic Glass, 60 days	0.12165	0.00781	7.60	43.75
400°C Rhyolitic Glass, 240 days	0.11307	0.00974	10.28	38.47
400°C Rhyolitic Glass, 240 days	0.10731	0.00963	11.29	37.93
Untreated Basaltic Glass	0.00517	0.00191	54.51	154.20
Untreated Basaltic Glass	0.00263	0.00010	83.63	173.79
200°C Basaltic Glass, 15 days	0.00240	0.00102	54.44	142.88
200°C Basaltic Glass, 60 days	0.00210	0.00088	81.75	154.19
200°C Basaltic Glass, 240 days	0.00425	0.00197	87.18	149.42
300°C Basaltic Glass, 15 days	0.00900	0.00365	67.70	132.90
300°C Basaltic Glass, 60 days	0.00499	0.00197	59.06	118.57
300°C Basaltic Glass, 240 days	0.00654	0.00248	52.87	106.66

300°C Basaltic Glass, 240 days	0.01825	0.00808	83.37	127.63
400°C Basaltic Glass, 15 days	0.01984	0.00912	83.75	136.95
400°C Basaltic Glass, 240 days	0.01449	0.00624	77.75	132.51
400°C Basaltic Glass, 60 days	0.03640	0.01508	71.70	122.82
400°C Basaltic Glass, 240 days	0.00193	0.00064	43.65	105.06

Figure 3.11: Day plots of artificially aged basaltic and rhyolitic samples. The basaltic samples had a higher M_r/M_s value and are seen in the top left corner of the Day plot. The rhyolitic samples had a lower M_r/M_s ratio and are located toward the bottom right of the chart. There were no trends found in the artificial aging treatment time or temperatures. Black stars = untreated; Blue = 200°C; Gold = 300°C; Red = 400°C. Circles = 15 day; Squares = 60 day; Triangles = 240 days. (magnetite mixing curves from Dunlop, 2002 shown for reference).

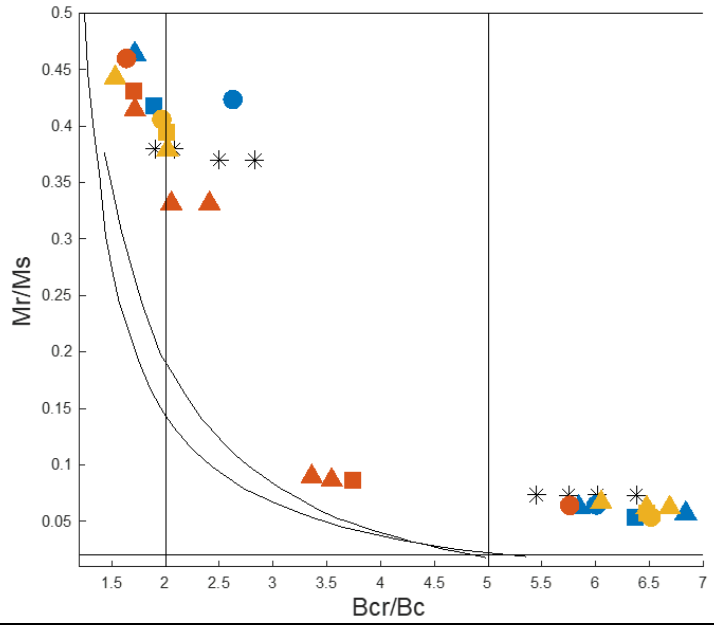

Based on this Day plot, there were no trends with treatment time or temperature for either the rhyolitic glass samples or the basaltic glass samples. Unlike the IRM acquisition experiments, these do not represent before and after data. All measurements were made on different specimens, which could explain why no trends are observed. The rhyolitic samples have a low remanence ratio and high coercivity ratio, consistent with PSD to MD behavior in the magnetic grain population (**Figure 3.11**). This means that the grain size of the rhyolitic glass is slightly larger than the basaltic samples, consistent with the observed lower coercivities from the

IRM acquisition experiments. With some notable exceptions, the artificially aged rhyolitic samples have also mostly shifted toward the MD endmember, suggesting an increasing average grain size over treatment time. The basaltic samples have a higher remanence and a lower ratio of B_{cr} to B_c , indicating PSD to SD behavior in samples with the highest coercivity and remanence. The slight variations in hysteresis parameters between specimens possibly arise from small heterogeneities in the starting magnetic mineral assemblage. These heterogeneities evidently result in bigger differences than those produced during the aging treatments (**Figure 3.11**).

3.1.4.2 First Order Reversal Curves

First order reversal curves (FORCs) provide much more in-depth information on the coercivity and interaction field distributions within a sample. FORC diagrams are based on data sampled from the entire area inside of a hysteresis loop (Harrison & Feinburg, 2008). **Figure 3.12** shows FORC distributions collected for both the basaltic and rhyolitic samples after their artificial aging treatments.

The rhyolitic FORC distributions are characteristic of PSD and MD domain behavior. The three-lobe pattern (e.g., **Figure 3.12, Untreated Rhyolite**) is characteristic of PSD-like behavior. The contours that do not close but spread along the vertical axis at x = 0 suggest very coarse PSD (e.g., **Fig. 3.12, Rhyolite 400°C**). There is little change in the rhyolitic glass FORC distributions when comparing the untreated sample to the artificially aged samples. The small differences in FORCs are likely due to sample heterogeneity, obscuring any possible trends related to aging.

Basaltic samples all show prominent horizontal spread on the coercivity (B_c) axis at B_u = 0, consistent with SD behavior. The basaltic samples also contain a sharp vertical ridge at zero

on the coercivity (B_c) axis, indicating a superparamagnetic component (**Figure 3.12**). Basaltic glasses were ~100 times weaker than the rhyolitic samples which lead to some noise in the data. One observable feature in the 200°C and 300°C samples is the creation of a "fish-tail" feature, or two distinct peaks on the horizontal axis, one at higher coercivities and one at very low coercivities and connected spatially to the vertical SP signature. This double peak is consistent with two very distinct magnetic mineral populations as opposed to a single population with a wide grain-size distribution. The 400°C sample was more comparable with the untreated basaltic glass FORC.

Figure 3.12: FORC diagrams of artificially aged rhyolitic glasses and basaltic glasses. The signal to noise ratio is higher in the rhyolitic glass specimens.

Untreated Rhyolite

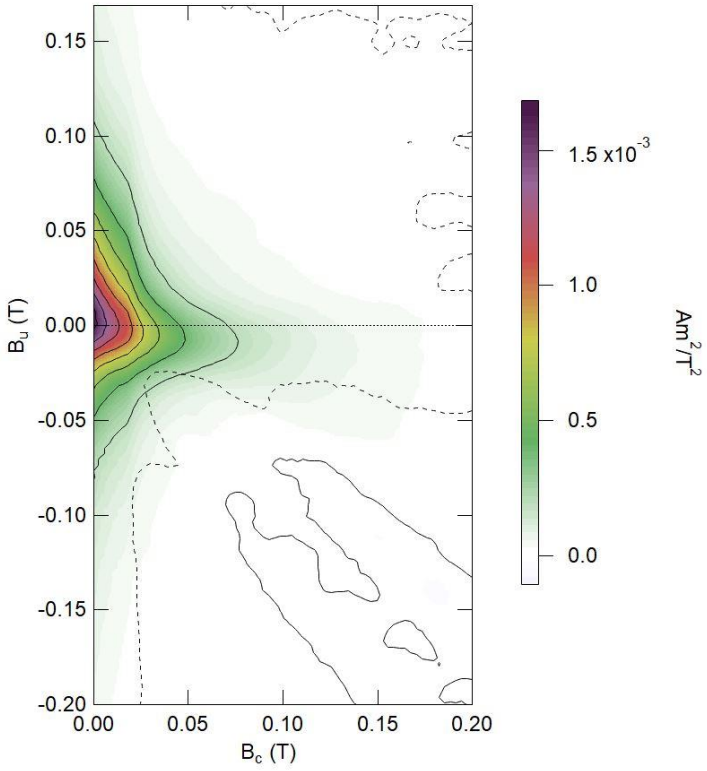

Rhyolite 200°C | **Rhyolite 300°C**

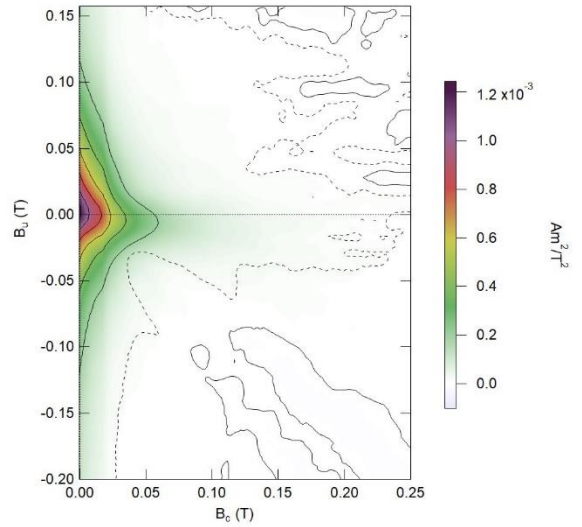

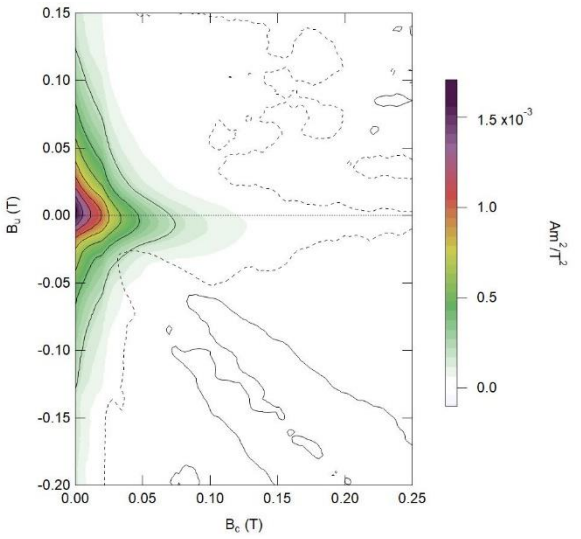

Rhyolite 400°C

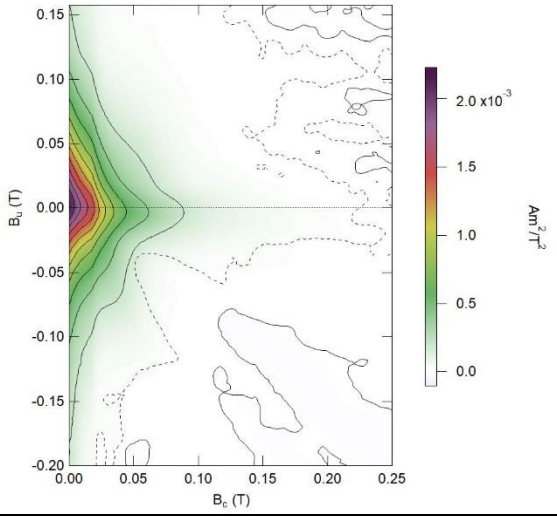

Untreated Basaltic Glass

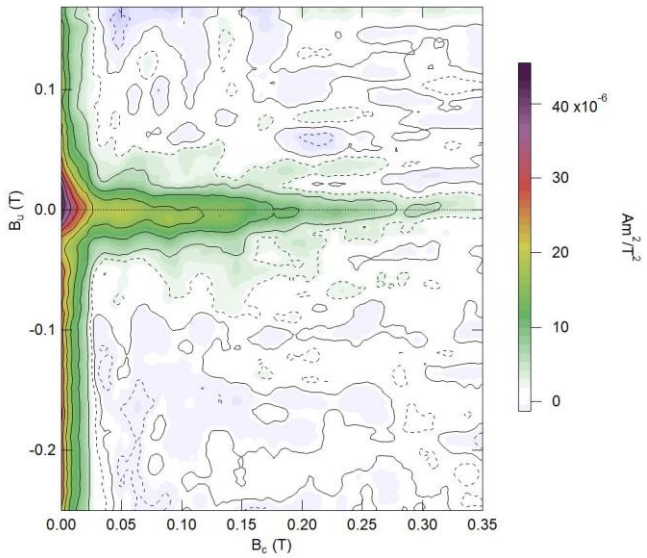

Basalt 200°C

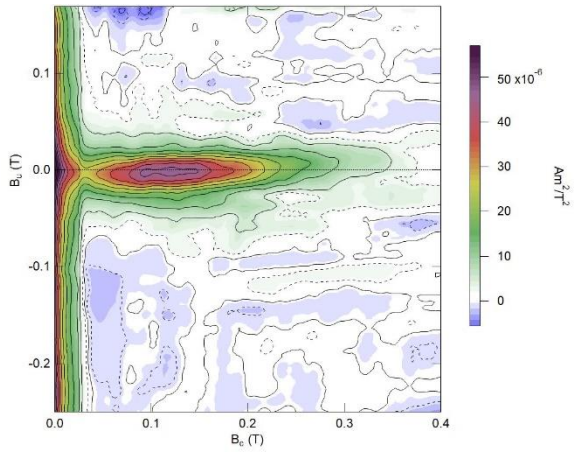

Basalt 300°C

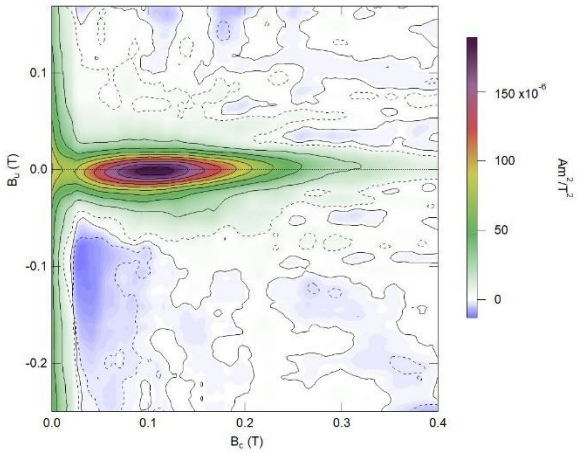

Basalt 400°C

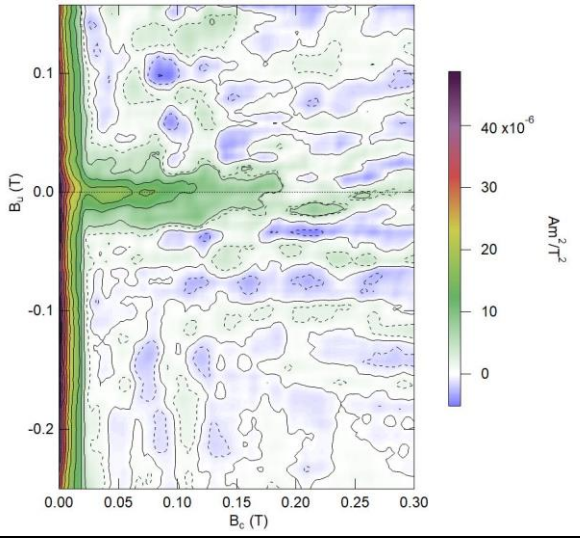

3.1.5 Paleointensity Experiments

As noted in the methods (see Sec. 2.1), the samples unfortunately did not carry any significant remanence prior to the aging experiments. However, some of the specimens likely acquired a thermoviscous remanence during the aging treatments, so they did carry some remanence prior to the paleointensity experiment. We can therefore look at this data from another viewpoint and see how they behaved during the paleointensity experiments. If the aging treatments were resulting in a lowering of the glass transition temperature, we might expect some pTRM checks to fail at lower temperatures compared to untreated specimens. pTRM check failure means that the repeat in-field step does not reproduce the original in-field step, suggesting the remanence-bearing capacity of the sample has changed via a change in magnetic mineralogy. **Figures 3.13 and 3.14** show the difference ratio sum (DRATS) in both rhyolitic and basaltic glasses. The different ratio (DRAT) is the difference between a single pTRM check and the prior pTRM measurement at the same temperature, normalized by the length of the best-fit line to NRM-pTRM data. The signed sum of the differences (DRATS) shows the trends of pTRM checks over the course of the paleointensity experiment (Tauxe and Staudigel, 2004). Positive DRATS means that most pTRM checks acquired more magnetization than the original pTRM measurement, while negative DRATS means that most pTRM checks acquired less magnetization than the original pTRM measurement. Rhyolitic glass DRATS did not trend with aging temperature, but basaltic glass showed an overall decrease in the maximum observed DRATS at increased aging temperatures. Basaltic glass DRATS had a lower range of values at higher aging temperatures. Overall, these paleointensity results should be taken lightly, due to the ARM experiments undertaken before the paleointensity experiments.

Figure 3.13: Rhyolitic glass DRATS with treatment temperature.

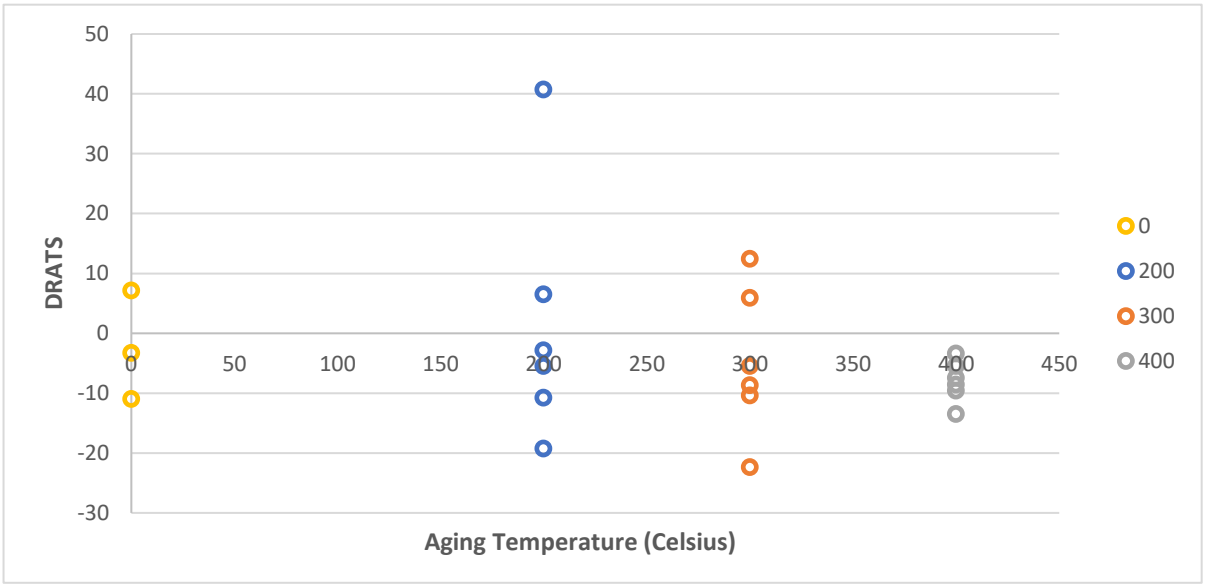

Figure 3.14: Basaltic glass DRATS with treatment temperature.

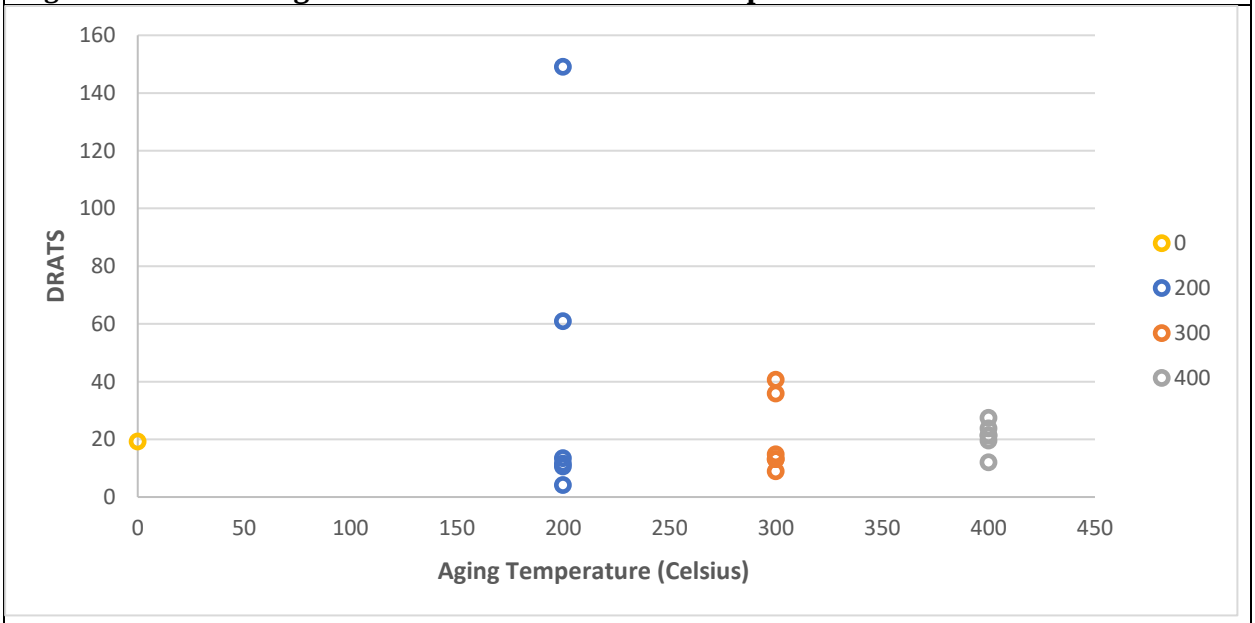

3.2 Hydration Results

3.2.1 IRM Experiments

3.2.1.1 Properties of IRM

Figure 3.15A-B shows the changes in the mass normalized saturation remanent magnetization over treatment time in both basaltic and rhyolitic glasses. In the rhyolitic glasses, longer treatment times at 300°C showed an increase, then decrease in normalized magnetization over treatment time. Samples hydrated at 450°C all showed a decrease during hydration treatment, with the 10-day step having the smallest decrease in magnetization. Magnetization changes in the rhyolites ranged between -34% and +13%. Basaltic glasses had significantly larger changes (-66% to +188%), and the 300°C treatment typically resulted in an increase in magnetization while the 450°C treatment resulted in more variable behavior.

Figure 3.15A: Change of the mass normalized saturation magnetization for rhyolitic glasses.

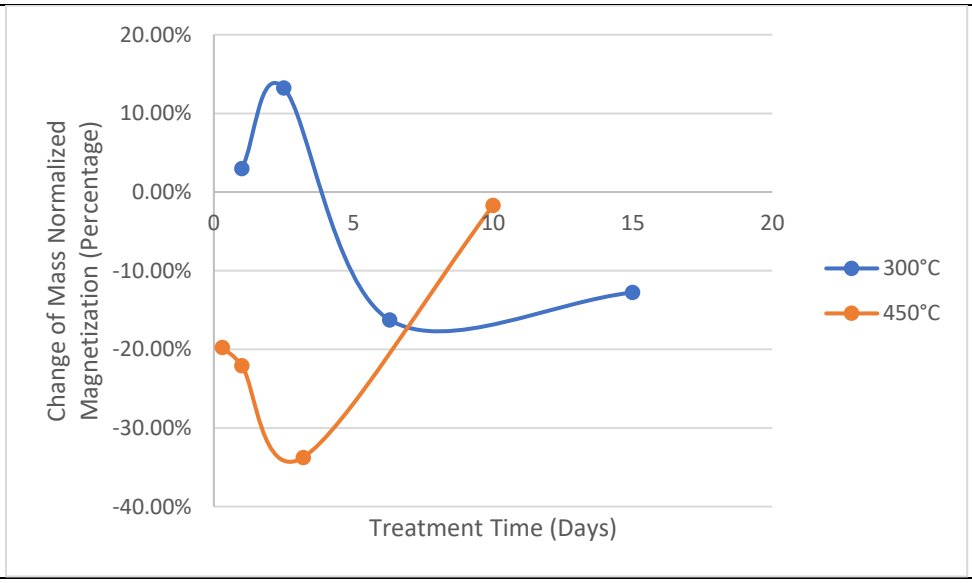

Figure 3.15B: Change of the mass normalized saturation magnetization for basaltic glasses.

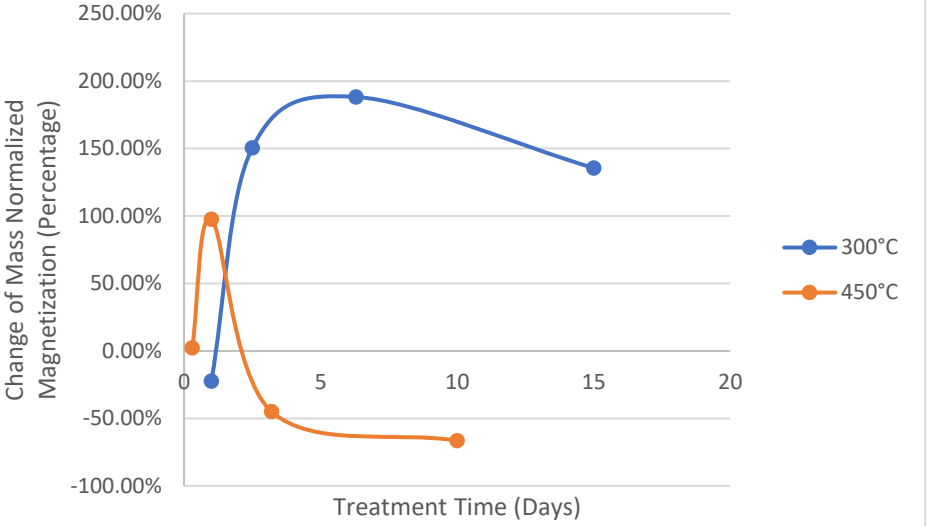

Figure 3.16A-B shows the change in the coercivity of remanence after hydration treatment. Rhyolitic glasses had a decreased B_{cr} over the course of treatment at the 300°C step. The 450°C step decreased, and then had an increased magnetization at the final treatment time. Hydrated basaltic glass samples show much higher variability in B_{cr} compared to rhyolitic samples. Basaltic glasses at 300°C decreased and then increased after longer treatments, while the 450°C step increased and then decreased at the final treatment time of 10 days.

Figure 3.16A: Change of the coercivity of remanence (B_{cr}) for rhyolitic glasses.

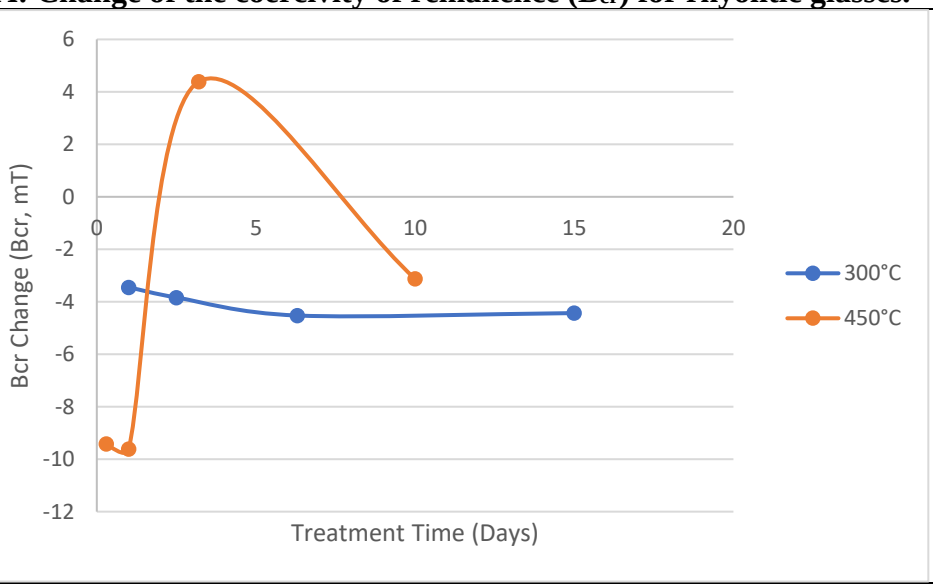

Figure 3.16B: Change of the coercivity of remanence (B_{cr}) for basaltic glasses.

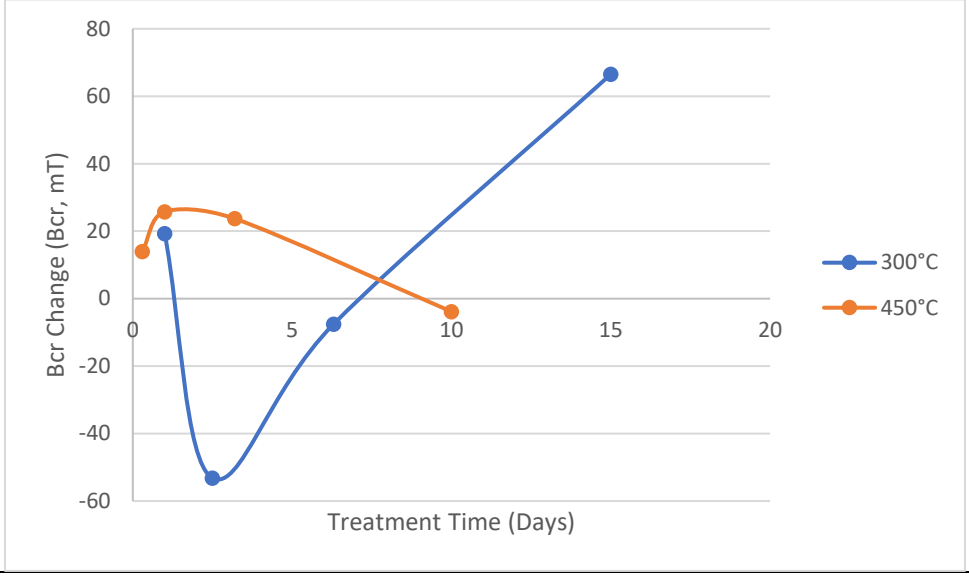

3.2.2 IRM Unmixing

IRM unmixing curves were calculated for hydrated glass specimens and can be seen in **Figures 3.17 and 3.18**. Typically, samples of hydrated rhyolitic glass (**Figure 3.17**) had two different components to the overall coercivity of the specimen, like those observed in the aging experiments. There were slight variations in the locations of the coercivity peaks before and after hydration treatment, but the rhyolitic glass typically had a decreased in the peak coercivity (B_h) of the primary component, except for the 450℃ treatments of 3.2 days and 10 days, which had an increase. The coercivity peak of the secondary component of the rhyolitic glasses also decreased, apart from the 300℃ treatment at 1 day, and 450℃ at 0.3 days and 3.2 days. All primary components of hydration experiments skewed to the left before and after treatment. All secondary components skewed to the right except for 450℃ at 10 days before hydration treatment. The extrapolated contribution of the primary component ranged from 72% to 100%, while the secondary component ranged from 5% to 28%. There were no trends before and after treatment with the relative contribution of the two components.

The basaltic hydrated specimen coercivity distributions (**Figure 3.18**) show slightly different trends to the rhyolitic specimens. Coercivity peaks (B_h) of the primary component ranged from 28 mT to 197 mT, and there were no trends with coercivity peaks before and after treatment. The secondary component ranged from 13 mT to 221 mT, with no overall trends with hydration treatment. The primary components skewed mainly to the left ($S < 1$), but two samples contained skewness to the right ($S > 1$) before treatment, and two different samples contained skewness to the right after treatment. The secondary components typically had mixed skewness with no trends over treatment. The extrapolated relative contribution of the primary component typically decreased, and the secondary component increased with treatment time at 300°C, but at no trends were observed at 450°C.

Figure 3.17: IRM MAX Unmix curves of hydrated rhyolitic glass. Untreated specimen (left), and specimen after hydration treatments (right). Specific statistical data for each sample will be provided in *Appendix B.*

C-02 - 300°C, 1 day	C-06 - 300°C, 2.5 days
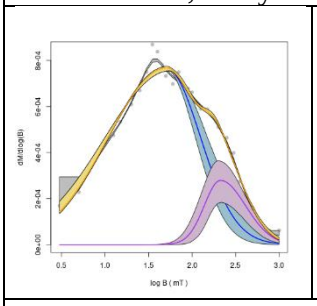	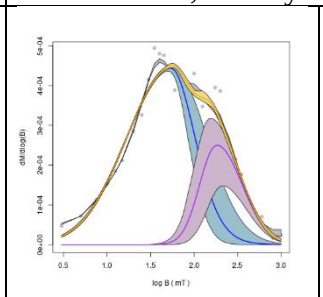
C-11 - 300°C, 6.3 days	C-15 - 300°C, 15 days
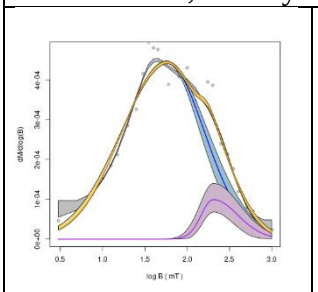	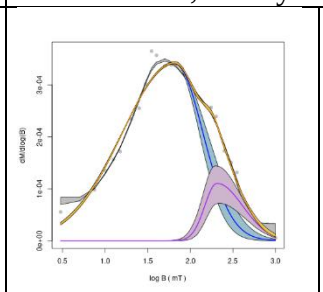
C-19 - 450°C, 0.3 days	C-25- 450°C, 1 day
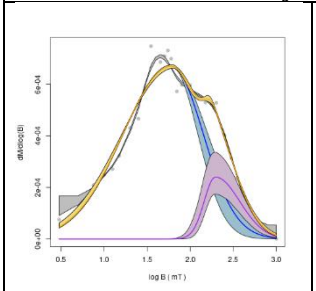	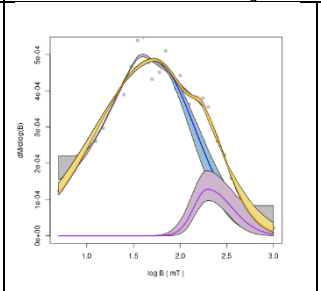
C-29- 450°C, 3.2 days	C-33 - 450°C, 10 days
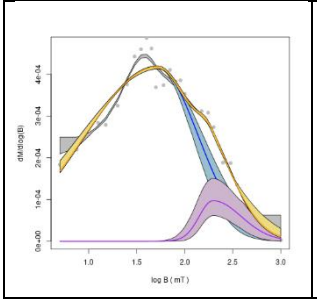	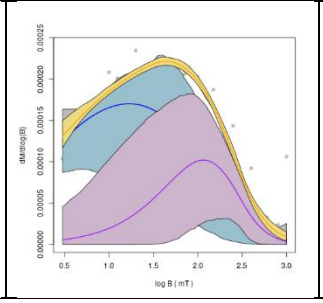

Figure 3.18: IRM MAX Unmix curves of hydrated basaltic glass. Untreated specimen (L), and specimen after hydration treatments (R). Specific statistical data for each sample will be provided in *Appendix B.*

C-50 - 300°C, 1 day		C-53 - 300°C, 2.5 days	
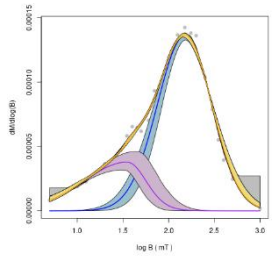	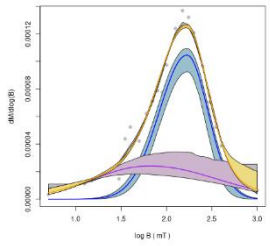	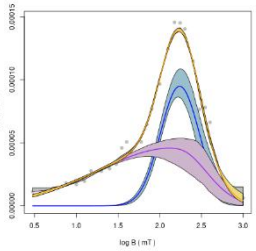	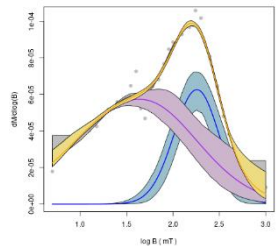
C-57 - 300°C, 6.3 days		C-65 - 300°C, 15 days	
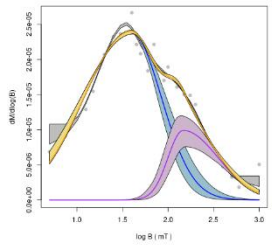	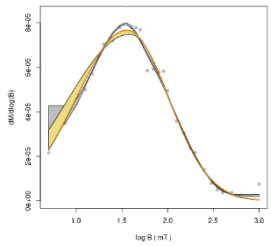	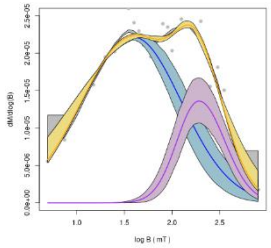	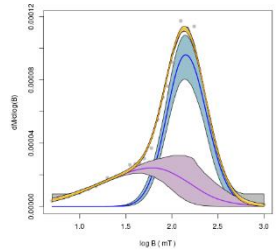
C-69 - 450°C, 0.3 days		C-71 - 450°C, 1 day	
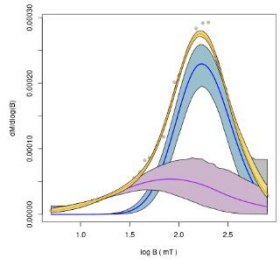	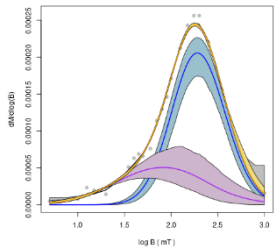	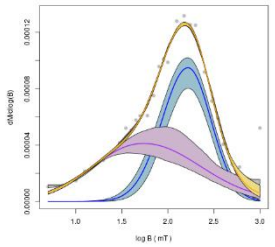	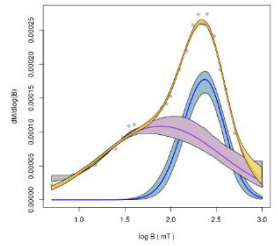
C-75 - 450°C, 3.2 days		C-79 - 450°C, 10 days	
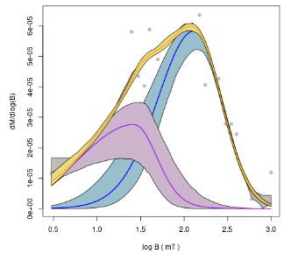	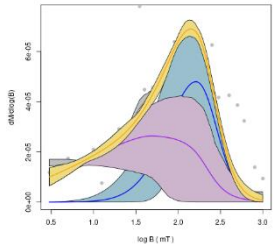	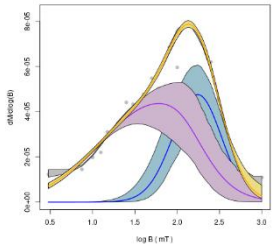	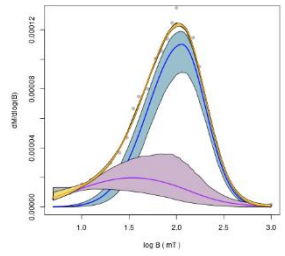

3.2.3 Hysteresis Experiments

3.2.3.1 Day Plot

B_{cr} in rhyolitic samples ranged from ~36 mT to ~58 mT, while the range of B_c was ~7 mT to ~12 mT. The hydrated basaltic specimens contained a much higher variance of range in both B_{cr} (~37 mT to ~162 mT) and B_c (~6 mT to ~38 mT) compared to the hydrated rhyolitic samples. Day plots (Day et al., 1977) can be seen in **Figure 3.19**. There were no obvious trends with time or treatment temperature in either the hydrated rhyolitic glass or the basaltic glass when comparing M_r/M_s and B_{cr}/B_c values. As with the artificially aged samples, heterogeneity in the starting material for the hydrated glass samples could potentially obscure trends found in both the basaltic and rhyolitic glass. In fact, the "before" IRM unmixing results for the basaltic samples show significant variability, suggesting that the starting material was not homogeneous.

Table 3.2: Day Plot parameters for hydrated samples. These values were used in calculations for the Day plot of **Figure 3.19**.

Type of Glass	Temperature/Time	M_s [Am/kg]	M_r [Am/kg]	B_c [mT]	B_{cr} [mT]
Rhyolitic Glass	Untreated	0.29780	0.021800	8.60	54.86
Rhyolitic Glass	Untreated	0.25670	0.018800	9.72	58.41
Rhyolitic Glass	300°C, 1 day	0.12990	0.005860	4.74	40.20
Rhyolitic Glass	300°C, 2.5 days	0.06640	0.006030	12.54	57.93
Rhyolitic Glass	300°C, 6.3 days	0.08940	0.005780	7.77	50.15
Rhyolitic Glass	300°C, 15 days	0.06700	0.004960	8.38	47.34
Rhyolitic Glass	450°C, 0.3 days	0.12400	0.007040	5.46	37.12
Rhyolitic Glass	450°C, 1 day	0.15100	0.006490	3.94	36.08
Rhyolitic Glass	450°C, 3.2 days	0.07780	0.005450	8.95	48.49
Rhyolitic Glass	450°C, 10 days	0.10210	0.003330	5.67	51.61
Basaltic Glass	Untreated	0.00517	0.001910	54.51	154.20
Basaltic Glass	Untreated	0.00263	0.000997	83.63	173.79
Basaltic Glass	300°C, 1 day	0.00695	0.001600	24.85	119.08
Basaltic Glass	300°C, 2.5 days	0.05782	0.004850	5.87	23.90
Basaltic Glass	300°C, 6.5 days	0.01120	0.000517	12.53	37.32
Basaltic Glass	300°C, 15 days	0.01080	0.002410	20.21	118.75
Basaltic Glass	450°C, 0.3 days	0.01160	0.002100	37.61	150.16
Basaltic Glass	450°C, 1 day	0.01180	0.002720	33.46	162.09
Basaltic Glass	450°C, 3.2 days	0.00447	0.001080	20.37	113.45
Basaltic Glass	450°C, 10 days	0.00556	0.000951	19.06	69.48

Figure 3.19: Day plots of hydrated samples (Day et al., 1977)

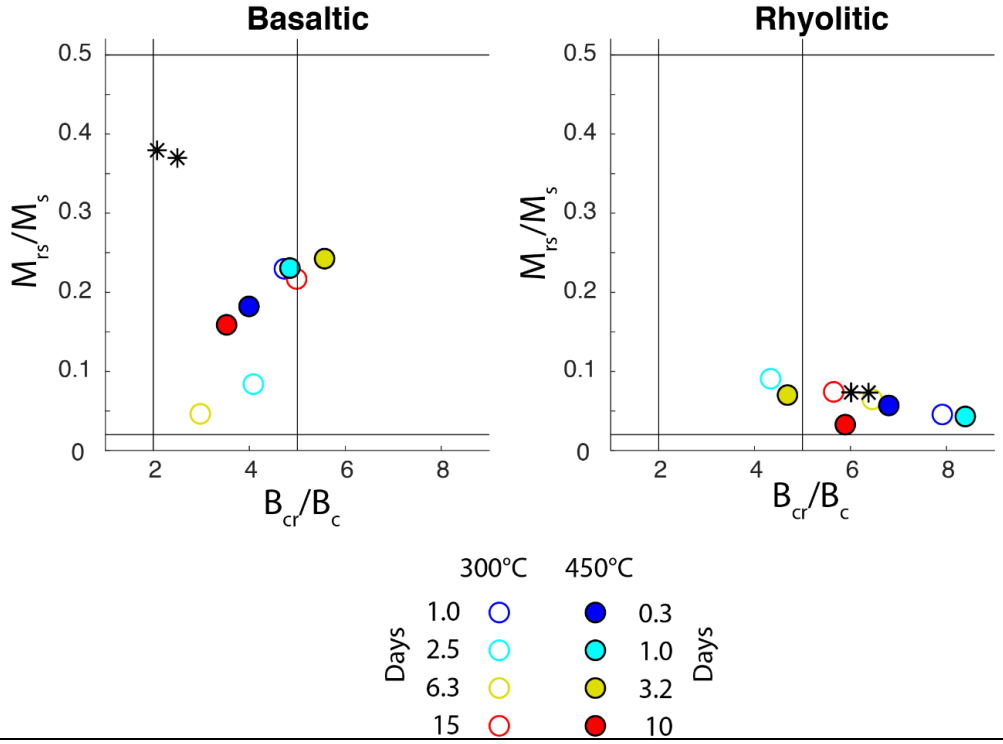

3.2.3.2 FORC Diagrams

Figure 3.20 shows examples of some FORC distributions from hydrated samples. **Figures 3.20 (R1-4)** show the rhyolitic glass samples. Axes for the FORCs have different scales in **Figure 3.20 (B1-4)**. FORC data for rhyolitic glass showed a PSD to MD component. **Figures 3.20 (B1-4)** show the example FORC distributions for basaltic glass, where larger variations are observed. The untreated basaltic samples showed a SD + SP state in FORC experiments. The hydrated basaltic glass specimens showed greater variability in their FORC distributions compared to the hydrated rhyolitic glasses, with some samples showing PSD behavior while others still showed some SD behavior. As noted above, however, this may result from heterogeneity in the starting materials.

Figure 3.20: FORCs of hydrated rhyolitic and basaltic samples. Figures R1 and R4 have larger scales than the other samples (10^{-3}, 10^{-4}) compared to other samples (10^{-6}). Rhyolitic (left

side) and basaltic (right side) all show a dashed line indicating the signal to noise threshold; data within the dotted line indicates real signal while noise is outside of these areas. Other FORCs collected can be found in *Appendix C*.	
R1) E-45, an untreated rhyolitic sample. A mixture of PSD to MD behavior is shown by the vertical spread at $B_c = 0$, and the horizontal spread at $B_u = 0$.	**B1)** D270-R2, an untreated basaltic sample. Doman behavior ranging from SP to SD. Possible SP due to spread along the horizontal on the coercivity (B_c) axis.
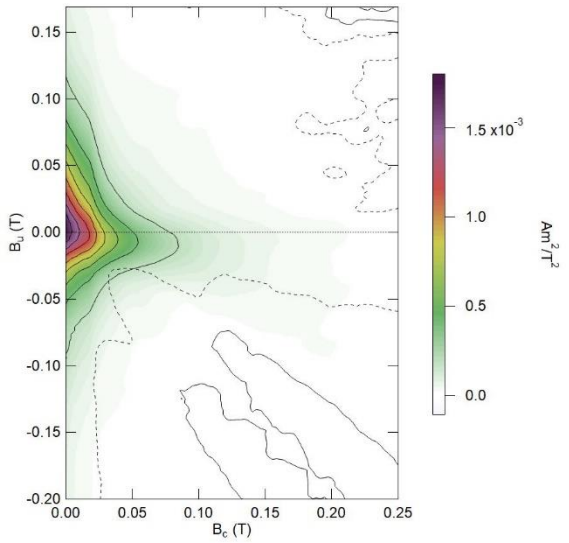	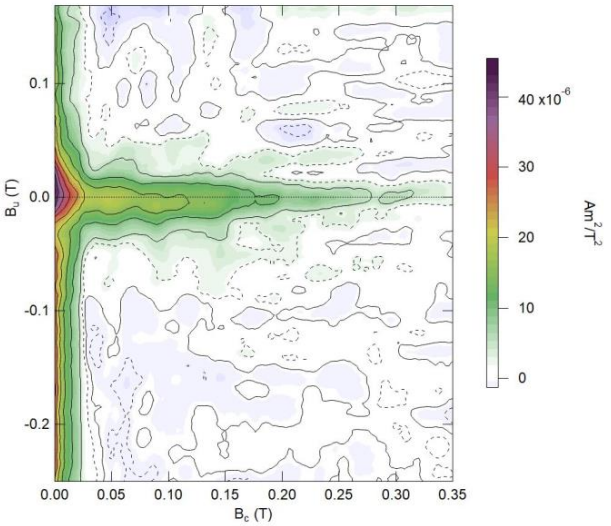
R2) C-06, a treated rhyolitic sample at 300°C for 1 day.	**B2)** C-53, a treated basaltic sample at 300°C for 3.2 days.
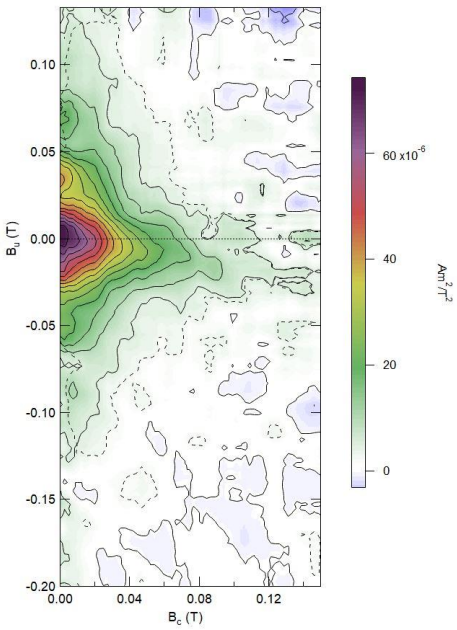	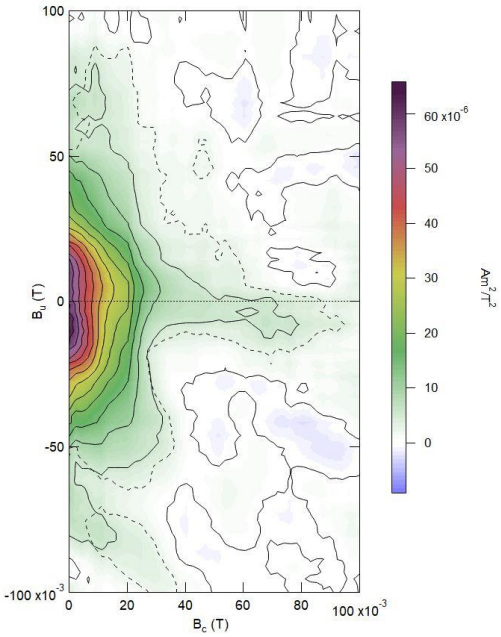
R3) Sample C-15, a hydrated rhyolitic sample at 300°C for 15 days.	**B3)** C-65 at a treated basaltic sample at 300°C for 15 days.

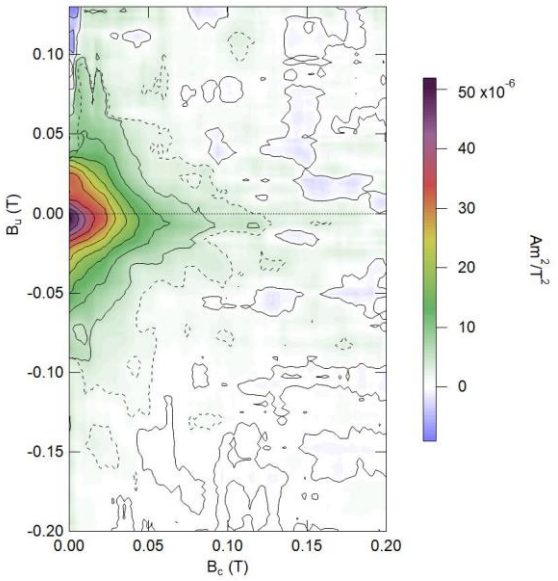

R4) C-33, a treated rhyolitic sample at 450°C for 10 days.

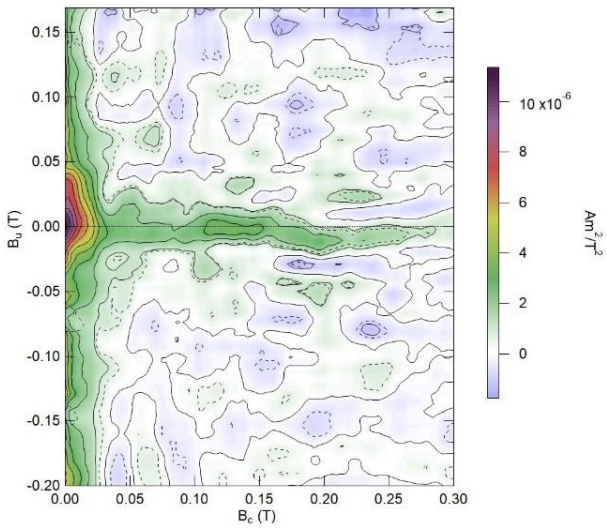

B4) C-71, a treated basaltic sample at 450°C for 1 day.

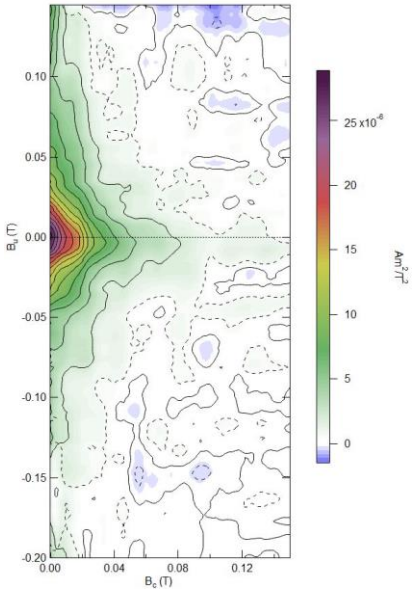

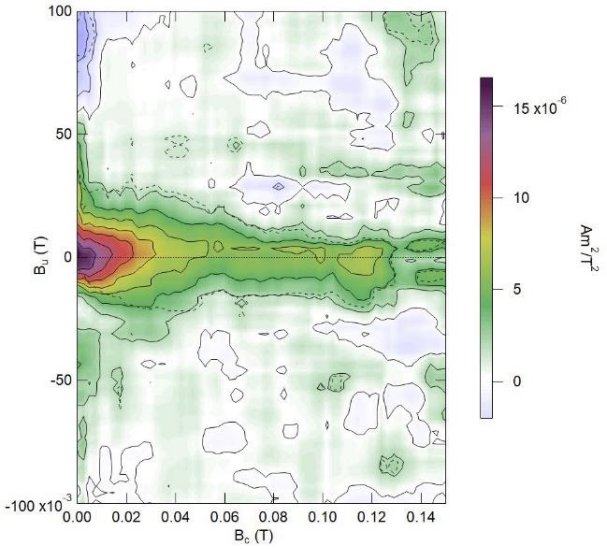

3.2.4 Hydration in Samples

Hydration effects from treatment were present in almost every hydrated rhyolitic sample in this study. It was generally found that the longer the hydration treatment, the larger the hydration rim present. There were no overall trends with any paleomagnetic properties and amount of material hydrated during treatment. While hydration rims were restricted to the

perimeter of most samples, some also had devitrified regions in the sample interior. C-02, the sample treated at 300°C for 1 day contained no hydration rim.

The basaltic specimens did not have the same trends in devitrification as the rhyolitic glasses. Basaltic samples were less devitrified than their rhyolitic counterparts. Higher temperature treatment resulted in overall more devitrification than lower temperature treatment, but the clear progression with treatment time was less evident. Basaltic samples also showed little to no devitrification within the interiors of the specimens, opposite to a majority of the rhyolitic samples.

Figure 3.21: Progressive hydration of rhyolitic glass samples. Calculated percentages of hydrated areas. Treatment temperature and time are listed. Image on left shows sample in full color, image on right shows mask which was the starting point for calculating the estimated hydrated area.

C-02, 0%, 300°C, 1 day

C-06 - 27% 300°C, 2.5 days

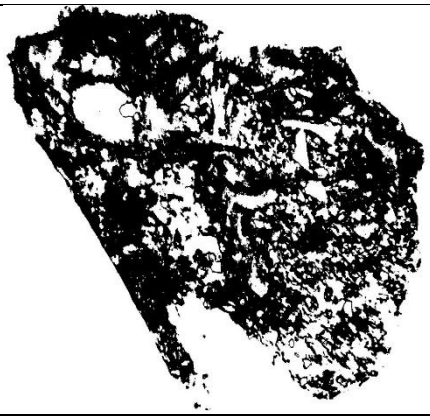

C-11 - 70%, 300°C, 6.3 days

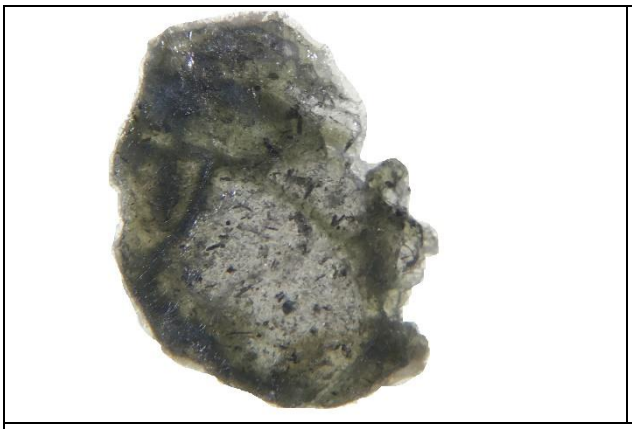
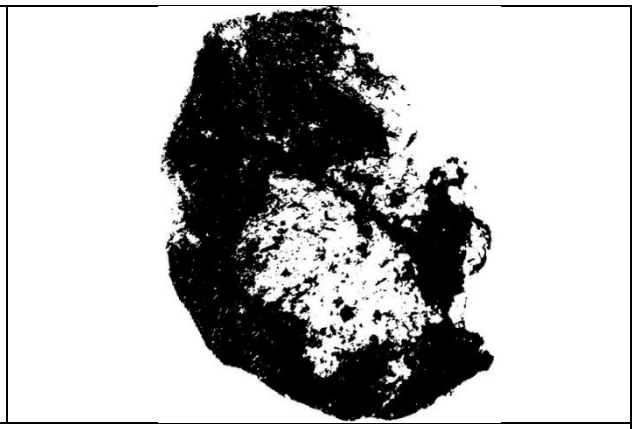

C-15 - 74%, 300°C, 15 days


C-19 - 42%, 450°C, 0.3 days


C-25 – 66%, 450°C, 1 day

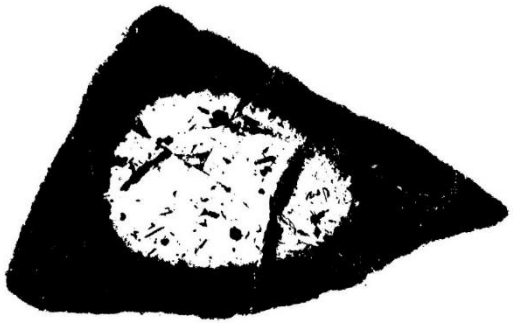

C-33 – 99%, 450°C, 10 days

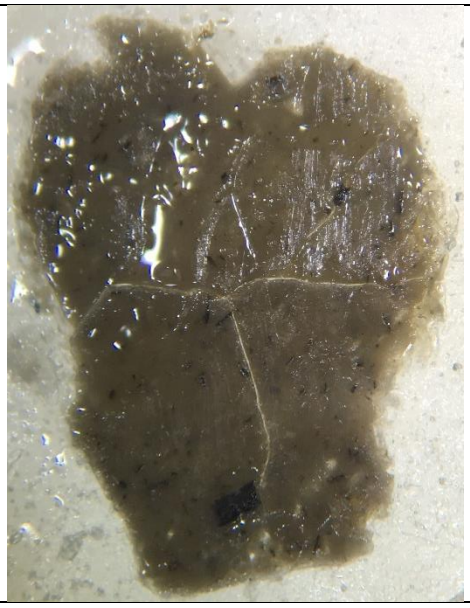

CHAPTER 4: DISCUSSION

4.1 Original Magnetic Mineralogy

The starting magnetic mineral assemblages of the fresh basaltic and rhyolitic natural glass samples vary drastically. The basaltic glass was mainly composed of SD, moderate-Ti titanomagnetite and with some superparamagnetic titanomagnetite. The rhyolitic glass had a different magnetic mineral assemblage of PSD to MD low-Ti titanomagnetite.

Rhyolitic glasses and basaltic glasses differed in several paleomagnetic properties observed when analyzing untreated samples. Saturation IRM experiments showed that rhyolitic glasses contained a higher volume of magnetic material compared to basaltic glasses. Rhyolitic glasses were found to have a lower coercivity and B_{cr} in both IRM and hysteresis experiments, supporting the theory that the magnetic mineral assemblage is mainly composed of PSD to MD grain sizes. Basaltic glasses had higher coercivity distributions and B_{cr} showing that the grain sizes of the magnetic remanence carrier were smaller. Hysteresis loops of basaltic glasses also showed SD behavior, with a higher remanence ratio compared to rhyolitic glasses, which had a smaller remanence ratio, more typical of non-uniform 'PSD'-like spin (**Figures 3.10-3.12**). Superparamagnetic components in the basaltic glasses were also seen in these FORC figures as vertical spread along the B_u axis near $x = 0$.

While both samples show different domain state behaviors, there is evidence for titanomagnetite in both sample compositions. Three-component IRM rhyolitic glass data showed a loss of IRM at around 500°C, indicating a low-Ti titanomagnetite component to the overall magnetic mineral assemblage (**Figure 3.7**). Basaltic glass three-component IRM data showed a

medium-Ti titanomagnetite component due to the lower temperature loss of IRM at 400°C compared to rhyolitic glasses (**Figure 3.8**).

4.2 Artificial Aging

4.2.1 Changes in Magnetic Mineralogy

The aging experiments attempted to accelerate the structural relaxation process that might normally occur over deep geologic time. Over deep geologic time, chemical and physical changes may occur to the magnetic mineral assemblages. Results presented here suggest that the changes of the magnetic mineral assemblages in these experiments were most likely a physical change rather than a chemical alteration. However, basaltic samples showed an increasing blocking temperature in three-component IRM experiments possibly showing oxidation effects.

Both rhyolitic and basaltic glasses showed an increase in sIRM values after artificial aging treatment (**Figure 3.2**). Higher temperatures provided greater change in sIRM to both rhyolitic and basaltic glasses over treatment time. This increase in sIRM could arise from grain growth if the glass transition temperature significantly lowered during the artificial aging process. An increase in sIRM could also imply a reduction in titanium, which would be accompanied by an increase in unblocking temperatures. While this is consistent with observations in the basaltic glass, the blocking temperatures in the rhyolitic glass do not change or decrease, inconsistent with a decrease in Ti.

Coercivity was investigated in both IRM acquisition and hysteresis experiments. IRM experiments were done on the same specimen over the course of the artificial aging treatment and are thus taken as a more reliable indicator of change than the hysteresis experiments which were all done post-treatment. A decrease in coercivity is typically associated with an increase in

average magnetic grain size. **Figures 3.3A-B** show the coercivity of remanence measurements of rhyolitic and basaltic glasses. Based on the IRM acquisition experiments, coercivity of remanence of basaltic glasses dropped over the artificial aging treatment, and the most drastic change took place at higher temperatures. This decrease in coercivity could support the idea of grain growth from SP and SD to larger SD or possibly small 'PSD'. The coercivity of rhyolitic glass showed more variability with time, but the overall trend was also a drop in coercivity, consistent with an increase in grain size.

In the IRM unmixing, rhyolitic specimens in the first aging experiment had primary components to the coercivity distribution skewed left while secondary components skewed to the right. Skew left distributions are commonly observed in natural mineral distributions. They typically are the result of thermal effects and interactions between different magnetic particles in a grain population (Heslop et al., 2004). Skew right distributions may indicate mixed mineralogy within a single-skew right component (Heslop et al., 2004). Skew-right distributions correlated with the growing extrapolated contribution of the secondary component to total MaxUnmix curves at longer treatment times in the 200°C and the 400°C MaxUnmix curves. Basaltic samples had a decreasing high-coercivity primary component and an increasingly prominent lower-coercivity secondary component of the total MaxUnmix curve at all temperature steps. Primary component curves of basaltic MaxUnmix curves typically skewed to the left.

The increase in sIRM combined with a decrease in coercivity are consistent with growth of existing magnetic grains as opposed to nucleation of new grains. The basaltic glass, dominated by the tiny SP to SD material, experienced a much larger change in sIRM and B_{cr} than the rhyolitic glass. Presuming grain growth proceeds by diffusion onto the surface area of the grain, the larger surface area to volume ratio of the SP-SD grains will result in a larger percentage

volume increase. The larger ‘PSD’-sized grains found in the rhyolitic glass have a smaller surface area to volume ratio, and a similar absolute increase in diameter will produce a smaller percentage increase in volume. The stable SD grain size range is also quite narrow, so magnetic mineral behavior could also change rapidly with a small increase in grain size, leading to the dramatic decrease in coercivity in the basaltic glass.

Figure 4.1 shows the normalized changes in magnetization and coercivity in the IRM acquisition experiments for the rhyolite samples. **Figure 4.1** is based on **Figure 1.5** from Ch. 1, which gives a summary of possible changes to magnetic mineralogy based on magnetization and coercivity. Over the course of artificial aging treatments, the first artificial aging IRM experiment to 240 days produced results that would support changes in magnetic properties due to grain growth within the magnetic mineral assemblage. This can be seen by the increase in normalized sIRM and the decrease in coercivity values in the IRM experiment. The second experiment, however, showed that the 200°C and 300°C samples have a decreased coercivity and a slightly decreased normalized magnetization after 30 days. This could possibly be the dissolution of material before grain growth within the sample. A decreased sIRM and a decreased coercivity could suggest the dissolution of the finest magnetic grains during artificial aging treatment. This would lead to a decrease in volume abundance with an increased average magnetic grain size.

Figure 4.1: Normalized changes in IRM experiments of rhyolitic glasses. The first IRM experiment was over 240 days. The second IRM experiment was over 30 days.

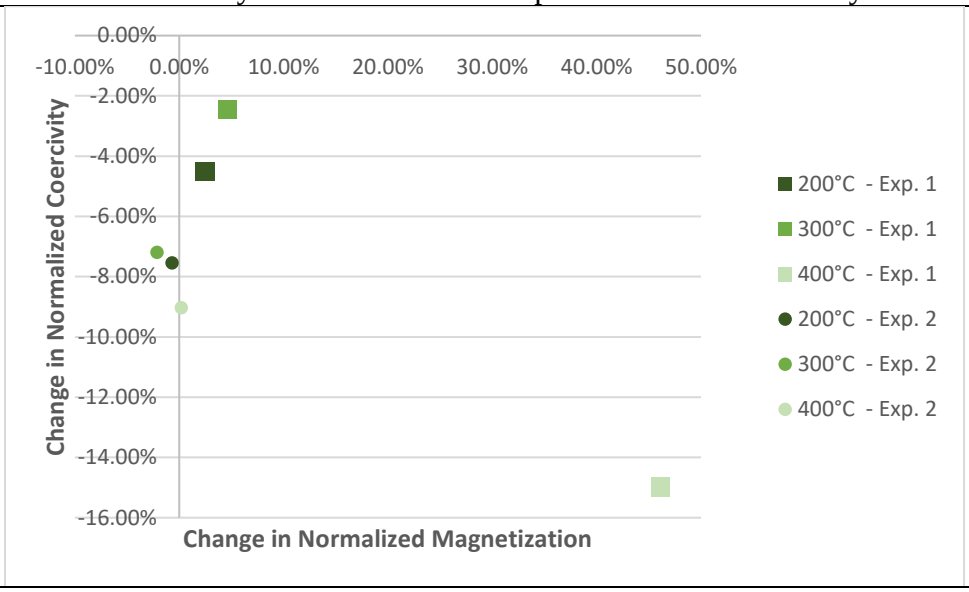

All the basaltic glass samples shown in **Figure 4.2** have changes in magnetic properties which could support magnetic grain growth within the specimens during artificial aging treatment. Basaltic glass samples had more "consistent" grain growth over different aging treatments while only the 400°C sample of rhyolitic glass showed a large change in sIRM.

Figure 4.2 Normalized changes in IRM experiments of basaltic glasses.

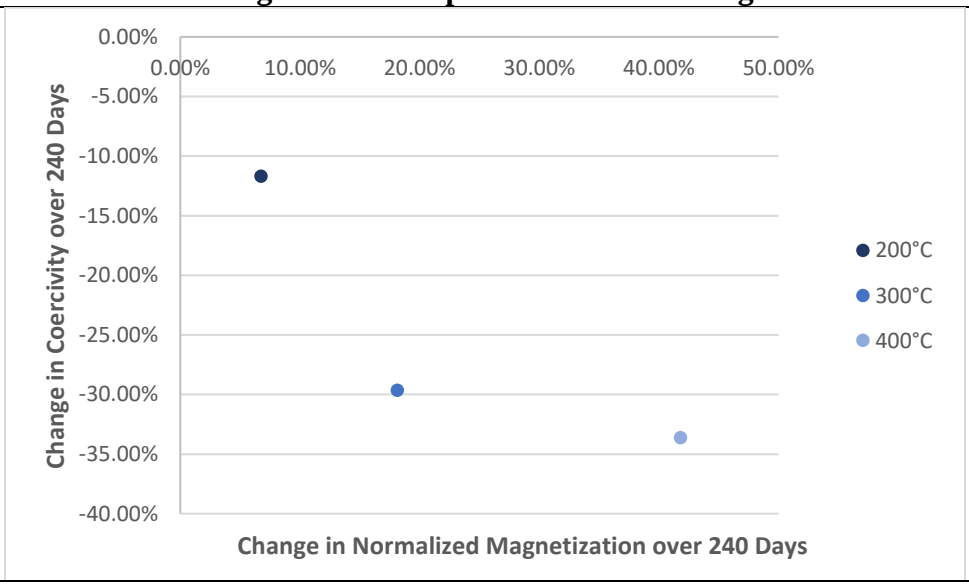

In the thermal demagnetization of IRM, basaltic samples typically lost a majority of the IRM at approximately 400℃, indicating a moderate-Ti titanomagnetite as the predominant magnetic carrier of the basaltic glass. However, continued unblocking up to 575°C suggests some crystals with less Ti, up to and including nearly pure magnetite. The rhyolitic glass had higher average blocking temperatures, with the greatest loss of IRM occurring ~500℃, consistent with low-Ti titanomagnetite. It also had a less prominent "hard" coercivity component over time, consistent with larger magnetic grain size.

In the thermal demagnetization of IRM experiment, most of the artificially aged basaltic glass samples had different properties compared to the unaged samples. A larger percentage of IRM was removed (unblocked) at higher thermal demagnetization temperatures in samples aged at higher temperature. This increase in unblocking temperatures could be caused by an increase in Ti-content of the titanomagnetite, but it may also be associated with the larger magnetic grain size. Blocking temperature increases with increasing grain size within the SD range. Another possibility is maghematization which would increase the Curie temperature of a the titanomagnetite.

4.2.2 Implications for Paleointensity

While exact paleointensity values could not be extracted from the data, TRM and pTRMs can be analyzed to determine possible changes in the magnetic mineral assemblages. In the paleointensity experiment, a majority of rhyolitic and basaltic samples failed a pTRM check, indicating that some alteration of magnetic materials was possible during heating phases of the paleointensity experiment. It should be kept in mind that because these samples had the NRM removed prior to the paleointensity experiment, the DRAT values may be artificially inflated. Nevertheless, DRATS show bigger failures in pTRMs for basaltic samples over the course of

paleointensity experiments, but this may partly be a function of the lower unblocking temperatures in the basaltic glass (**Figure 3.14**). Because of the higher unblocking temperatures in the rhyolitic glass, the rhyolitic glasses do not acquire as much pTRM at lower temperatures, leading to fewer pTRM check failures (**Figure 3.13**). If these pTRM failures in the basaltic glass samples are related to structural aging of the glass, then it may be the case that older basaltic glasses will be more likely to fail in paleointensity experiments.

These experiments were not analogous to what would happen in nature, but some observations have shown that magnetic mineral assemblage can change during artificial aging treatment. The data are mostly consistent with growth of pre-existing titanomagnetite grains, but there may also be some compositional changes. If these changes were to occur at ambient temperatures during natural aging, it could invalidate paleointensity experiments due to the changes in the magnetic recording assemblage. This means that the TRM acquired in nature will not be carried by the same mineral assemblage as the laboratory TRM, which in turn means paleointensity measurements of rhyolitic and basaltic glasses could vary based on age and not save magnetic remanence over "deep time" from formation.

4.3 Hydration Experiments

4.3.1 Introduction

Hydration treatments were conducted on samples at two different temperatures and four different time intervals to provide an idea into how hydration or rehydration in nature could affect paleomagnetic properties over deep time. Hydration effects occurred in both basaltic and rhyolitic glasses during hydration treatment. The rhyolitic glasses showed a higher percentage of

hydrated areas over treatment compared to their basaltic counterparts and could be further analyzed.

4.3.2 Hydration of Samples

Hydration of samples occurred in both the basaltic and rhyolitic glasses. In some cases, it was evident that the "perlitization" effect could be restricted to the perimeters of these samples. In some cases, cracks or fractures might arise in samples during hydration treatment. This could lead to hydrated areas of the interior of the sample. Typically, in both rhyolitic and basaltic glasses, the higher the temperature of the treatment, and the longer the treatment, the more hydration effects present on the exterior and the interior for rhyolitic glasses (**Figure 3.21**). **Figure 4.3** shows an example of hydration that took place in rhyolitic sample C-15 as slight interior alteration took place. **Figure 4.4** shows an example of a typical basaltic sample, which did not have an altered interior during hydration treatment.

Figure 4.3: A hydrated rhyolitic glass sample under transmitted light. Green and darker brown areas are hydrated material while the clearer color is the original rhyolitic glass present before hydration treatment. This sample, C-15, was hydrated at 300°C for 15 days.

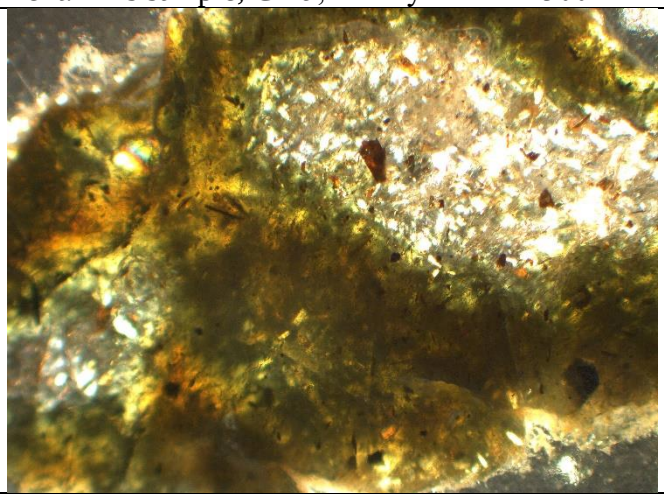

Figure 4.4: **A basaltic glass sample under transmitted light**. Lack of sufficient color contrast made it difficult to calculate specific percentages of devitrification over hydration treatment. Sample C-57 was hydrated at 300℃ for 6.2 days.

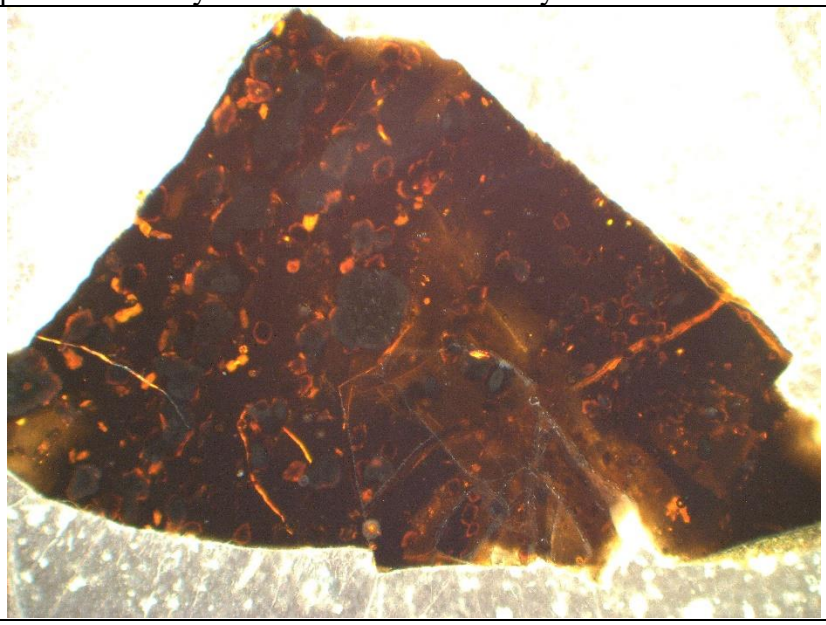

Hydrated rim percentages were used as an analog instead of previously proposed FTIR experiments. Unfortunately, basaltic glass was difficult to analyze in the same way due to the lack of color contrast. Samples with a decreased coercivity had higher percentages of hydrated areas.

4.3.3 Changes in Paleomagnetic Properties after Hydration

IRM acquisition experiments were conducted before and after treatment to provide an idea into how the samples' coercivity spectra and remanent magnetization were altered over treatment time. While B_{cr} did change during treatment in both rhyolitic and basaltic glasses, there were no clear and consistent trends to these changes, except for significantly larger changes in the basaltic glass compared to the rhyolitic glass, and an almost consistent decrease in B_{cr} at 300°C treatments in rhyolitic glasses over treatment time. Changes in B_{cr} of rhyolitic samples displayed smaller changes of ~0-10 mT, while basaltic samples had a change of ~5-60 mT

(**Figure 3.19**). Grain size change could lead to these changes in B_{cr}, and this means most samples experienced some type of physical change during hydration treatment. The increase in hydration may correlate with the decrease in coercivity at 300℃ only, and mineralogical changes are likely associated with the hydration rim.

To better understand what physical changes might have occurred within both the basaltic and rhyolitic glass samples, the change in sIRM is plotted against the change in B_{cr}, where both parameters were derived from the IRM acquisition experiments (**Figures 4.5 and 4.6)**. Assuming no major changes in composition, decreased coercivity suggests an increase in average magnetic grain size and increased coercivity suggests reduction of grain size. An increase in sIRM suggests a volume increase in magnetic particles, likewise assuming composition remains unchanged. Changes in coercivity and magnetization can be broken down into four different quadrants to explain changes in magnetic mineral assemblages.

If the sIRM of a sample increased, and the coercivity of remanence decreased (lower right quadrant of **Figs. 4.5 and 4.6**), that could indicate changes in magnetic properties due to grain growth within samples. If samples had a decreasing sIRM and a decreasing coercivity (lower left quadrant), this could suggest the dissolution of the finest magnetic grains during hydration experiments (decrease in volume abundance coupled with increased average grain size). This would theoretically only leave the coarser material and grains left within the magnetic mineral assemblage. If the coercivity increased and the sIRM decreased, (upper left quadrant) it suggests a net volume reduction in magnetic material that results in a finer magnetic grain size and/or a change in magnetic mineral composition. An increase in both sIRM and B_{cr} (upper right quadrant) can be explained by nucleation and growth of new fine-grained magnetic minerals without significantly growing the existing minerals. Other possibilities include a compositional

change in addition to domain state changes, such as might arise via oxidation-exsolution of titanomagnetite. This results in subdivision of the grains into Fe-rich and Ti-rich regions, which effectively reduces magnetic grain size and increases saturation remanence. Other explanations are also possible, but we do not have enough information to constrain these changes.

Five out of eight rhyolitic samples in **Figure 4.5** have a decreased normalized magnetization and a decreased coercivity of remanence, meaning the select dissolution of finer magnetic grains over hydration treatment. Two samples indicated a growth of grains through hydration treatment. One sample had reduced magnetization and increased coercivity, meaning grain size increased but the overall abundance of magnetic particles decreased during treatment.

Figure 4.5: Rhyolitic glass change in normalized magnetization versus change of coercivity of remanence.

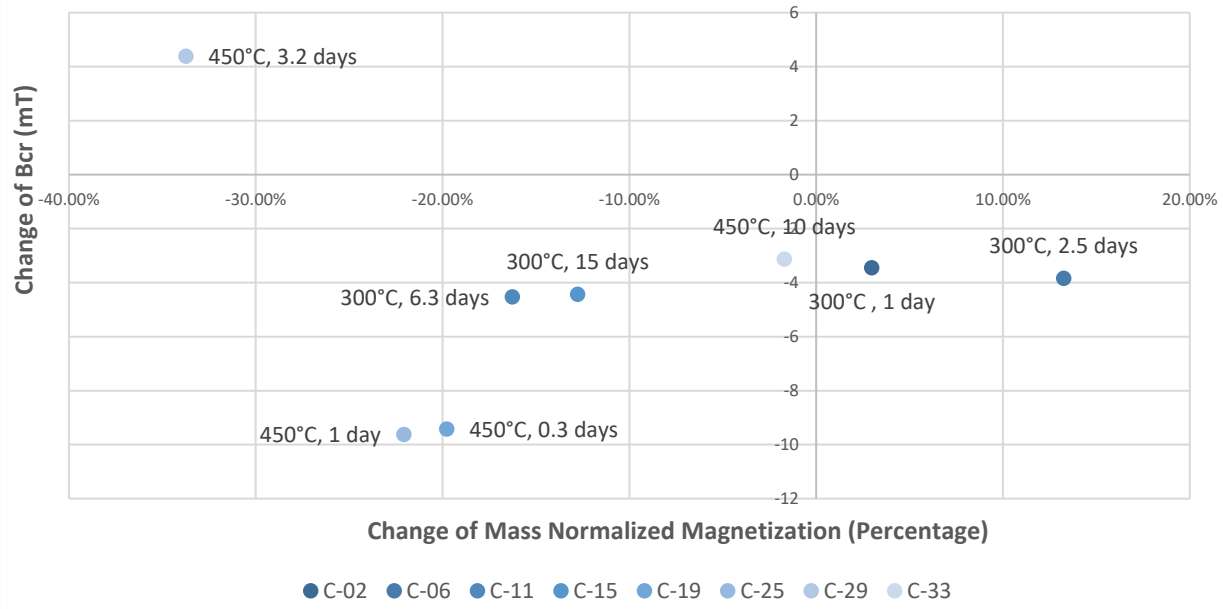

Basaltic samples in **Figure 4.6** have different trends compared to the rhyolitic glasses over hydration treatment. Three out of eight basaltic glasses showed an increased coercivity and an increased sIRM (upper right quadrant). This could possibly be explained by nucleation and

growth of new magnetic minerals. It could also be explained by chemical transformation, or the oxidation on the perimeter of the grain. The oxidized outer layers could lead to an increase in coercivity. One basaltic glass sample may have experienced select dissolution of finer grained particles (lower left quadrant), similar to half of the hydrated rhyolitic glasses. Two basaltic samples with increased coercivity and decreased magnetization possibly showed a net volume reduction in magnetic material that results in a finer magnetic grain size and/or a change in magnetic mineral composition.

Figure 4.6: Basaltic glass change in normalized magnetization versus change of normalized coercivity of remanence.

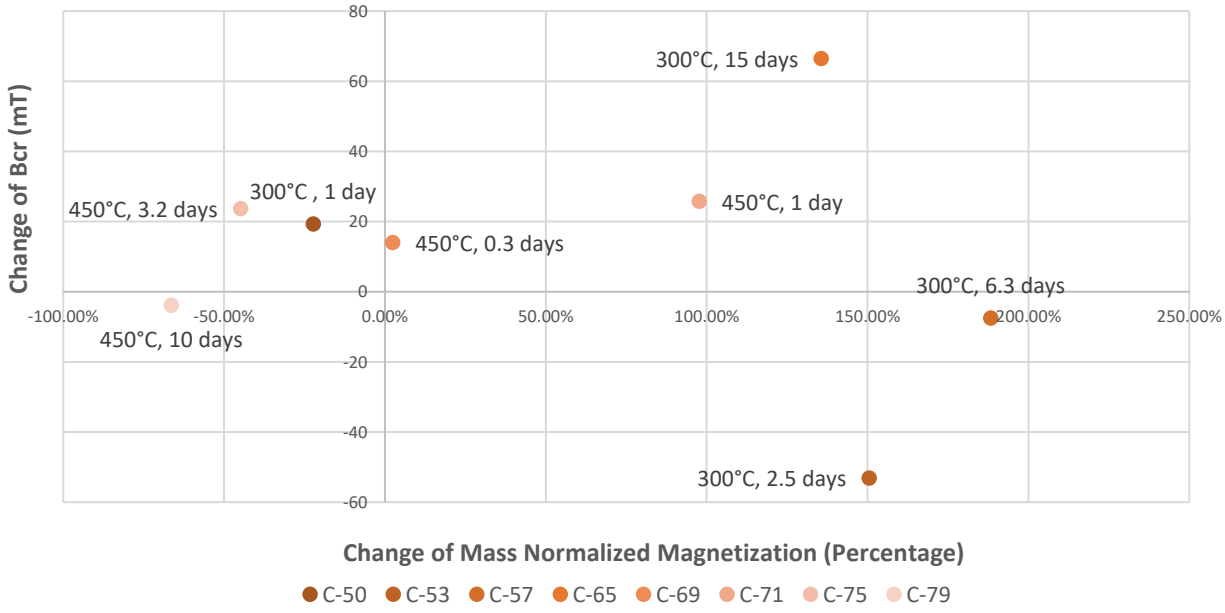

4.3.4 Comparison to Previous Studies

Comparing the data of this thesis to naturally occurring hydration values coupled with paleomagnetic data will provide insight into long term magnetization retention over deep time. Ferk et al. (2012) studied paleointensities and rock magnetic properties on rhyolitic glasses of

various hydration states in Iceland and conducted a similar study on phonolitic obsidian from Tenerife, Canary Islands, Spain (Ferk et al., 2011). Both Ferk et al. studies found that B_{cr}, M_{rs}, and M_s decreased if assumed hydration increased outward within the samples. There was also a trend toward more PSD-like behavior from SD with increasing hydration results (Ferk et al., 2011). The authors interpreted this as a preferential loss of the high coercivity minerals, which would be consistent with loss of the finest magnetic particles with increasing hydration.

Hydrated samples from our experiments showed a variety of behaviors, as seen in **Figure 4.5 and 4.6**. In a controlled environment in this study we experienced similar trends in some of the rhyolitic glasses from Ferk et al. (2012). A decreased sIRM and a decreased coercivity was prevalent in half of the rhyolitic glass samples from the experiments of this thesis. B_{cr} in rhyolitic glasses hydrated at 300℃ showed a consistent decrease in B_{cr} with increasing area of hydration. This would fit with the idea of a larger average grain size and partial dissolution of magnetic mineral particles within the rhyolitic glass samples. The results in the 300℃-temperature bracket of rhyolitic glasses matched the coercivity trends found in nature with hydrated material if hydration rims were an analog for water content in the rhyolitic samples. The normalized magnetization trends were found to have partially matched with the decreasing trend from Ferk et al., 2012, with only three rhyolitic glass samples experiencing an increased sIRM over treatment. Basaltic glasses had five samples increase in coercivity, but it was not consistent over treatment time. These results would not match the Ferk et al., 2012 study as they experienced opposite trends with the naturally occurring rhyolitic glass. While a simplistic interpretation of the hysteresis results suggests all hydrated basaltic glasses had decreased coercivity compared to untreated samples, these measurements were all made on different samples in this thesis. The

IRM acquisition data clearly show much more variable behavior, where some basaltic samples increased in coercivity and some decreased.

5.3.5 Future Work

Additional work that will aid in interpretation of the data presented here includes Fourier transform infrared spectroscopy (FTIR) experiments to explore the water content in parts of the specimens. A limited transect from core to rim would be ideal for the basaltic glasses, as only the exterior showed any hydration effects. It would be best to make compositional maps of water content for the rhyolitic glass samples since they experienced interior hydration effects. It is possible that the lack of clear trends in the magnetic data is linked to variability in rehydration that does not strictly correspond to treatment time or temperature. FTIR will allow for an assessment of intra- and inter-sample variability in water contents.

Glass transition temperature data will also help us understand how the rehydration may have influenced the glass structure.

5.3.6 Final Remarks on Hydration Experiments

Between basaltic and rhyolitic glasses, changes in the magnetic mineral assemblage occurred in both basaltic and rhyolitic glasses over hydration treatment. In rhyolites, a mixture of a partial dissolution of the finest grain sizes occurred, with a possible combination of increased average grain growth. No “new” nucleation took place within the rhyolitic glasses, with only the growth of existing grains seen in IRM studies.

This controlled hydration study indicates that the hydration state should be considered before selecting volcanic glass samples for paleointensity studies. As shown throughout the hydration discussion (**Sec 4.2**), fundamental changes in paleomagnetic properties in both

rhyolitic and basaltic glasses were created by the changes in grain behavior after hydration treatment. Grain growth, possible oxidation in basaltic glasses, change in average grain size, and the dissolution of the finest sized magnetic particles are all examples of what could occur to specimens if hydrated in nature. These changes in the magnetic mineral assemblages could yield drastic changes to paleointensity estimates on hydrated volcanic glasses. As explained in the background, there are numerous ways hydration or rehydration can occur in nature, and it is a common occurrence in obsidians. Hydration or rehydration of natural glass can skew our understanding of past magnetic field readings over "deep time" due to bias in paleointensity. Before paleointensity estimates should be considered for older volcanic glasses, hydration measurements should be undertaken to determine possible changes to the magnetic mineral assemblage over geologic time.

Chapter 5: CONCLUSION

To better understand how structural aging and hydration might alter magnetic mineralogy and influence paleointensity results, young, fresh basaltic and rhyolitic glasses were subjected to artificial aging and hydration treatments. The starting magnetic mineralogy of the basaltic glass was a mixture of SD and SP moderate-Ti titanomagnetite while rhyolitic glasses contained PSD to MD low-Ti titanomagnetite. The magnetic grains of these samples changed in both hydrated and artificial aging treatments, but with slightly different results.

Artificial aging experiments produced results which provided a deeper look into how change in structural relaxation over geologic time might affect paleointensity estimates of glass. Three different artificial aging experiments at 200°C, 300°C, and 400°C were conducted over 240 days. Over the course of artificial aging treatments, saturation IRM increased and coercivity decreased in both basaltic and rhyolitic glasses, but basaltic glasses had more drastic decreases in coercivity over treatment time and temperature. These changes in saturation magnetization and coercivity are interpreted to arise from grain growth due to a possible lowering of the glass transition temperature. Paleointensity experiments conducted on aged specimens show changes in the pTRM acquisition over the experiment in both rhyolitic and basaltic glasses, but this effect is much more prevalent in basaltic glasses. The sense of these changes is consistent with continued grain growth during reheating for the paleointensity experiments, and again suggests a lowering of the glass transition temperature. Looking at artificially aged glasses in a controlled laboratory setting shows that age would most likely affect the paleointensity of the sample.

Hydration treatments were conducted at 300°C and 450°C over four different periods of time. Hydration and rehydration of volcanic glasses are common in nature, and previous work

(Ferk et al., 2011; 2012) has shown that re-hydration in obsidian can affect coercivity, magnetization, and paleointensity in naturally occurring samples. In this study, similar (but not entirely consistent) trends were found in coercivity measurements. The observed changes in magnetic properties could be explained by a variety of processes, including grain nucleation, grain growth, select dissolution of the finest grains, and possible compositional changes, including oxidation. Hydration rims were observed in nearly all the samples. In both volcanic glasses, increased hydration effects occurred during longer treatment times and higher temperatures. The 300°C rhyolitic glass, experienced a decreased B_{cr} with an increased area of hydration within the sample. No other clear trends were found between hydration treatment, coercivity, and magnetization. Because changes in the magnetic mineralogy arising from hydration will adversely impact paleointensity estimates, natural glasses should be assessed for their water content and possible magnetic grain changes before paleointensity experiments.

References

Angell, C. A., Ngai, K. L., McKenna, G. B., McMillan, P. F., and Martin, S. W. (2000). Relaxation in glass forming liquids and amorphous solids. *Journal of Applied Physics,* **88**(6), 3113–3157. DOI:10.1063/1.1286035

Anovitz, L. M., Cole, D. R., and Fayek, M. (2008). Mechanisms of rhyolitic glass hydration below the glass transition. *American Mineralogist,* **93**(7), 1166–1178. DOI: 10.2138/am.2008.2516

Biggin, A. J., Piispa, E. J., Pesonen, L. J., Holme, R., Paterson, G. A., Veikkolainen, T., and Tauxe, L. (2015). Palaeomagnetic field intensity variations suggest Mesoproterozoic inner-core nucleation. *Nature,* **526**(7572), 245–248. DOI:10.1038/nature15523

Bono, R K. Tarduno, J.A. Nimmo, F., and Cottrell, R.D. (2019). Young inner core inferred from Ediacaran ultra-low geomagnetic field intensity. *Nature Geoscience*, **12**(2), 143–147. DOI:10.1038/s41561-018-0288-0

Bowles, J., Gee, J. S., Kent, D. V., Bergmanis, E., and Sinton, J. (2005). Cooling rate effects on paleointensity estimates in submarine basaltic glass and implications for dating young flows. *Geochemistry, Geophysics, Geosystems*, **6**(7), 1–24. DOI:10.1029/2004GC000900

Bowles, J., Gee, J. S., Kent, D., Perfit, M., Soule, S., and Fornari D. (2006), Paleointensity applications to timing and extent of eruptive activity, 9°–10°N East Pacific Rise. *Geochemistry, Geophysics, Geosystems,* **7**(6), Q06006, DOI: 10.1029/2005GC001141

Bowles, J. A., Gee, J. S., Burgess, K., and Cooper, R. F. (2011). Timing of magnetite formation in basaltic glass: Insights from synthetic analogs and relevance for geomagnetic paleointensity analyses. *Geochemistry, Geophysics, Geosystems,* **12**(2), Q02001. DOI:10.1029/2010GC003404

Carlut, J., and Kent, D. V. (2000). Paleointensity record in zero-age submarine basalt glasses: Testing a new dating technique for recent MORBs. *Earth and Planetary Science Letters,* **183**(3), 389–401. DOI:10.1016/S0012-821X(00)00291-0

Carlut, J., and Kent, D. V. (2002). Grain-size dependent paleointensity results from very recent mid-oceanic ridge basalts. *Journal of Geophysical Research,* **107**(B3), EPM 2-1 – EPM 2-12. DOI:10.1029/2001JB000439

Carlut, J., Cormier, M. H. Kent, D. V. Donnelly, K. E. and Langmuir C. H. (2004). Timing of volcanism along the northern East Pacific Rise based on paleointensity experiments on basaltic glasses. *Journal of Geophysical Research,* **109**, B04104. DOI:10.1029/2003JB002672.

Caress, D.W., Clague, D.A., Paduan, J.B., Martin, J.F., Dreyer, B.M., and Chadwick Jr., W.W. (2011). Repeat bathymetric surveys at 1-metre resolution of lava flows erupted at Axial Seamount. *Nature Geoscience,* **5**, 483–488. DOI: 10.1029/2020GC009136

Cerling T. E., Brown F. H. and Bowman J. R., (1985). Low-temperature alteration of volcanic glass: hydration, Na, K, ^{18}O, and Ar mobility. *Chemical Geology,* **52**(3-4), 281–293. DOI: 10.1016/0168-9622(85)90040-5

Coe, R. S. (1967). The determination of paleointensities of the earth's magnetic field with emphasis on mechanisms which could cause non-ideal behavior in Thellier's method. *Journal of Geomagnetism and Geoelectricity*, **19**(3), 157–179. DOI: 10.5636/jgg.19.157

Danyushevsky, L.V., Batiza, R., Eggins, S.M., Christie, D.M. (2000). H_2O abundance in depleted to moderately enriched mid-ocean ridge magmas; Part I: incompatible behaviour, implications for mantle storage, and origin of regional variations. *Journal of Petrology*, **41**(8), 1329–1364. DOI: 10.1093/petrology/41.8.1329

DeGroat-Nelson, P.J., Cameron, B.I., Fink, J.H., and Holloway, J.R. (2001). Hydrogen isotope analysis of rehydrated silicic lavas: implications for eruption mechanisms. *Earth and Planetary Science Letters*, **185**(3–4), 331-341. DOI:10.1016/S0012-821X(00)00379-4.

Denton, J., Tuffen, H., Gilbert, J., and Odling, N. (2009). The hydration and alteration of perlite and rhyolite. *Journal of the Geological Society*. **166**(5), 895–904. DOI: 10.1144/0016-76492008-007

Deubener J, Mueller R, Behrens H., and Heide G. (2003). Water and the glass transition temperature of silicate melts. *Journal of Non-Crystalline Solids*. **330**(1-3), 268–273. DOI: 10.1016/S0022-3093(03)00472-1

Dingwell, D. B. and Webb, S. L. (1990). Relaxation in silicate melts. *European Journal of Mineralogy*, **2**(2), 427–449. DOI: 10.1127/ejm/2/4/0427

Dunlop, D. J. (2002). Theory and application of the Day plot (M_{rs}/M_s versus H_{cr}/H_c): 1. Theoretical curves and tests using titanomagnetite data, *Journal of Geophysical Research*, **107**(B3), 2056. DOI: 10.1029/2001JB000487

Ferk, A., Aulock, F. W. v., Leonhardt, R., Hess, K.-U., and Dingwell, D. B. (2010). A cooling rate bias in paleointensity determination from volcanic glass: An experimental demonstration. *Journal of Geophysical Research*, **115**, B08102. DOI:10.1029/2009JB006964.

Ferk, A., Leonhardt, R., von Aulock, F.W., Hess, K.U., and Dingwell, D.B. (2011). Paleointensities of phonolitic obsidian: influence of emplacement rotations and devitrification. *Journal of Geophysical Research.*, **116**, B12113, 1–18. DOI:10.1029/2011JB008397

Ferk, A., Denton, J. S., Leonhardt, R., Tuffen, H., Koch, S., Hess, K. U., and Dingwell, D. B., (2012). Paleointensity on volcanic glass of varying hydration states. *Physics of the Earth and Planetary Interiors*, **208–209**, 25–37. DOI: 10.1016/j.pepi.2012.06.004

Frahm, E., and Feinberg, J. M. (2013). From flow to quarry: magnetic properties of obsidian and changing the scale of archaeological sourcing. *Journal of Archaeological Science*, **40**(10), 3706-3721. DOI: 10.1016/j.jas.2013.04.029

Friedman I., Smith R. L., and Long W. D. (1966). Hydration of natural glass and formation of perlite. *Geological Society of America Bulletin*, **77**(3), 323-328. DOI: 10.1130/0016-7606(1966)77[323:HONGAF]2.0.CO;2

Glatzmaier, G. and Roberts, P. (1996). Rotation and magnetism of Earth's inner core. *Science*, **274**(5294), 1887–1891. DOI: 10.1126/science.274.5294.1887

Hamilton, L. H. (1992). The oldest abundant volcanic glass on Earth. *Australian Journal of Earth Sciences*, **39**(1), 55-59. DOI: 10.1080/08120099208728000

Heide, K., Woermann, E., and Ulmer., G. (2008). Volatiles in pillows of the Mid-Ocean-Ridge Basalt (MORB) and vitreous basaltic rims. *Chemie der Erde.* **68**(4), 353-368. DOI: 10.1016/j.chemer.2008.07.001

Heslop, D., McIntosh, G., and Dekkers, M.J. (2004). Using time and temperature dependent Preisach models to investigate the limitations of modelling isothermal remanent magnetization acquisition curves with cumulative log Gaussian functions. *Geophysical Journal International*, **157**(1), 55-63. DOI: 10.1111/j.1365-246X.2004.02155.x

Jacobs, J. (1953). The Earth's Inner Core. *Nature*, **172**, 297–298. DOI:10.1038/172297a0

Jantzen, C. M., Brown, K. G., and Pickett, J. B. (2010). Durable Glass for Thousands of Years. *International Journal of Applied Glass Science*, **1**(1), 38–62. DOI:10.1111/j.2041-1294.2010.00007.x

Kelley, K. A., and Cottrell, E. (2009). Water and the Oxidation State of Subduction Zone Magmas. *Science*, **325**(5940), 605–607. DOI:10.1126.science.1174156.

Kruber, C., Thorseth, I. H., and Pedersen R. B. (2008). Seafloor alteration of basaltic glass: Textures, geochemistry, and endolithic microorganisms. *Geochemistry, Geophysics, Geosystems*, **9**(12), Q12002, DOI:10.1029/2008GC002119.

Leonhardt, R., Matzka, J., Nichols, A. R. L., and Dingwell, D. B. (2006). Cooling rate correction of paleointensity determination for volcanic glasses by relaxation geospeedometry. *Earth and Planetary Science Letters*, **243**(1), 282–292. DOI: 10.1016/j.epsl.2005.12.038

Lofgren, G. (1971). Experimentally produced devitrification textures in natural rhyolitic glass. *Geological Society of America Bulletin*, **82**(1), 111-124. DOI: 10.1130/0016-7606(1971)82[111:EPDTIN]2.0.CO;2

Lowrie, W. (1990). Identification of ferromagnetic minerals in a rock by coercivity and unblocking temperature properties. *Geophysical Research Letters.* **17**(2), 159-162. DOI: 10.1029/GL017i002p00159

McElhinny, M. and McFadden, P. (2000). Paleomagnetism: Continents and Oceans. *Academic Press.*

Millar, C.I., King, J.C., Westfall, R.D., Alden, H.A., and Delany, D.L. (2006), Late Holocene forest dynamics, volcanism, and climate change at Whitewing Mountain and San Joaquin Ridge, Mono County, Sierra Nevada, CA, USA, *Quaternary Research*, **66**(2), 273–287. DOI: 10.1016/j.yqres.2006.05.001

Miller, C. D. (1985). Holocene eruptions at the Inyo volcanic chain, California: implications for possible eruptions in Long Valley caldera. *Geology*, **13**, 14–17. DOI: 10.1130/0091-7613

Moynihan, C.T., Crichton, S.N., and Opalka, S.M. (1991). Linear and non-linear structural relaxation. *Journal of Non-Crystalline Solids*, **131–133**(Part 1), 420-434. DOI: 10.1016/0022-3093(91)90335-4.

Newman S., Epstein S. and Stolper E. (1988) Water, carbon dioxide, and hydrogen isotopes in glasses from the ca. 1340 A.D. eruption of the Mono Craters, California: constraints on degassing phenomena and initial volatile content. *Journal of Volcanology and Geothermal Research,* **35**(1–2), 75–96. DOI: 10.1016/0377-0273(88)90007-8

Nolan G.S. and Bindeman I.N. (2013). Experimental investigation of rates and mechanisms of isotope exchange (O, H) between volcanic ash and isotopically-labeled water. *Geochimica et Cosmochimica Acta*, **111**, 5–27. DOI: 10.1016/j.gca.2013.01.020

Parruzot B., Jollivet P., Rébiscoul D., and Gin S. (2015). Long-term alteration of basaltic glass: mechanisms and rates. *Geochimica et Cosmochimica Acta,* **154**, 28-48. DOI: 10.1016/j.gca.2014.12.011

Perfit, M., Cann, J., and Fornari, D., Engels, J., Smith, D., Ridley, W., and Edwards, M. (2003). Interaction of sea water and lava during submarine eruptions at mid-ocean ridges. *Nature*, **426**(6962)**,** 62–65. DOI:10.1038/nature02032

Pick, T., and Tauxe, L. (1993). Holocene paleointensities: Thellier experiments on submarine basaltic glass from the East Pacific Rise. *Journal of Geophysical Research*, **98**(B10), 17949–17964. DOI: 10.1029/93JB01160

Robertson, D.J., and France, D.E. (1994). Discrimination of remanence-carrying minerals in mixtures, using isothermal remanent magnetisation acquisition curves, *Physics of Earth and Planetary Interiors*, **82**(3-4), 223-234. DOI: 10.1016/0031-9201(94)90074-4

Seligman, A.N., Bindeman, I.N., Watkins, J. M., and Ross, A.M. (2016). Water in volcanic glass: From volcanic degassing to secondary hydration. *Geochimica et Cosmochimica Acta*, **191**, 216-238. DOI:10.1016/j.gca.2016.07.010

Selkin, P., and Tauxe, L. (2000). Long-term variations in paleointensity. *Philosophical Transactions of the Royal Society*, **358**(1768), 1065–1088. DOI: 10.1098/rsta.2000.0574

Shaw, J. (1974). A new method of determining the magnitude of the paleomagnetic field application to 5 historic lavas and five archeological samples. *The Geophysical Journal of the Royal Astronomical Society*, **39**(1), 133–141. DOI: 10.1111/j.1365-246X.1974.tb05443.x

Smirnov, A. V., and Tarduno J. A., (2003). Magnetic hysteresis monitoring of Cretaceous submarine basaltic glass during Thellier paleointensity experiments: Evidence for alteration and attendant low field bias. *Earth and Planetary Science Letters,* **206**, 571–585. DOI:10.1016/S0012-821X(02)01123-8

Stewart, L., Christopher A., Fortunato, C., Fortunato, L., Vallino, J., Huber, J., Butterfield, D., and Holden, J. (2019). Fluid geochemistry, local hydrology, and metabolic activity define methanogen community size and composition in deep-sea hydrothermal vents. *The ISME Journal*, **13**(7). 1711-1721. DOI:10.1038/s41396-019-0382-3

Stroncik N. A. and Schmincke H., (2002). Palagonite – a review. *International Journal of Earth Sciences,* **91**(4), 680-697. DOI: 10.1007/s00531-001-0238-7

Tarduno, J. A., Cottrell, R. D., Davis, W. J., Nimmo, F., and Bono, R. K. (2015). A Hadean to Paleoarchean geodynamo recorded by single zircon crystals. *Science*, **349**(6247), 521-524. DOI: 10.1126/science.aaa9114

Tarduno, J. A., Cottrell, R. D., Bono, R. K., Oda, H., Davis, W. J., Fayek, M., Erve, O. van 't, Nimmo, F., Huang, W., Thern, E. R., Fearn, S., Mitra, G., Smirnov, A. V, and Blackman, E. G. (2020). Paleomagnetism indicates that primary magnetite in zircon records a strong Hadean geodynamo. *Proceedings of the National Academy of Sciences*, **117**(5), 2309 – 2318. DOI:10.1073/pnas.1916553117

Tauxe, L., Mullender, T. A. T., and Pick, T. (1996). Potbellies, wasp-waists, and superparamagnetism in magnetic hysteresis. *Journal of Geophysical Research,* **101**(B1), 571–583. DOI: 10.1029/95JB03041

Tauxe, L., and Love, J. J., (2003). Paleointensity in Hawaiian Scientific Drilling Project Hole (HSDP2): Results from submarine basaltic glass. *Geochemistry, Geophysics, Geosystems,* **4**(2), 8702. DOI:10.1029/2001GC000276

Tauxe, L., and Staudigel, H. (2004). Strength of the geomagnetic field in the Cretaceous Normal Superchron: New data from submarine basaltic glass of the Troodos Ophiolite. *Geochemistry, Geophysics, Geosystems,* **5**(2), Q02H06. DOI:10.1029/2003GC000635

Tauxe, L., (2006). Long-term trends in paleointensity: The contribution of DSDP/ODP submarine basaltic glass collections. *Physics of the Earth and Planetary Interiors,* **156**(3–4), 223-241. DOI: 10.1016/j.pepi.2005.03.022

Tauxe, L., Gee, J. S., Steiner, M. B., and Staudigel, H., (2013). Paleointensity results from the Jurassic: New constraints from submarine basaltic glasses of ODP Site 801C. *Geochemistry, Geophysics, Geosystems,* **14**(10), 4718-4733. DOI: 10.1002/2013GC004704

Tauxe, L, Banerjee, S.K., Butler, R.F. and van der Voo R, (2018). Essentials of Paleomagnetism, 5th Web Edition.

Thellier, E., and O. Thellier, (1959). Sur l'intensité du champ magnétique terrestre dans le passé historique et géologique. *Annales Geophysicae,* **15**, 285–378.

Valle N., Verney-Carron A., Sterpenich J., Libourel G., Deloule E.and Jollivet P., (2010). Elemental and isotopic (^{29}Si and ^{18}O) tracing of glass alteration mechanisms. *Geochimica et Cosmochimica Acta,* **74**(12), 3412–3431. DOI: 10.1016/j.gca.2010.03.028

Verney-Carron, A. Vigier, N. and Millot, R., (2011). Experimental determination of the role of diffusion on Li isotope fractionation during basaltic glass weathering. *Geochimica et Cosmochimica Acta,* **75**(12), 3452-3468. DOI: 10.1016/j.gca.2011.03.019

Zhou, W., Van der Voo, R., Peacor, D., Zhang Y., (2000). Variable Ti-content and grain size of titanomagnetite as a function of cooling rate in very young MORB. *Earth and Planetary Science Letters,* **179**, 9-20. DOI: 10.1016/S0012-821X(00)00100-X

Appendix A:

Table A1: The coercivity peaks (B_h) of artificially aged samples in MaxUnmix peaks. The "sd" is the standard deviation of the coercivity peak from each component. Rhyolitic glasses have two experiments, one over 240 days, and one over 30 days (Exp. 2).

	Component 1		Component 2	
Rhyolitic Glass				
	Bh	sd	Bh	sd
200°C Rhyolite, 0 Days	52.05208401	1.095487064		
200°C Rhyolite, 15 Days	51.14921849	1.081092478		
200°C Rhyolite, 30 Days	50.30329281	1.009477688		
200°C Rhyolite, 60 Days	43.82438933	1.045574535	272.4060863	1.071190161
200°C Rhyolite, 120 Days	44.485443	1.052576879	264.1705664	1.083781947
200°C Rhyolite, 240 Days	42.66077706	1.063773692	281.9454905	1.068545869
300°C Rhyolite, 0 Days	45.71061651	1.108553233		
300°C Rhyolite, 15 Days	41.06366029	1.112284606		
300°C Rhyolite, 30 Days	43.27187751	1.013070142		
300°C Rhyolite, 60 Days	45.83895518	1.005770545		
300°C Rhyolite, 120 Days	42.90157353	1.002959316		
300°C Rhyolite, 240 Days	44.84302462	1.014222738		
400°C Rhyolite, 0 Days	45.12889289	1.150001389		
400°C Rhyolite, 15 Days	42.1339252	1.161083744		
400°C Rhyolite, 30 Days	34.66948361	1.070159371	259.1370453	1.051466311
400°C Rhyolite, 60 Days	23.16148209	1.084558997	172.7275333	1.110590245
400°C Rhyolite, 120 Days	29.07865347	1.092165859	227.4287218	1.132386159
400°C Rhyolite, 240 Days	33.45252482	1.038302367	275.9997925	1.103977316
Exp. 2				
200°C Rhyolite, 0 Days	42.93472093	1.070690515	296.5592391	1.120186324
200°C Rhyolite, 7 Days	34.43993172	1.073521106	241.9218239	1.100347444
200°C Rhyolite, 15 Days	43.58734524	1.097054154	255.3488534	1.16844183
200°C Rhyolite, 30 Days	35.46824577	1.056002158	247.4270654	1.051050698
300°C Rhyolite, 0 Days	31.98822466	1.090657834	229.6326507	1.090245296
300°C Rhyolite, 7 Days	35.41968192	1.076758531	241.5749527	1.077542466
300°C Rhyolite, 15 Days	40.61391804	1.062929246	267.0821964	1.035949898
300°C Rhyolite, 30 Days	35.94370094	1.062311642	255.6719387	1.069021871
400°C Rhyolite, 0 Days	37.48433582	1.07475175	248.9771136	1.057535328
400°C Rhyolite, 7 Days	38.44745213	1.055830322	269.0207137	1.054089817
400°C Rhyolite, 15 Days	36.07827987	1.050619753	256.9709973	1.050664436
400°C Rhyolite, 30 Days	32.38611762	1.062714494	230.6622166	1.086735582
Basaltic Glass				
200°C Basalt, 0 Days	162.5235398	1.00761807		
200°C Basalt, 15 Days	159.2812503	1.013756244		
200°C Basalt, 30 Days	158.646092	1.003708105		
200°C Basalt, 60 Days	168.0270084	1.014655824	114.3742429	1.078325456
200°C Basalt, 120 Days	170.1277005	1.025453502	85.44508257	1.250118926

200°C Basalt, 240 Days	165.3273827	1.020809403	114.5524062	1.042610803
300°C Basalt, 0 Days	176.2747922	1.00893353		
300°C Basalt, 15 Days	156.3744586	1.007356708		
300°C Basalt, 30 Days	166.305598	1.018899104	90.76877503	1.140898641
300°C Basalt, 60 Days	153.6237984	1.015538273	98.13887026	1.076688202
300°C Basalt, 120 Days	149.5234947	1.023728446	65.71275435	1.250181459
300°C Basalt, 240 Days	139.4714857	1.027312723	45.41323337	1.187490392
400°C Basalt, 0 Days	143.5184481	1.007416667		
400°C Basalt, 15 Days	104.830387	1.006024331		
400°C Basalt, 30 Days	132.6769669	1.086655601	64.59250161	1.228280357
400°C Basalt, 60 Days	114.645074	1.0614861	79.4363868	1.146186251
400°C Basalt, 120 Days	104.6170336	1.03606399	80.4818445	1.051643491
400°C Basalt, 240 Days	112.4924141	1.039676878	71.45385014	1.044137859

Table A2: The dispersion parameters (DP) of artificially aged samples in MaxUnmix curves. The "sd" is the standard deviation of the dispersion parameters from each component. Rhyolitic glasses have two experiments, one over 240 days, and one over 30 days (Exp. 2).

	Component 1		Component 2	
Rhyolitic Glass				
	DP	sd	DP	sd
200°C Rhyolite, 0 Days	3.82942	1.06291		
200°C Rhyolite, 15 Days	3.6947	1.05253		
200°C Rhyolite, 30 Days	3.4728	1.00675		
200°C Rhyolite, 60 Days	3.21499	1.02836	1.66468	1.053
200°C Rhyolite, 120 Days	3.3646	1.02949	1.58945	1.07158
200°C Rhyolite, 240 Days	3.1348	1.03609	1.66866	1.06459
300°C Rhyolite, 0 Days	4.03586	1.0719		
300°C Rhyolite, 15 Days	3.98079	1.07723		
300°C Rhyolite, 30 Days	3.67236	1.00974		
300°C Rhyolite, 60 Days	3.56353	1.00431		
300°C Rhyolite, 120 Days	3.87538	1.00204		
300°C Rhyolite, 240 Days	3.64556	1.00966		
400°C Rhyolite, 0 Days	4.23816	1.09649		
400°C Rhyolite, 15 Days	4.08896	1.10323		
400°C Rhyolite, 30 Days	3.14961	1.03899	1.67175	1.0295
400°C Rhyolite, 60 Days	2.48979	1.02729	1.8349	1.0491
400°C Rhyolite, 120 Days	2.73966	1.04282	1.74521	1.01941
400°C Rhyolite, 240 Days	2.69735	1.01885	1.7868	1.02947
Exp. 2				
200°C Rhyolite, 0 Days	0.537206658	0.004576159	0.819095476	0.126892104
200°C Rhyolite, 7 Days	0.518463135	0.009344958	0.724929495	0.17913938
200°C Rhyolite, 15 Days	0.492213393	0.013314228	0.64713814	0.119513209
200°C Rhyolite, 30 Days	0.494493275	0.01344403	0.645050998	0.108151673

300°C Rhyolite, 0 Days	0.531329908	0.00641416	0.754782525	0.096429956
300°C Rhyolite, 7 Days	0.501821759	0.005380268	0.712217252	0.085478773
300°C Rhyolite, 15 Days	0.500210347	0.007871367	0.668377716	0.100309952
300°C Rhyolite, 30 Days	0.444942924	0.022097161	0.498435322	0.080150523
400°C Rhyolite, 0 Days	0.507554893	0.006912477	0.687155602	0.08439439
400°C Rhyolite, 7 Days	0.496800355	0.00644294	0.68810326	0.099118267
400°C Rhyolite, 15 Days	0.487947945	0.004029587	0.739361333	0.108464746
400°C Rhyolite, 30 Days	0.484324856	0.014281028	0.579683944	0.105663182
Basaltic Glass				
200°C Basalt, 0 Days	1.935936807	1.007684331		
200°C Basalt, 15 Days	1.936005444	1.008823966		
200°C Basalt, 30 Days	1.873148853	1.00478549		
200°C Basalt, 60 Days	1.688853954	1.011242222	3.12608136	1.109528509
200°C Basalt, 120 Days	1.701731176	1.014440751	2.487271893	1.138499532
200°C Basalt, 240 Days	1.585827902	1.013898874	2.397210303	1.046755774
300°C Basalt, 0 Days	1.894914509	1.008161657		
300°C Basalt, 15 Days	3.032268	1.019964	3.18041	1.177608
300°C Basalt, 30 Days	1.967652267	1.007309825		
300°C Basalt, 60 Days	1.706588906	1.011363508	2.891950598	1.098830002
300°C Basalt, 120 Days	1.700309086	1.012408235	2.139851978	1.131538782
300°C Basalt, 240 Days	1.674468357	1.014031999	1.733874693	1.066189376
400°C Basalt, 0 Days	2.100948592	1.007111679		
400°C Basalt, 15 Days	2.234051849	1.004960709		
400°C Basalt, 30 Days	1.788625347	1.031432219	2.331976049	1.141759213
400°C Basalt, 60 Days	1.780281752	1.036764729	2.925851885	1.129798553
400°C Basalt, 120 Days	1.877579868	1.027125846	3.558820248	1.147881679
400°C Basalt, 240 Days	1.795900708	1.025578711	2.722157903	1.066850269

Table A3: The proportional height (P) of components part of the total curve of artificially aged samples in MaxUnmix curves. The "sd" is the standard deviation of the proportional heights from each component. Rhyolitic glasses have two experiments, one over 240 days, and one over 30 days (Exp. 2).

Proportional height of components to full curve	Component 1		Component 2	
Rhyolitic Glass				
	P	sd	P	sd
200°C Rhyolite, 0 Days	0.98224	0.00489		
200°C Rhyolite, 15 Days	0.98385	0.00473		
200°C Rhyolite, 30 Days	0.95213	0.00625		
200°C Rhyolite, 60 Days	0.95933	0.0097	0.16236	0.03897
200°C Rhyolite, 120 Days	0.98346	0.0031	0.14397	0.04416
200°C Rhyolite, 240 Days	0.97984	0.0047	0.19169	0.05634
300°C Rhyolite, 0 Days	0.97706	0.00402		

300°C Rhyolite, 15 Days	0.97615	0.00386		
300°C Rhyolite, 30 Days	0.97822	0.00314		
300°C Rhyolite, 60 Days	0.95538	0.00435		
300°C Rhyolite, 120 Days	0.95061	0.00177		
300°C Rhyolite, 240 Days	0.96899	0.00306		
400°C Rhyolite, 0 Days	0.97861	0.00376		
400°C Rhyolite, 15 Days	0.97666	0.00439		
400°C Rhyolite, 30 Days	0.96941	0.00565	0.239	0.06097
400°C Rhyolite, 60 Days	0.93583	0.04126	0.5549	0.04628
400°C Rhyolite, 120 Days	0.95068	0.00762	0.3045	0.08378
400°C Rhyolite, 240 Days	0.96163	0.00454	0.18813	0.03497
Exp. 2				
200°C Rhyolite, 0 Days	1.007398742	0.005488694	0.088439434	0.016644928
200°C Rhyolite, 7 Days	0.967979942	0.020185544	0.103574116	0.030144153
200°C Rhyolite, 15 Days	0.947586501	0.029775652	0.168902627	0.046028129
200°C Rhyolite, 30 Days	0.936588971	0.028035257	0.167702432	0.044459515
300°C Rhyolite, 0 Days	0.982331255	0.014063467	0.104069083	0.024224663
300°C Rhyolite, 7 Days	0.934306376	0.01834054	0.137696492	0.018701454
300°C Rhyolite, 15 Days	0.925254989	0.026411005	0.153497914	0.027181201
300°C Rhyolite, 30 Days	0.826718251	0.027954648	0.394182669	0.078739738
400°C Rhyolite, 0 Days	0.963020429	0.0215286	0.123719936	0.026008407
400°C Rhyolite, 7 Days	0.936673752	0.022985323	0.144398661	0.02245516
400°C Rhyolite, 15 Days	0.882761137	0.024348173	0.164703736	0.016942415
400°C Rhyolite, 30 Days	0.905993395	0.031945918	0.202445471	0.052165438
Basaltic Glass				
200°C Basalt, 0 Days	0.962869391	0.007265202		
200°C Basalt, 15 Days	0.981513374	0.007190337		
200°C Basalt, 30 Days	0.993192415	0.004008185		
200°C Basalt, 60 Days	0.872833819	0.028303312	0.131159006	0.029328008
200°C Basalt, 120 Days	0.878239374	0.053124321	0.15501433	0.04459134
200°C Basalt, 240 Days	0.703370576	0.054208627	0.309330868	0.048486575
300°C Basalt, 0 Days	0.982618362	0.00741309		
300°C Basalt, 15 Days	0.986934241	0.005351392		
300°C Basalt, 30 Days	0.888123281	0.039773042	0.145950847	0.038553399
300°C Basalt, 60 Days	0.890792427	0.028623388	0.129838113	0.031520154
300°C Basalt, 120 Days	0.899598686	0.051511859	0.153172532	0.04000258
300°C Basalt, 240 Days	0.962744713	0.044421046	0.159436727	0.037580366
400°C Basalt, 0 Days	0.966735937	0.005428672		
400°C Basalt, 15 Days	1.004300052	0.002807104		
400°C Basalt, 30 Days	0.740132537	0.113833972	0.354621666	0.096898533
400°C Basalt, 60 Days	0.739724783	0.084669275	0.298088827	0.088749615
400°C Basalt, 120 Days	0.818274665	0.053528799	0.189820901	0.061105947
400°C Basalt, 240 Days	0.743298634	0.055495236	0.315538369	0.063400483

Table A4: The skewness (S) of components part of the total curve of artificially aged samples in MaxUnmix peaks. If S > 1, there is a right skew, if S < 1, that is a left skew. The "sd" is the standard deviation of the skewness from each component. Rhyolitic glasses have two experiments, one over 240 days, and one over 30 days (Exp. 2).

	Component 1		Component 2	
Rhyolitic Glass				
	S	sd	S	sd
200°C Rhyolite, 0 Days	0.958163914	0.044187746		
200°C Rhyolite, 15 Days	0.92659787	0.039826991		
200°C Rhyolite, 30 Days	0.910250893	0.01066215		
200°C Rhyolite, 60 Days	0.854330139	0.028446572	1.570418803	0.155500795
200°C Rhyolite, 120 Days	0.838618122	0.032501075	1.53013428	0.16963144
200°C Rhyolite, 240 Days	0.842356858	0.043056467	1.507739363	0.16013367
300°C Rhyolite, 0 Days	0.911081326	0.041387292		
300°C Rhyolite, 15 Days	0.85976905	0.035416254		
300°C Rhyolite, 30 Days	0.832463497	0.0084912		
300°C Rhyolite, 60 Days	0.855561887	0.004840407		
300°C Rhyolite, 120 Days	0.8027456	0.002182418		
300°C Rhyolite, 240 Days	0.85127808	0.010784016		
400°C Rhyolite, 0 Days	0.933400126	0.054655498		
400°C Rhyolite, 15 Days	0.917673272	0.056971088		
400°C Rhyolite, 30 Days	0.832463497	0.0084912	1.410626052	0.156512418
400°C Rhyolite, 60 Days	0.855561887	0.004840407	1.547825946	0.202943776
400°C Rhyolite, 120 Days	0.69817328	0.07594211	1.432310549	0.184070227
400°C Rhyolite, 240 Days	0.729405889	0.033393764	1.707131292	0.153023732
Exp. 2				
200°C Rhyolite, 0 Days	1.012850687	0.013604419	0.543137622	0.115632795
200°C Rhyolite, 7 Days	1.051478278	0.038067638	0.684209247	0.169292152
200°C Rhyolite, 15 Days	1.076872152	0.052359376	0.643888202	0.204735906
200°C Rhyolite, 30 Days	1.120315744	0.050873434	0.710875544	0.21979313
300°C Rhyolite, 0 Days	1.030718918	0.020240434	1.009005522	0.206685405
300°C Rhyolite, 7 Days	1.119621821	0.019802641	0.977021292	0.133647983
300°C Rhyolite, 15 Days	1.139327921	0.030212671	0.914589693	0.190115579
300°C Rhyolite, 30 Days	1.070276998	0.084386085	0.495680808	0.090787748
400°C Rhyolite, 0 Days	1.054189757	0.025233628	0.953348452	0.213232554
400°C Rhyolite, 7 Days	1.116257723	0.023384666	0.920452603	0.154134663
400°C Rhyolite, 15 Days	1.169885156	0.016353408	0.995391525	0.114637277
400°C Rhyolite, 30 Days	1.194612218	0.065017442	0.74988658	0.232442825
Basaltic Glass				
200°C Basalt, 0 Days	0.881589734	0.01006987		
200°C Basalt, 15 Days	0.927349692	0.02719872		
200°C Basalt, 30 Days	0.988307009	0.02006978		
200°C Basalt, 60 Days	0.928787164	0.018119288	1.202573432	0.133252992
200°C Basalt, 120 Days	0.988948476	0.029266849	1.037341497	0.133162827
200°C Basalt, 240 Days	0.996194959	0.030527323	1.012092201	0.098785485

300°C Basalt, 0 Days	0.940274782	0.018668227		
300°C Basalt, 15 Days	0.908903015	0.015509181		
300°C Basalt, 30 Days	0.995958092	0.024319653	1.228923071	0.143179362
300°C Basalt, 60 Days	0.963820464	0.020233461	1.344619692	0.123019577
300°C Basalt, 120 Days	0.998714091	0.024217384	1.028058383	0.120251862
300°C Basalt, 240 Days	1.03517483	0.027286953	0.825487998	0.089435205
400°C Basalt, 0 Days	0.829796003	0.01315555		
400°C Basalt, 15 Days	0.842103474	0.01056504		
400°C Basalt, 30 Days	0.983566083	0.068084285	0.962952014	0.11530305
400°C Basalt, 60 Days	0.90446021	0.06121201	1.082126062	0.128256723
400°C Basalt, 120 Days	0.82452611	0.024304702	1.108443516	0.134669656
400°C Basalt, 240 Days	0.893997985	0.030073912	1.152650811	0.079129744

Table A5: The original contribution (OC) of the total curve of artificially aged samples in MaxUnmix peaks. These were user created before the calculation of the extrapolated contribution (EC). The "sd" is the standard deviation of the original contribution from each component. Rhyolitic glasses have two experiments, one over 240 days, and one over 30 days (Exp. 2).

Original Contribution	Component 1		Component 2	
Rhyolitic Glass				
	Oc.mean	sd	Oc.mean	sd
200°C Rhyolite, 0 Days	1	0		
200°C Rhyolite, 15 Days	1	0		
200°C Rhyolite, 30 Days	1	0		
200°C Rhyolite, 60 Days	0.93222	0.05526	0.06778	0.05824
200°C Rhyolite, 120 Days	0.94629	0.06238	0.05371	0.058
200°C Rhyolite, 240 Days	0.92171	0.06914	0.07829	0.07415
300°C Rhyolite, 0 Days	1	0		
300°C Rhyolite, 15 Days	1	0		
300°C Rhyolite, 30 Days	1	0		
300°C Rhyolite, 60 Days	1	0		
300°C Rhyolite, 120 Days	1	0		
300°C Rhyolite, 240 Days	1	0		
400°C Rhyolite, 0 Days	1	0		
400°C Rhyolite, 15 Days	1	0		
400°C Rhyolite, 30 Days	0.89971	0.08993	0.10029	0.08276
400°C Rhyolite, 60 Days	0.70746	0.15655	0.29254	0.12508
400°C Rhyolite, 120 Days	0.84742	0.12527	0.15258	0.11424
400°C Rhyolite, 240 Days	0.90138	0.04961	0.09862	0.05326
Exp. 2				
200°C Rhyolite, 0 Days	0.941313204	0.025967349	0.058681873	0.035444197
200°C Rhyolite, 7 Days	0.906281733	0.071520388	0.093784393	0.088135706
200°C Rhyolite, 15 Days	0.841950719	0.102481764	0.158082138	0.112176059

200°C Rhyolite, 30 Days	0.840774021	0.115211459	0.159208548	0.11801619
300°C Rhyolite, 0 Days	0.900441399	0.059171706	0.09955916	0.070290658
300°C Rhyolite, 7 Days	0.849371136	0.057372816	0.150628864	0.077900309
300°C Rhyolite, 15 Days	0.839438091	0.092848515	0.160561909	0.10503093
300°C Rhyolite, 30 Days	0.680512377	0.12218329	0.319487623	0.165394273
400°C Rhyolite, 0 Days	0.872990824	0.07533668	0.126990555	0.088228639
400°C Rhyolite, 7 Days	0.844612673	0.078704162	0.155387327	0.092586396
400°C Rhyolite, 15 Days	0.798788421	0.074386697	0.201211785	0.102437958
400°C Rhyolite, 30 Days	0.81105902	0.119363451	0.18894098	0.129236084
Basaltic Glass				
200°C Basalt, 0 Days	1	0		
200°C Basalt, 15 Days	1	0		
200°C Basalt, 30 Days	1	0		
200°C Basalt, 60 Days	0.765120301	0.10738855	0.234875355	0.118454134
200°C Basalt, 120 Days	0.770682195	0.17936172	0.229317805	0.188041536
200°C Basalt, 240 Days	0.549558918	0.156711611	0.450439136	0.171299338
300°C Basalt, 0 Days	1	0		
300°C Basalt, 15 Days	1	0		
300°C Basalt, 30 Days	0.780698484	0.15791682	0.219301516	0.156447279
300°C Basalt, 60 Days	0.785499074	0.107771872	0.214511547	0.112250661
300°C Basalt, 120 Days	0.804338427	0.187090033	0.195655685	0.174449997
300°C Basalt, 240 Days	0.84932337	0.120106861	0.22873673	0.13012014
400°C Basalt, 0 Days	1	0		
400°C Basalt, 15 Days	1	0		
400°C Basalt, 30 Days	0.594618136	0.337747205	0.405381864	0.340250748
400°C Basalt, 60 Days	0.582551351	0.279703781	0.417448649	0.313986721
400°C Basalt, 120 Days	0.694898252	0.20222175	0.305101748	0.190830619
400°C Basalt, 240 Days	0.586031226	0.197350007	0.413968774	0.214156633

Table A6: The extrapolated contribution (EC) of artificially aged samples in MaxUnmix peaks. The "sd" is the standard deviation of the extrapolated contribution from each component. Rhyolitic glasses have two experiments, one over 240 days, and one over 30 days (Exp. 2).

Extrapolated Contribution	Component 1		Component 2	
Rhyolitic Glass				
	EC	sd	EC	sd
200°C Rhyolite, 0 Days	1	0		
200°C Rhyolite, 15 Days	1	0		
200°C Rhyolite, 30 Days	1	0		
200°C Rhyolite, 60 Days	0.93213	0.05546	0.06787	0.05884
200°C Rhyolite, 120 Days	0.94643	0.06258	0.05357	0.05736
200°C Rhyolite, 240 Days	0.91932	0.06741	0.08068	0.07891
300°C Rhyolite, 0 Days	1	0		

300°C Rhyolite, 15 Days	1	0		
300°C Rhyolite, 30 Days	1	0		
300°C Rhyolite, 60 Days	1	0		
300°C Rhyolite, 120 Days	1	0		
300°C Rhyolite, 240 Days	1	0		
400°C Rhyolite, 0 Days	1	0		
400°C Rhyolite, 15 Days	1	0		
400°C Rhyolite, 30 Days	0.90033	0.08882	0.09967	0.08155
400°C Rhyolite, 60 Days	0.71068	0.15314	0.28932	0.12283
400°C Rhyolite, 120 Days	0.84786	0.12277	0.15214	0.11401
400°C Rhyolite, 240 Days	0.89962	0.04585	0.10039	0.05523
Exp. 2				
200°C Rhyolite, 0 Days	0.942036913	0.026399065	0.057965336	0.034772508
200°C Rhyolite, 7 Days	0.907243141	0.07041559	0.092756859	0.086936548
200°C Rhyolite, 15 Days	0.843452358	0.102754822	0.156571143	0.110486313
200°C Rhyolite, 30 Days	0.842347986	0.113940765	0.157652014	0.116508568
300°C Rhyolite, 0 Days	0.901648593	0.059914206	0.098350276	0.069447979
300°C Rhyolite, 7 Days	0.850481677	0.057005119	0.149518323	0.077694461
300°C Rhyolite, 15 Days	0.840798802	0.092861066	0.159201198	0.10438907
300°C Rhyolite, 30 Days	0.68250877	0.121884332	0.31749123	0.163284446
400°C Rhyolite, 0 Days	0.874349431	0.07604138	0.125650857	0.08752547
400°C Rhyolite, 7 Days	0.845732604	0.077831773	0.154267396	0.092357844
400°C Rhyolite, 15 Days	0.799936201	0.074430852	0.200063287	0.102635282
400°C Rhyolite, 30 Days	0.812959242	0.119426684	0.187040758	0.127284683
Basaltic Glass				
200°C Basalt, 0 Days	1	0		
200°C Basalt, 15 Days	1	0		
200°C Basalt, 30 Days	1	0		
200°C Basalt, 60 Days	0.76203507	0.098010195	0.23796493	0.123427584
200°C Basalt, 120 Days	0.770603702	0.171536473	0.229383836	0.06417049
200°C Basalt, 240 Days	0.548254266	0.202613812	0.451745734	0.172013531
300°C Basalt, 0 Days	1	0		
300°C Basalt, 15 Days	1	0		
300°C Basalt, 30 Days	0.779326826	0.152973627	0.220673174	0.158657467
300°C Basalt, 60 Days	0.781001705	0.102185744	0.218998295	0.117080448
300°C Basalt, 120 Days	0.804255257	0.188153199	0.195744743	0.175280195
300°C Basalt, 240 Days	0.8497857	0.148243011	0.1502143	0.138531156
400°C Basalt, 0 Days	1	0		
400°C Basalt, 15 Days	1	0		
400°C Basalt, 30 Days	0.594840947	0.33554137	0.405122142	0.340545797
400°C Basalt, 60 Days	0.578583888	0.272787097	0.421416112	0.317751193
400°C Basalt, 120 Days	0.68809299	0.193104527	0.311824349	0.196122505
400°C Basalt, 240 Days	0.582514024	0.193396518	0.417443276	0.215620622

Appendix B

Table B1: The coercivity peaks (B_h) of hydrated samples in MaxUnmix peaks. The "sd" is the standard deviation of the coercivity peak from each component.				
	Component 1		Component 2	
Rhyolitic Glass				
	Bh	sd	Bh	sd
300°C 1 day; Before	30.69698188	1.070707406	256.7559159	1.047061104
300°C 1 day; After	30.17928699	1.076944248	261.1977509	1.046193128
300°C 2.5 days; Before	48.93413972	1.058748642	279.551629	1.121218854
300°C 2.5 days; After	45.12579558	1.047754221	250.7216618	1.022270429
300°C 6.3 days; Before	49.30003938	1.053425874	266.5323562	1.051144141
300°C 6.3 days; After	37.11778108	1.076067736	261.4748399	1.064880547
300°C 15 days; Before	38.9851036	1.047277986	275.5833777	1.040137069
300°C 15 days; After	38.00139751	1.046819957	241.8281621	1.062531246
450°C 0.3 day; Before	42.5605912	1.055179007	259.5121618	1.028072447
450°C 0.3 day; After	37.80688468	1.064098591	285.3210401	1.123338555
450°C 1 day; Before	38.98232959	1.056200771	242.8997687	1.059109536
450°C 1 day; After	27.79265789	1.061037371	226.0834064	1.101375774
450°C 3.2 days; Before	28.4616793	1.066273361	260.74324	1.06694891
450°C 3.2 days; After	36.23932241	1.041581928	275.5648125	1.167304062
450°C 10 days; Before	10.23826094	1.336088345	91.57051492	1.582615689
450°C 10 days; After	37.92433518	1.030880374		
Basaltic Glass				
300°C 1 day; Before	148.1779952	1.04274437	21.05025178	1.139058694
300°C 1 day; After	147.1291869	1.02219814	82.24129868	1.238204315
300°C 2.5 days; Before	175.0935176	1.036741481	54.73507415	1.098868067
300°C 2.5 days; After	178.5889378	1.056252679	37.8551853	1.161192801
300°C 6.3 days; Before	28.15113628	1.049592948	220.6832273	1.063645049
300°C 6.3 days; After	29.60506627	1.03704144		
300°C 15 days; Before	36.66925612	1.088922835	206.43562	1.05017418
300°C 15 days; After	147.2666473	1.029277038	43.63699128	1.232522846
450°C 0.3 day; Before	180.6409548	1.067572529	77.22729041	1.506296888
450°C 0.3 day; After	197.7687966	1.04746373	76.32924241	1.238303132
450°C 1 day; Before	156.2516431	1.036643196	63.15096914	1.100588
450°C 1 day; After	224.8326844	1.03211837	83.94914611	1.099157274
450°C 3.2 days; Before	104.9718759	1.124361979	13.24408221	1.261379511
450°C 3.2 days; After	134.5181215	1.187549238	20.61324091	1.73079344
450°C 10 days; Before	170.2072184	1.107481348	39.79549734	1.156062361
450°C 10 days; After	93.99535335	1.043346509	31.15117127	1.26175977

Table B2: The dispersion parameters (DP) of hydrated samples in MaxUnmix curves. The "sd" is the standard deviation of the dispersion parameter from each component.				
	Component 1		Component 2	
Rhyolitic Glass				
	DP	sd	DP	sd
300°C 1 day; Before	3.484629484	1.055268567	1.737449536	1.030887154
300°C 1 day; After	3.795434233	1.051210229	1.736806546	1.044230052
300°C 2.5 days; Before	3.391519362	1.031764532	1.551348938	1.099392878
300°C 2.5 days; After	2.706191351	1.029009584	1.698826377	1.014139676
300°C 6.3 days; Before	3.088401561	1.032344768	1.667910847	1.048794225
300°C 6.3 days; After	2.975718737	1.041425673	1.719959795	1.023140887
300°C 15 days; Before	3.043317305	1.025191623	1.695948585	1.017982622
300°C 15 days; After	2.754733096	1.030418784	1.825322741	1.03871228
450°C 0.3 day; Before	2.974748163	1.034556527	1.633494678	1.017440782
450°C 0.3 day; After	3.589830378	1.042172494	1.852091135	1.092826667
450°C 1 day; Before	3.368914047	1.034996684	1.614865198	1.058618493
450°C 1 day; After	4.159456391	1.046030115	1.677518141	1.075870494
450°C 3.2 days; Before	3.998311063	1.03717183	1.683821779	1.060747331
450°C 3.2 days; After	2.886199733	1.035678965	2.053878267	1.117982164
450°C 10 days; Before	6.462832334	1.269796341	2.671325737	1.294150228
450°C 10 days; After	3.62653212	1.021168875		
Basaltic Glass				
300°C 1 day; Before	1.988371274	1.025249431	2.281854117	1.035117887
300°C 1 day; After	1.862711435	1.017197524	4.861661741	1.187354249
300°C 2.5 days; Before	1.713338015	1.023133818	4.588998327	1.050737453
300°C 2.5 days; After	1.755400969	1.026916127	4.490524947	1.10869206
300°C 6.3 days; Before	2.705840164	1.032462718	1.934984869	1.019191269
300°C 6.3 days; After	3.200257946	1.026569515		
300°C 15 days; Before	3.372343483	1.064777602	1.785700667	1.035358406
300°C 15 days; After	1.648256335	1.014325043	2.999490247	1.13113494
450°C 0.3 day; Before	1.904714988	1.036252014	3.464046342	1.28717036
450°C 0.3 day; After	1.93702977	1.020568155	3.008550783	1.134913213
450°C 1 day; Before	1.850133353	1.019220061	3.785333377	1.083381511
450°C 1 day; After	1.69253513	1.016906948	4.44960775	1.077685031
450°C 3.2 days; Before	2.372761217	1.079361258	2.972264223	1.124545387
450°C 3.2 days; After	1.995883297	1.093093463	5.247726694	1.393690877
450°C 10 days; Before	1.935182041	1.034183553	3.768595876	1.087792424
450°C 10 days; After	2.029147465	1.02382513	3.469669435	1.15846129

Table B3: The proportional height of components (P) of total curve of hydrated samples in MaxUnmix curves. The "sd" is the standard deviation of the proportional height from each component.				
	Component 1		Component 2	
Rhyolitic Glass				
	P	sd	P	sd
300°C 1 day; Before	0.954392337	0.007076183	0.347865299	0.056211558
300°C 1 day; After	0.942039828	0.00678058	0.258560903	0.051540766
300°C 2.5 days; Before	0.992835105	0.003304802	0.149425634	0.05130762
300°C 2.5 days; After	0.964626387	0.004258544	0.341215254	0.04418631
300°C 6.3 days; Before	0.985453566	0.004857263	0.220149332	0.043413527
300°C 6.3 days; After	0.976530556	0.006222881	0.316191209	0.073352555
300°C 15 days; Before	0.985522516	0.002870117	0.318242729	0.051872969
300°C 15 days; After	0.960113211	0.004458034	0.333082887	0.045812399
450°C 0.3 day; Before	0.944239526	0.005427781	0.33867334	0.054112057
450°C 0.3 day; After	1.001985109	0.01350602	0.122502261	0.055404698
450°C 1 day; Before	0.971524769	0.00496742	0.256361179	0.042507931
450°C 1 day; After	0.962280852	0.009609353	0.124754352	0.038901106
450°C 3.2 days; Before	0.937311162	0.005137932	0.218759778	0.04910025
450°C 3.2 days; After	0.953129131	0.007310375	0.164825853	0.038356141
450°C 10 days; Before	0.784861929	0.160108212	0.473201139	0.191396391
450°C 10 days; After	0.95188913	0.005394915		
Basaltic Glass				
300°C 1 day; Before	0.988267432	0.012947447	0.276654218	0.026934821
300°C 1 day; After	0.818598697	0.032569215	0.191386618	0.030711224
300°C 2.5 days; Before	0.674823451	0.039026201	0.330301714	0.024764466
300°C 2.5 days; After	0.637725226	0.051764775	0.588006551	0.020889468
300°C 6.3 days; Before	0.953390895	0.005271454	0.39458348	0.04346919
300°C 6.3 days; After	0.958849383	0.005088089		
300°C 15 days; Before	0.936379179	0.008378641	0.574465691	0.05958376
300°C 15 days; After	0.852465528	0.065824265	0.223426938	0.025346712
450°C 0.3 day; Before	0.825915536	0.066192502	0.204496868	0.046454605
450°C 0.3 day; After	0.837605018	0.056918578	0.212020787	0.04413715
450°C 1 day; Before	0.748235282	0.04554113	0.328825053	0.039727186
450°C 1 day; After	0.678802107	0.034858809	0.418236872	0.0266354
450°C 3.2 days; Before	0.961516319	0.037933912	0.456704871	0.085095031
450°C 3.2 days; After	0.692369103	0.177364558	0.411964577	0.115665198
450°C 10 days; Before	0.603747657	0.104267489	0.562917362	0.065632919
450°C 10 days; After	0.883762199	0.057061697	0.166919106	0.05421363

Table B4: The skewness (S) of total curve of hydrated samples in MaxUnmix curves. The "sd" is the standard deviation of the proportional height from each component.				
	Component 1		Component 2	
Rhyolitic Glass				
	S	sd	S	sd
300°C 1 day; Before	0.773113437	0.039701923	1.259756146	0.094608894
300°C 1 day; After	0.810993629	0.041648617	1.535401759	0.178329054
300°C 2.5 days; Before	0.772507492	0.035266039	1.770107923	0.147748624
300°C 2.5 days; After	0.910225264	0.034045402	1.429109511	0.078667142
300°C 6.3 days; Before	0.921954586	0.033884639	1.442953009	0.147195292
300°C 6.3 days; After	0.773863604	0.049882308	1.349350822	0.135545204
300°C 15 days; Before	0.734634943	0.030773207	1.471338832	0.096390774
300°C 15 days; After	0.85977156	0.031886957	1.51094119	0.097634355
450°C 0.3 day; Before	0.81209055	0.037049807	1.487438602	0.111358293
450°C 0.3 day; After	0.759040862	0.032581662	1.523575994	0.168266079
450°C 1 day; Before	0.860699201	0.033975129	1.351846797	0.14057075
450°C 1 day; After	0.804906546	0.027340848	1.282787214	0.181505031
450°C 3.2 days; Before	0.755678346	0.034976752	1.447133967	0.139130453
450°C 3.2 days; After	0.871710208	0.030151061	2.305266385	0.761153282
450°C 10 days; Before	0.867954652	0.297836597	0.821137353	0.194296905
450°C 10 days; After	0.973294247	0.01944499		
Basaltic Glass				
300°C 1 day; Before	0.986273395	0.043690592	0.638254628	0.052139305
300°C 1 day; After	0.874942249	0.024870901	1.12230813	0.118642823
300°C 2.5 days; Before	1.016685359	0.045812368	0.633653052	0.080372387
300°C 2.5 days; After	0.987555196	0.07440586	0.939761233	0.104730841
300°C 6.3 days; Before	0.810411679	0.035652295	1.544416117	0.075554442
300°C 6.3 days; After	0.899817522	0.020030585		
300°C 15 days; Before	0.966470324	0.050870601	1.09699713	0.108919548
300°C 15 days; After	1.056326296	0.044061206	0.753090623	0.127105529
450°C 0.3 day; Before	1.063552068	0.074787905	0.944521344	0.198727195
450°C 0.3 day; After	1.037950079	0.049042899	0.965171988	0.140146162
450°C 1 day; Before	0.944897163	0.036243493	1.102644825	0.126433611
450°C 1 day; After	0.943683585	0.04362705	1.050404047	0.113383979
450°C 3.2 days; Before	0.859786583	0.064781656	0.6432249	0.081083661
450°C 3.2 days; After	0.842242117	0.151775782	0.555570472	0.214885074
450°C 10 days; Before	0.974012922	0.068981301	0.79188116	0.142793271
450°C 10 days; After	0.840028946	0.023009168	1.013401584	0.192898732

Table B5: The original contribution (OC) of total curve of hydrated samples in MaxUnmix curves. The "sd" is the standard deviation of the original contribution from each component.				
Original Contribution	Component 1		Component 2	
Rhyolitic Glass				
	OC	sd	OC	sd
300°C 1 day; Before	0.856466532	0.077416966	0.143658311	0.084531451
300°C 1 day; After	0.896199382	0.076761942	0.104049849	0.079438658
300°C 2.5 days; Before	0.947929074	0.059891392	0.052257482	0.056950596
300°C 2.5 days; After	0.843349889	0.06086859	0.156582517	0.067400107
300°C 6.3 days; Before	0.909213051	0.057361694	0.090744034	0.063432414
300°C 6.3 days; After	0.860454087	0.093242107	0.139387025	0.102575691
300°C 15 days; Before	0.867829312	0.057823499	0.132170688	0.066417553
300°C 15 days; After	0.832023746	0.057391371	0.167942577	0.069671186
450°C 0.3 day; Before	0.862516746	0.07768543	0.137483254	0.073276326
450°C 0.3 day; After	0.943096211	0.061238786	0.056951689	0.071031492
450°C 1 day; Before	0.901643565	0.056348782	0.098290194	0.067274443
450°C 1 day; After	0.948401831	0.060993687	0.051580313	0.054855885
450°C 3.2 days; Before	0.910826549	0.06475641	0.089072282	0.073610862
450°C 3.2 days; After	0.90668847	0.034834768	0.094056306	0.062303679
450°C 10 days; Before	0.693776478	0.513396578	0.306223522	0.444342428
450°C 10 days; After	1	0		
Basaltic Glass				
300°C 1 day; Before	0.765933182	0.084588388	0.234186013	0.079676395
300°C 1 day; After	0.653222888	0.133117438	0.346777112	0.137415606
300°C 2.5 days; Before	0.442690688	0.115327367	0.557309312	0.136781645
300°C 2.5 days; After	0.313534719	0.138022824	0.686465281	0.144825386
300°C 6.3 days; Before	0.784330766	0.0629358	0.215658822	0.06976082
300°C 6.3 days; After	1	0		
300°C 15 days; Before	0.765395958	0.091608084	0.234604042	0.096713298
300°C 15 days; After	0.647577324	0.157896747	0.352422676	0.169123534
450°C 0.3 day; Before	0.692583795	0.20804646	0.307416205	0.217201558
450°C 0.3 day; After	0.708660611	0.177353348	0.291339389	0.172827161
450°C 1 day; Before	0.526781181	0.13676596	0.473218819	0.13373691
450°C 1 day; After	0.38375357	0.089401407	0.61624643	0.090732671
450°C 3.2 days; Before	0.659414155	0.160518248	0.340635972	0.180855272
450°C 3.2 days; After	0.470023877	0.380678688	0.529976123	0.415495857
450°C 10 days; Before	0.361616404	0.217331142	0.638383596	0.222194671
450°C 10 days; After	0.76886065	0.196183305	0.23113935	0.187623064

Table B6: The extrapolated contribution (EC) of total curve of hydrated samples in MaxUnmix curves. The "sd" is the standard deviation of the extrapolated contribution from each component.

Extrapolated Contribution	Component 1		Component 2	
Rhyolitic Glass				
	EC	Sd	EC	sd
300°C 1 day; Before	0.858041144	0.075459403	0.141958856	0.081106774
300°C 1 day; After	0.898130248	0.075452622	0.101869752	0.077151682
300°C 2.5 days; Before	0.947337294	0.059980174	0.054705999	0.057844163
300°C 2.5 days; After	0.84411907	0.060379119	0.155969347	0.06647136
300°C 6.3 days; Before	0.908820941	0.057902762	0.091880762	0.064597374
300°C 6.3 days; After	0.860798495	0.091988611	0.139138415	0.100443587
300°C 15 days; Before	0.867478992	0.05578826	0.133684451	0.065453157
300°C 15 days; After	0.831528644	0.052730286	0.167348493	0.070151559
450°C 0.3 day; Before	0.863004705	0.077424476	0.136996752	0.073290011
450°C 0.3 day; After	0.944336575	0.057912399	0.05583258	0.068305437
450°C 1 day; Before	0.905695685	0.053027785	0.094755535	0.065499314
450°C 1 day; After	0.953325154	0.052025542	0.046612189	0.047934041
450°C 3.2 days; Before	0.918129904	0.057995772	0.082390955	0.068805837
450°C 3.2 days; After	0.903340589	0.021469107	0.094368891	0.068611812
450°C 10 days; Before	0.723806257	0.490160548	0.276142671	0.403712033
450°C 10 days; After	1	0		
Basaltic Glass				
300°C 1 day; Before	0.756266535	0.081447314	0.243733465	0.084202476
300°C 1 day; After	0.630673768	0.11442418	0.369320507	0.159328762
300°C 2.5 days; Before	0.435826675	0.131045765	0.564173325	0.137124235
300°C 2.5 days; After	0.295001113	0.115664556	0.704998887	0.148737156
300°C 6.3 days; Before	0.788885731	0.061098622	0.211114269	0.068994403
300°C 6.3 days; After	1	0		
300°C 15 days; Before	0.772684681	0.092900512	0.227157082	0.089361778
300°C 15 days; After	0.643930341	0.153808826	0.356069659	0.168733768
450°C 0.3 day; Before	0.680458646	0.183354168	0.319541354	0.246044357
450°C 0.3 day; After	0.705771906	0.175476955	0.294224086	0.179014614
450°C 1 day; Before	0.51547636	0.124480732	0.484776599	0.143187609
450°C 1 day; After	0.36696796	0.070035667	0.632888018	0.101260089
450°C 3.2 days; Before	0.640870899	0.148216381	0.359129101	0.185017043
450°C 3.2 days; After	0.450413906	0.35583816	0.549586094	0.416169353
450°C 10 days; Before	0.355294468	0.206263295	0.644638733	0.222637419
450°C 10 days; After	0.757433172	0.182114253	0.242566828	0.19658008

Appendix C

Table C1: FORC diagrams for artificially aged and hydration samples. Samples designated with "B" were artificially aged samples. Samples designated with a "C" are hydrated samples. Other samples are listed as untreated samples.

B-27 - 300°C Rhyolitic Glass	B-28 - 400°C Rhyolitic Glass
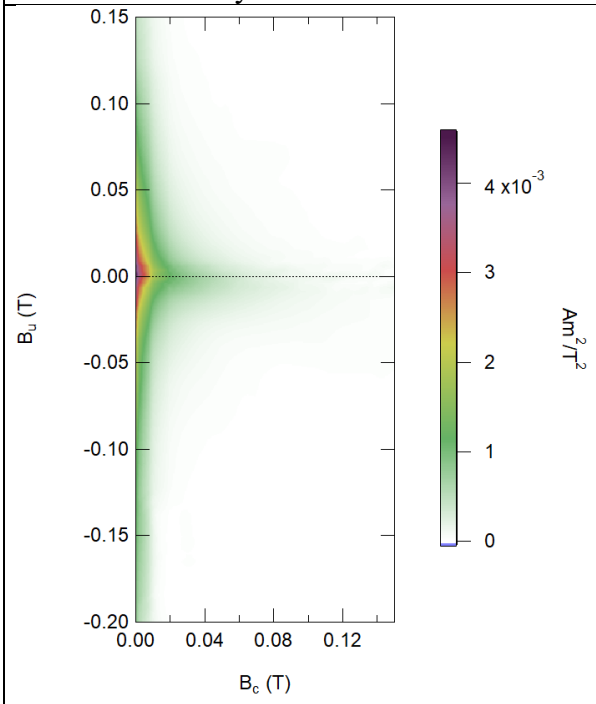	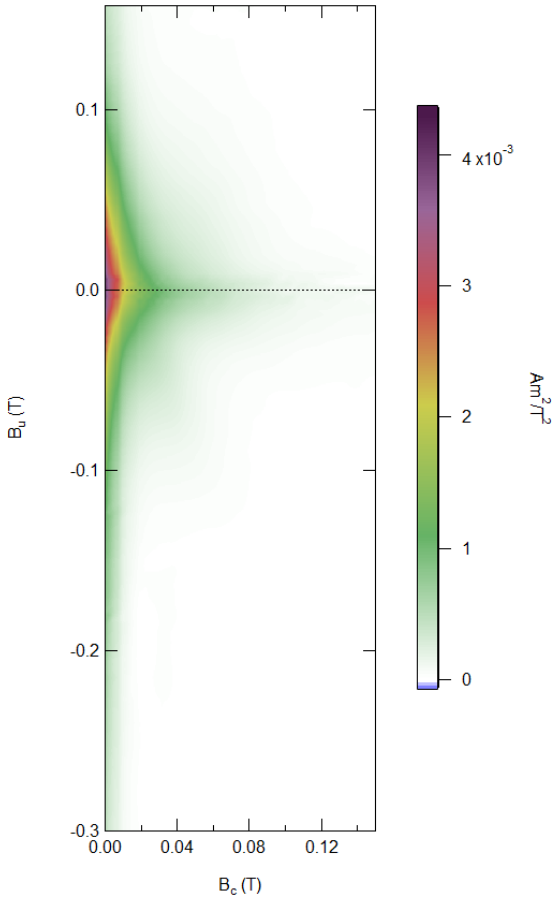
B-29 - 200°C Rhyolitic Glass	**B-41 - 300°C Basaltic Glass**

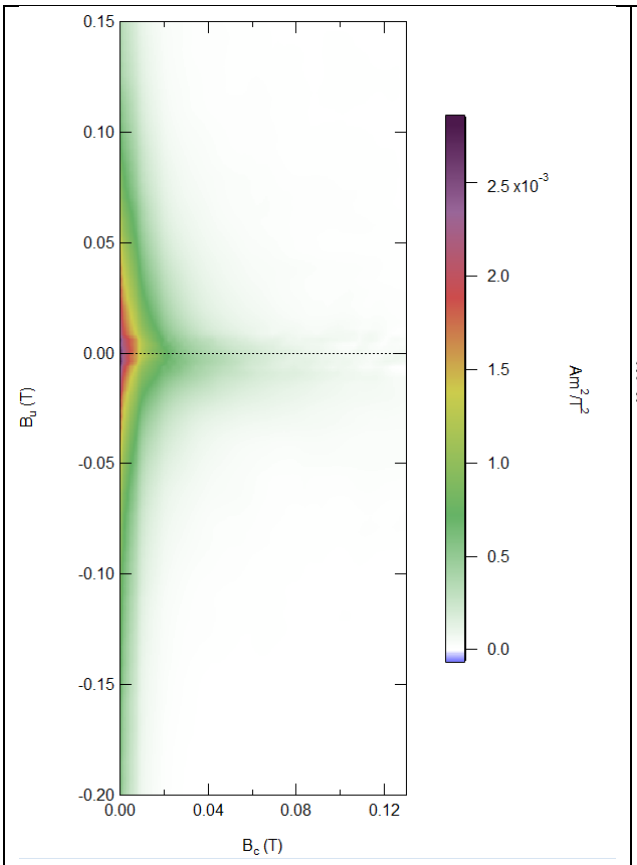

B-42 - 400°C Basaltic Glass

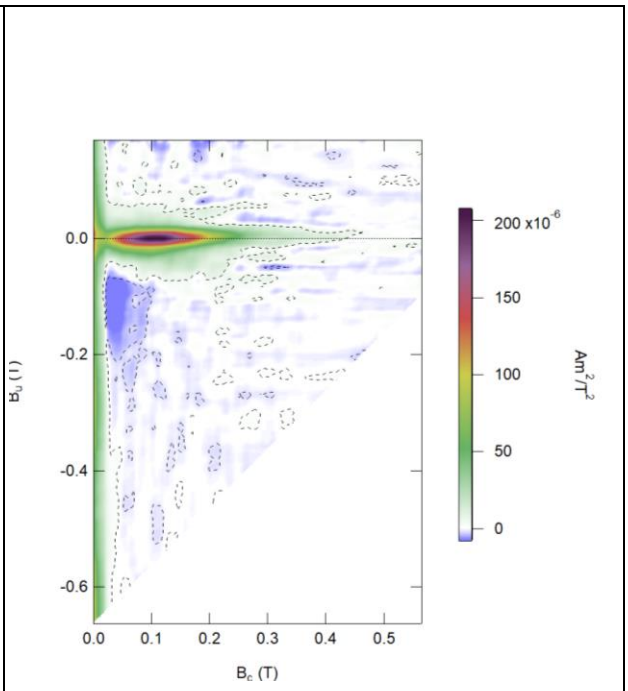

B-66 - 200°C Basaltic Glass

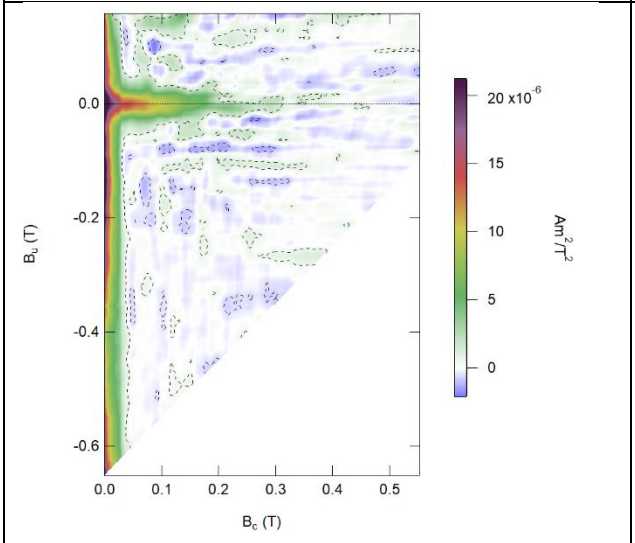

C-02 - 300°C 1 day; Rhyolitic Glass

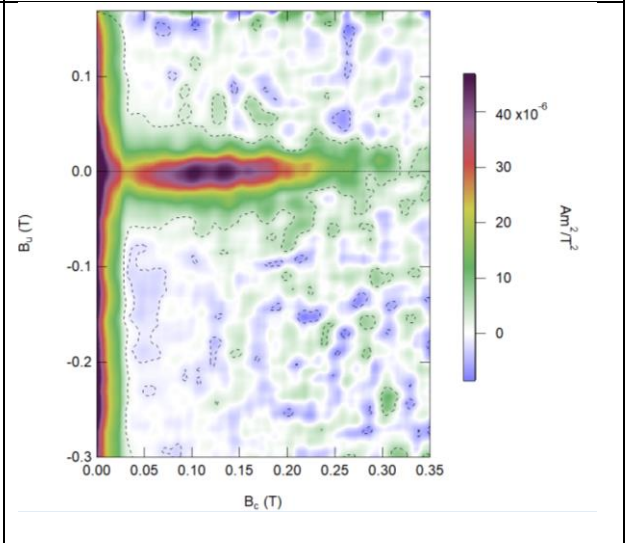

C-06 - 300°C 2.5 days; Rhyolitic Glass

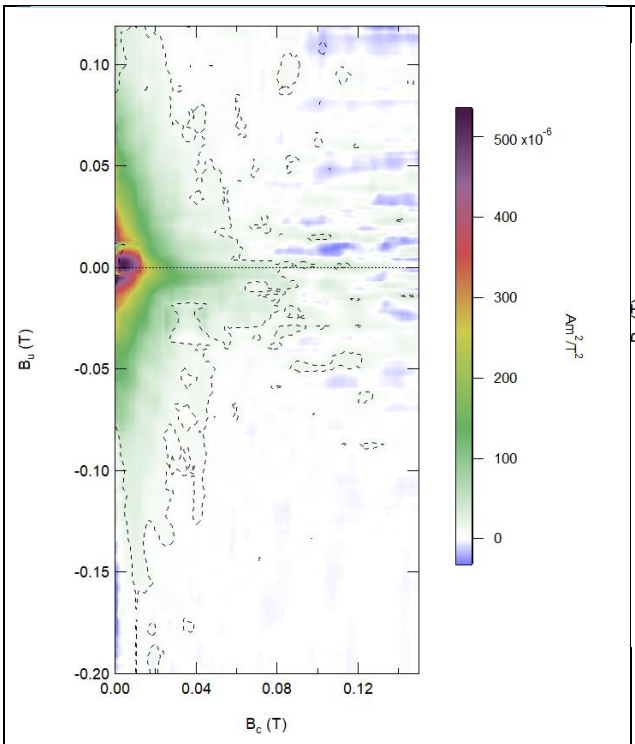

C-15 - 300°C 15 days; Rhyolitic Glass

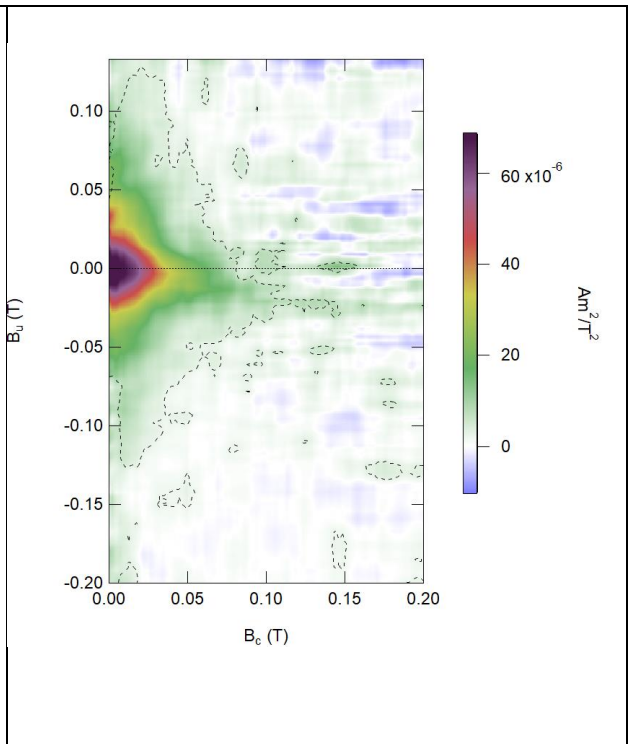

C-19 - 450°C 0.3 days; Rhyolitic Glass

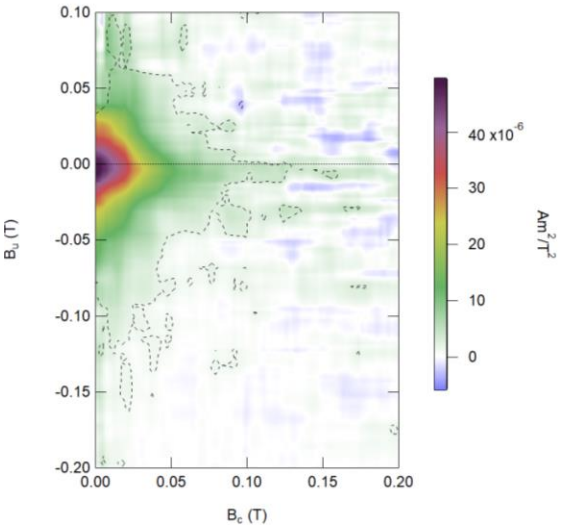

C-25 - 450°C 1 day; Rhyolitic Glass

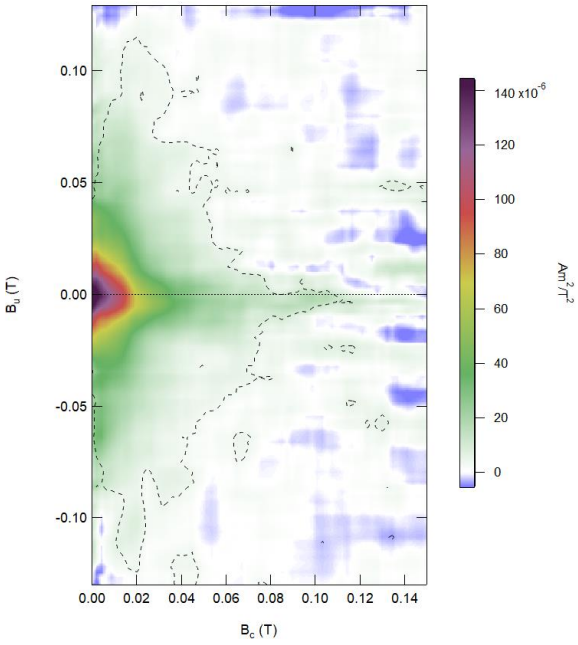

C-29 - 450°C 3.2 day; Rhyolitic Glass

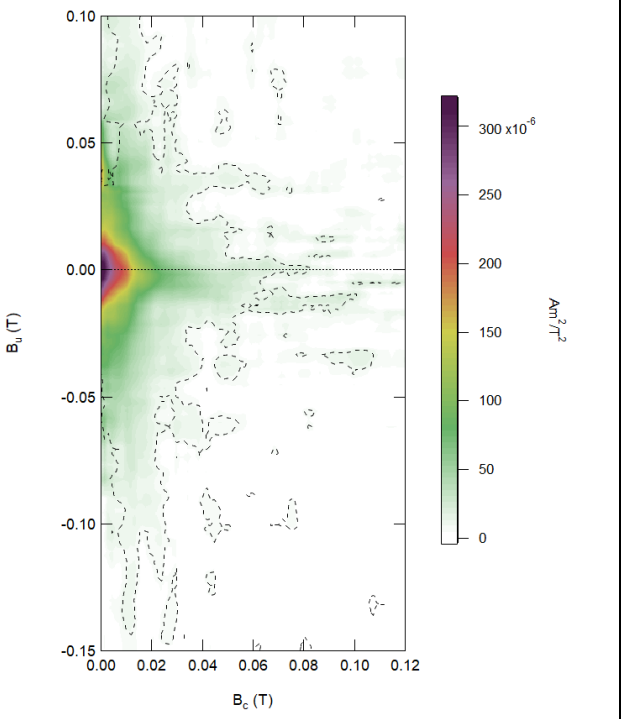

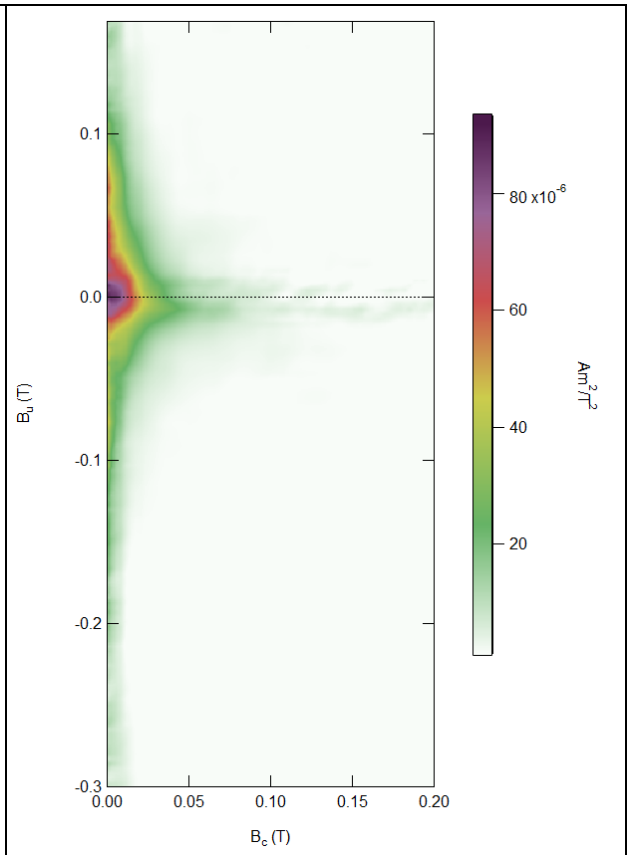

C-33- 450°C 10 days; Rhyolitic Glass

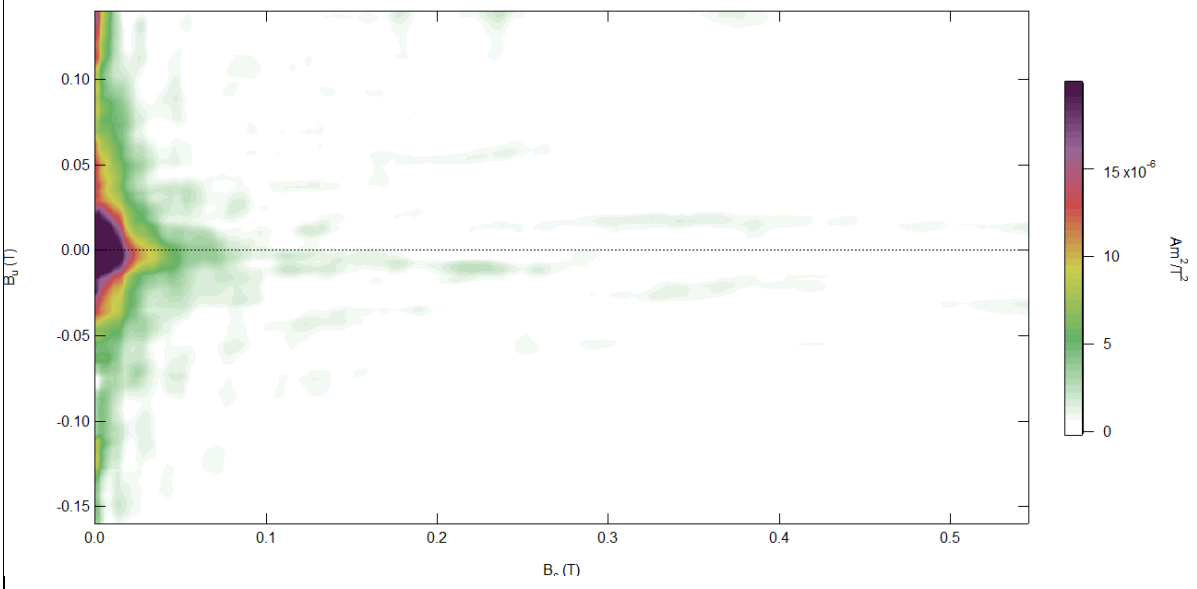

C-53- 300°C 2.5 days; Basaltic Glass

C-65 - 300°C 6.3 days; Basaltic Glass

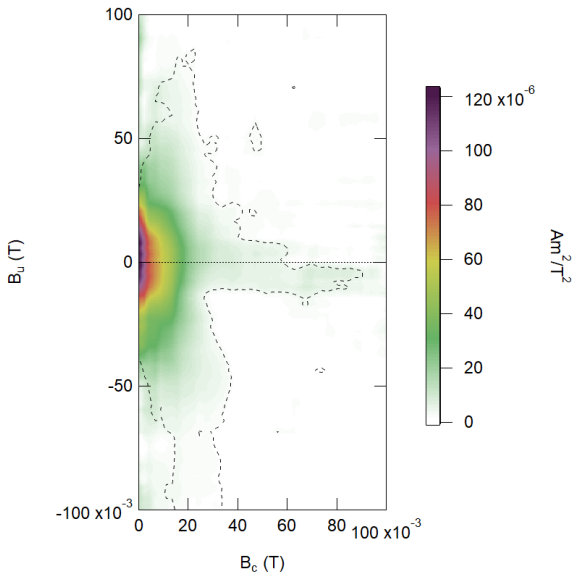

C-71 - 450°C 1.0 day; Basaltic Glass

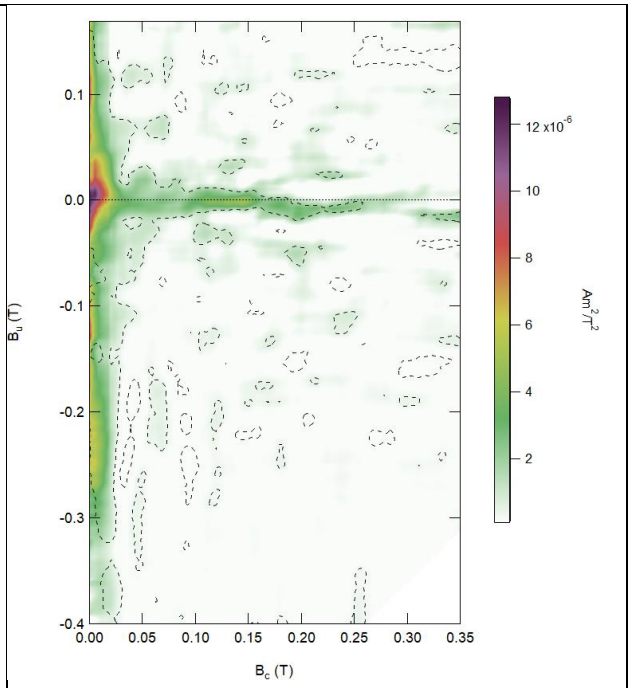

C-79 - 450°C 10 days; Basaltic Glass

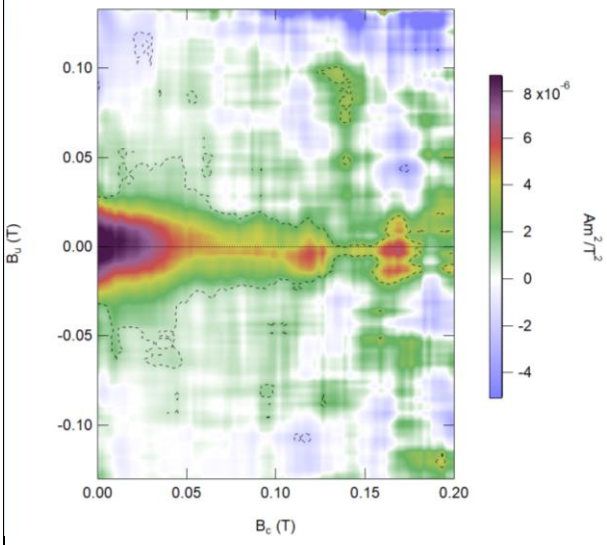

D270-R2 - Untreated Basaltic Glass

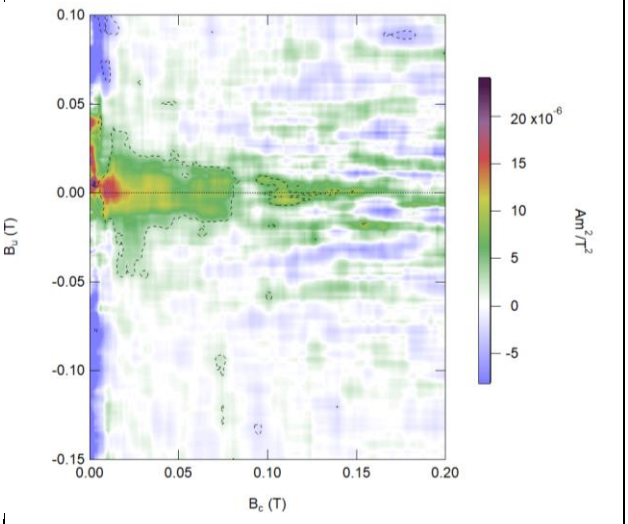

D657-R4 - Untreated Basaltic Glass

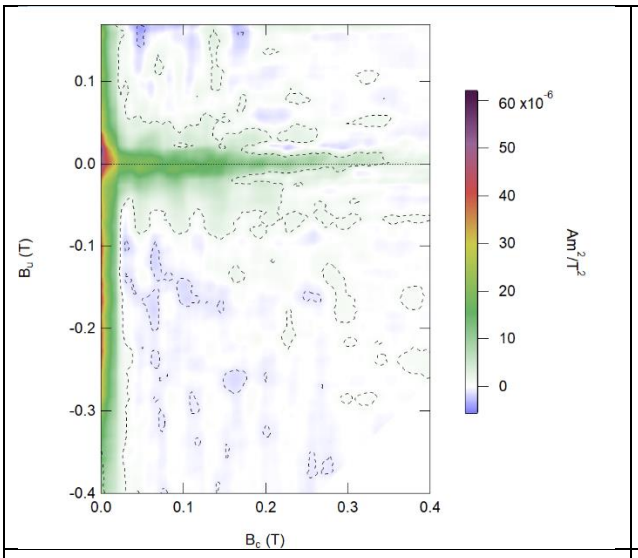

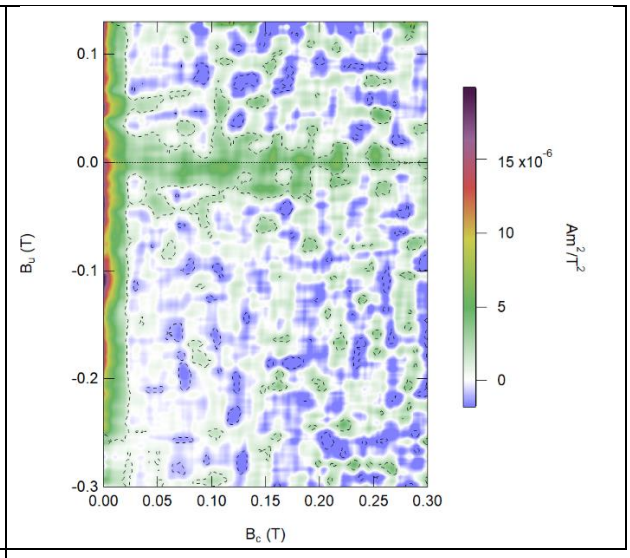

E-01 - Untreated Rhyolitic Glass